Seismic investigation of an isolated sedimentary basin to reconstruct glacially controlled sedimentation processes in the Pine Island Bay, West Antarctica

Masterarbeit im Studiengang Marine Geosciences

Fachbereich Geowissenschaften
Universität Bremen

von

Philip Schneider
Bremen, 2020

1. Gutachter: PD Dr. Karsten Gohl
2. Gutachter: Dr. Tilmann Schwenk

i. Declaration

Philip Schneider

Name

Declaration acc. to § 10 Paragraph 11 Common Part of the Master Examination Regulations

I hereby declare that I wrote my Master Thesis independently and that I did not use other sources and auxiliary means than the ones indicated.

This Master Thesis is not submitted in another examining procedure.

I further declare that the Master thesis might be / might not be* made available to the public in this version.

*Please mark where applicable

Place/Date: Bremen, 22.6.2020

Signature: _____

ii. Abstract

The study carries out a seismic investigation in an isolated sedimentary basin of the inner Pine Island Bay, offshore Pine Island Glacier, West Antarctica. Aim of the study is to derive information on glacially controlled sedimentation processes and to gain knowledge about characteristics of the sedimentary basin. The seismic data employed in the study was recorded on cruise PS104 in 2017. After carrying out of a complete seismic processing, seismic reflection data (paired with bathymetric and Parasound data) is analysed with the aim of then creating a conceptual model of the study area. The investigation reveals a sedimentary basin with up to 300 m horizontally and parallelly deposited sediments, which are strongly consolidated by the earlier overlaying ice sheet. A grounding zone wedge indicates former stillstand of ice sheet in the basin. The crystalline bedrock has up to 90 m deep incisions scoured by meltwater flow. The basin flanks rise up to water depths of ~900 m, while the greatest water depth is ~1070m in the central part of the basin. The all in all successful data processing and investigation of the sedimentary basin provides well interpretable seismic profiles. As a starting point for future work in the study area would be the resolution of the GZW in a high-resolution bathymetric map; research into sediment cores from the consolidated sediments in the basement and the internal structure of the GZW; an age determination for the sediment; and the addition of further seismic lines to carry out a real 3D survey in the sedimentary basin.

iii.   Acknowledgements

Table of contents

List of Figures

1. Introduction

A collapse of the unstable and sensitive West Antarctic Ice Sheet (WAIS) would lead to a global sea level rise of 3-5m. The particularly vulnerable Pine Island Glacier has the largest discharge (66 Gt yr-1) of all ice streams of the WAIS (Hillenbrand et al., 2013; Payne et al., 2004). In scientific circles, it has been debated for decades whether the current rapid retreat of the WAIS represents a phase of ongoing ice retreat since the Last Glacial Maximum (LGM) or if climatic or oceanographic changes influenced the recent changes. Therefore, one of the main objectives of research at the Amundsen Sea sector of West Antarctica is the reconstruction of the ice retreat since LGM, with the goal of possibly being able to predict its future behaviour.

The present thesis carries out a seismic investigation of an isolated sedimentary basin, offshore Pine Island Glacier, West Antarctica. The aim of this investigation is to reconstruct glacially controlled sedimentation processes in the inner Pine Island Bay, and to derive information of the retreat history of the Pine Island Glacier.

This work is based on seismic reflection data that had been acquired during RV Polarstern cruise PS104 in 2017. Seven seismic profiles have been recorded and have, in the context of this thesis, undergone a seismic processing. Moreover, three already processed seismic profiles from expedition ANTXXVI/3 in 2010 have been included in the results, as they have been recorded in the same sedimentary basin. After the seismic processing, key units were identified and picked. For receiving better spatial resolution of the sedimentary basin, 2D grids of the key units were created. In addition to the seismic reflection data, bathymetric maps and Parasound data have been analysed. While seismic reflection data provides information about the deeper areas of the sedimentary basin, Parasound resolves the uppermost meters. The knowledge gained in the study area then has been applied to create a conceptual model of the isolated sedimentary basin.

2. Study Area

The present study focuses on the area of Pine Island Bay (PIB), located in the Amundsen Sea of the South Pacific (West Antarctica). As showed in Fig. 1, the eastern side of the area is occupied by Ellsworth Land, while Marie Byrd Land lies in the southwestern side. A deep, narrow trench occupied by the Pine Island Glacier separates the two sides at the southern end of the bay. PIB borders on Thurston Island in the north and on Thwaities Glacier in the west. The Amundsen Sea lies in between the Bellingshausen Sea (east) and the Ross Sea (west).

Fig. 1: Map of Antarctica and its key geographical information. The red rectangle marks the Amundsen Sea in West Antarctica (Fig. 2). Modified after Abrahamsen (2012).

The specific location of interest for the upcoming analysis is the inner Pine Island Bay, offshore Pine Island Glacier, where seven seismic profiles have been recorded in an isolated sedimentary basin.
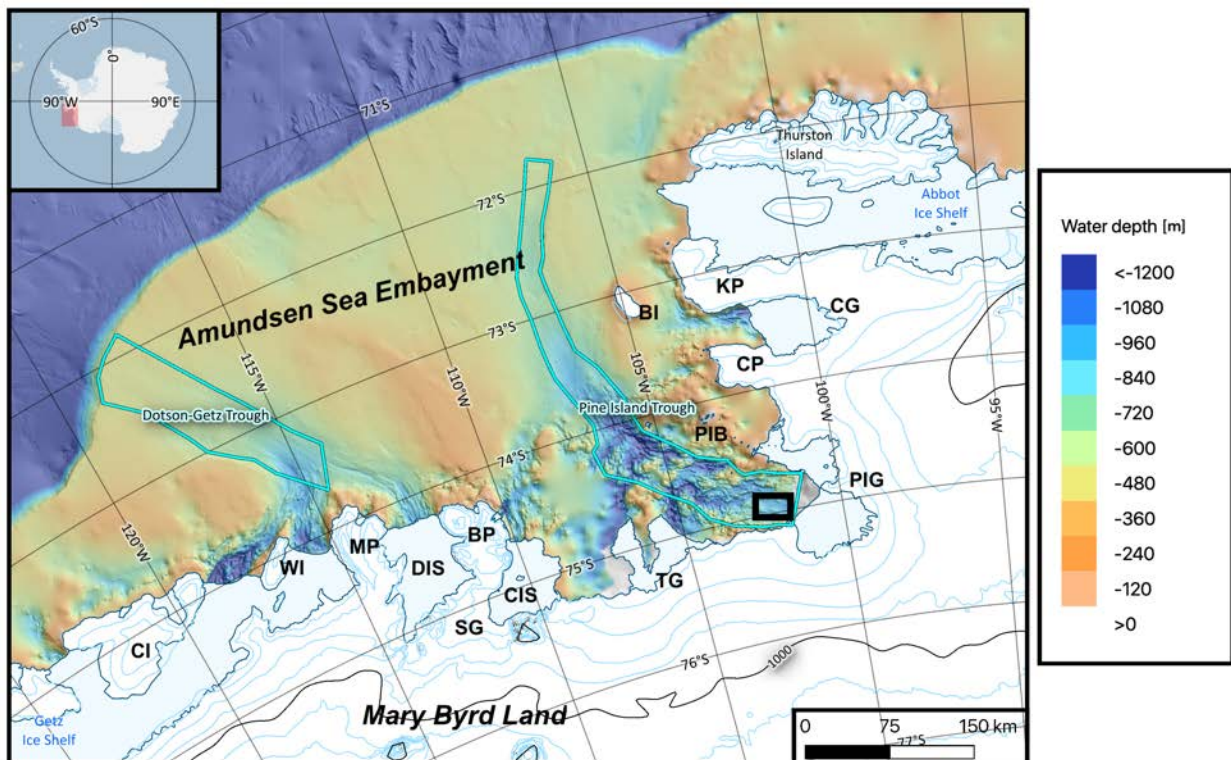
Fig. 2: Map showing key geographical information of the Amundsen Sea sector. Study area (back rectangle) in the Pine Island Bay, offshore Pine Island Glacier. CI=Carney Island, WI=Wright Island, MP=Martin Peninsula, DIS=Dotson Ice Shelf, BP=Bear Peninsula, SG=Smith Glacier, CIS=Crosson Ice Shelf, TG=Thwaites Glacier, PIG=Pine Island Glacier, PIB=Pine Island Bay, CP=Canisteo Peninsula, CG=Cosgrove Glacier, KP=King Peninsula, BI=Burke Island. Bathymetric map created with "Quantarctica 3" from the Norwegian Polar Institute (Matsuoka et al., 2018).

The seven seismic profiles have been recorded at the basin during RV Polarstern cruise PS104 and will be labelled as follows: AWI-20170001, AWI-20170002, AWI-20170003, AWI-20170004, AWI-20170005, AWI-20170006 and AWI-20170007. More detailed information about the profiles cf. Tab. 1. Additionally, three seismic profiles acquired during expedition ANTXXVI/3 in 2010 (labelled as AWI-20100123, AWI-20100124 and AWI-20100125) will be analysed in the present study as well.

The center of the isolated sedimentary basin is roughly at -74.11 N -102.75 E. The orientation of the profiles and their exact location are illustrated on a bathymetric map (Fig. 3).
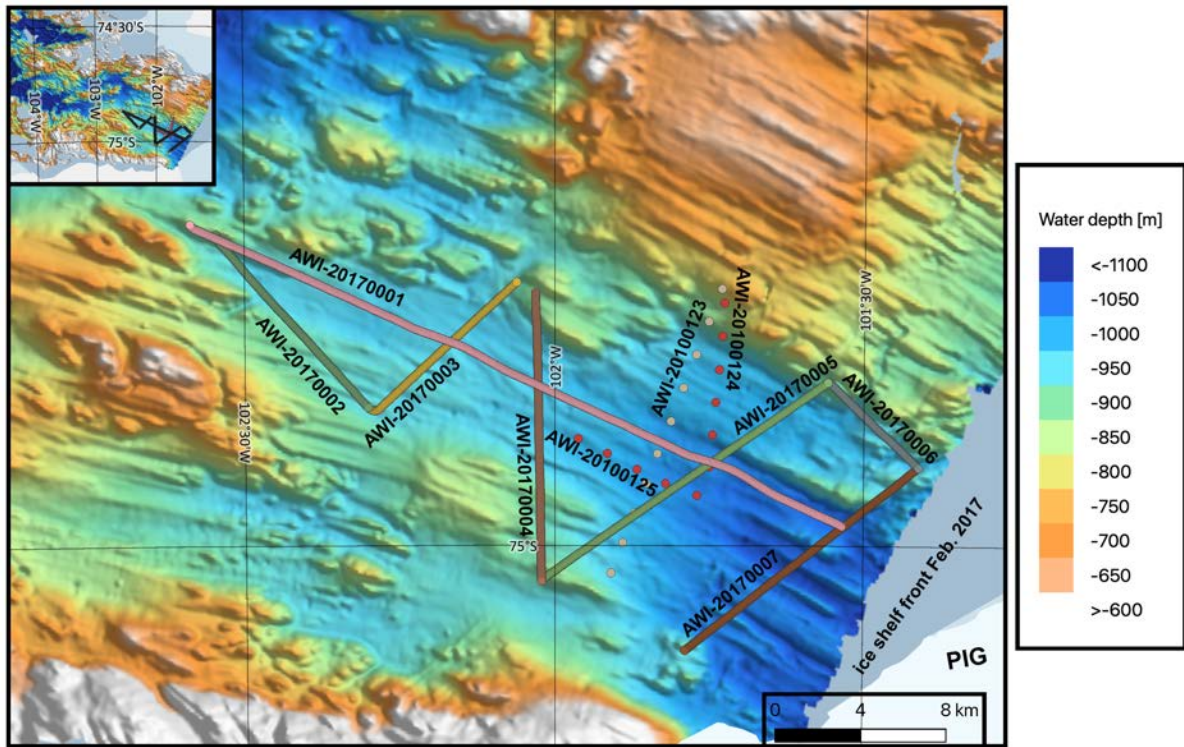
Fig. 3: Isolated sedimentary basin: Marked are seven seismic reflection profiles from PS104 in 2017 and three seismic reflection profiles from cruise ANTXXVI/3 in 2010. PIG=Pine Island Glacier. Bathymetric map created with a basemap from "Quantarctica 3" from the Norwegian Polar Institute Matsuoka et al. (2018) and a 100 m grid provided by the bathymetry department from AWI, Bremerhaven.

3. Background

3.1.   Tectonic evolution of Antarctica

The origin of today's continent Antarctica is the result of a series of very complex tectonic processes, which began with the breakup of the supercontinent Pangaea and the relative movements of the continental plates. All continents formed a single supercontinent before breaking up and drifting to their present locations.

The scientific research on the Antarctic continent already began at the beginning of the 20th century. In 1912, Roald Amundsen and his Norwegian companions won the race to the South Pole by one month against Robert Falcon Scott, Dr. Edward A. Wilson and Lieutenant H.R. Bowers. On their way back to their supply camp, the disappointed and defeated party from Scott took some time to collect rock samples from the Transantarctic Mountains. Unfortunately, a blizzard on the Ross Ice Shelf made it impossible for the researchers to return to the camp, causing them to perish in their tent from cold, exhaustion and lack of food supplies. Their remains were recovered in the following summer (Dalziel, 1992).

Several decades of scientific research and technological progress later, today there are numerous contributions to the paleogeographical reconstruction of the supercontinents Rodinia, Pangaea, Gondwana and Laurasia. Among these, Pangaea (Fig. 4) was identified as the last supercontinent to combine all landmasses in the geological history. The supercontinent was surrounded by the superocean Panthalassa (Veevers, 2012).
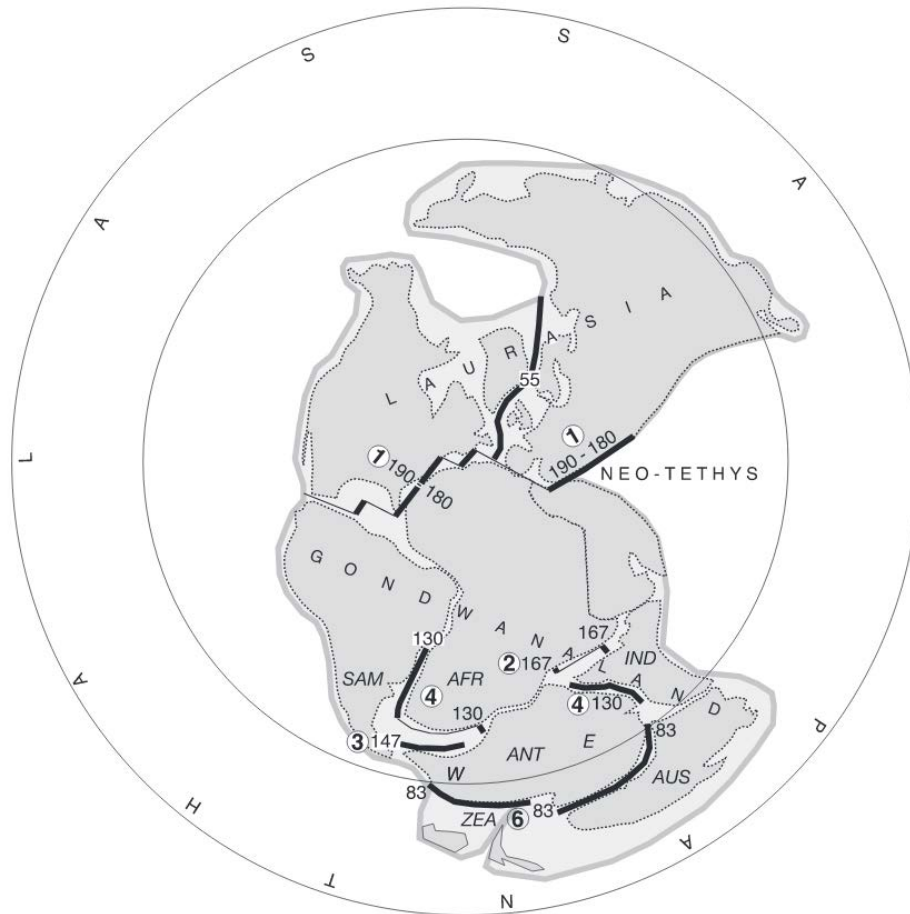
Fig. 4: Reconstruction of Middle/Late Triassic Pangaea and Panthalassa with the re-entrant of Neo-Tethys, showing the order of different breakup processes (stages: numbers in circles) with ages (Ma BP) of onsets of seafloor spreading (thick lines); from Veevers (2012).

Due to seafloor spreading at the Central Atlantic Province between Africa and America, Pangaea split into a northern area (Laurasia) and a southern area (Gondwana) at 190-180 Ma BP. Through six subsequent stages, beginning from the Lower Jurassic era until today, East Antarctica (E ANT) and West Antarctica (W ANT) separated from their five adjacent pieces – South America (SAM), Africa (AFR), Sri Lanka/India (SL/IND), Australia (AUS), Zealandia (ZEA) (Veevers, 2012).

The Antarctic continent is divided into the tectonically active West Antarctica and the stable East Antarctica. While West Antarctica consists of several microplates, East Antarctica is an Archean craton. There are four major entities in West Antarctica (Fig. 4), which accreted onto the East Antarctic craton as the Phoenix Plate subducted under the Antarctic plate: the Ellsworth-Whitmore Mountains crustal block (EWM), the Thurston Island block (TI), the Marie Byrd Land block (MBL) and the Antarctic Peninsula (AP). Antarctica is divided in two parts by the Transantarctic Mountains. The microplates essentially reached their present

location (around 83 Ma BP) when New Zealand drifted away from Marie Byrd Land (Dalziel, 1992; Dalziel and Lawver, 2001; Storey et al., 1988; Veevers, 2012).
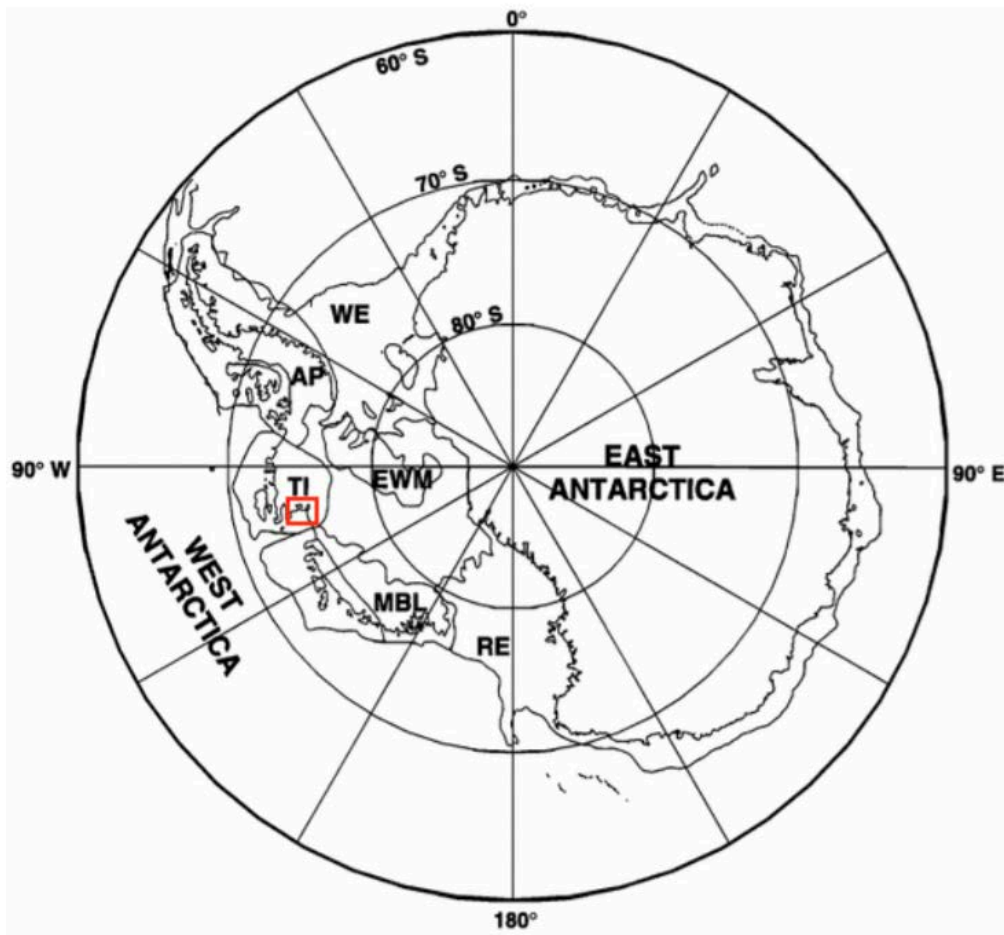
Fig. 5: Locations of the microplates in West Antarctica. The study area is marked by a red rectangle. Ellsworth-Whitmore Mountains (EWM), Thurston Island (TI), Marie Byrd Land (MBL), Antarctic Peninsula (AP), Weddell Embayment (WE), Ross Embayment (RE). Modified from Dalziel and Lawver (2001).

A majorly notable geological feature of West Antarctica is the West Antarctic Rift System (WARS), which developed with the initial breakup of Gondwana due to lithospheric thinning. At the early Oligocene, around 29 to 33 Ma BP, Antarctica was isolated (Lawver and Gahagan, 2003; Siddoway, 2007).

3.2.   The West Antarctic Ice Sheet

The Antarctic Ice Sheet, divided into the East Antarctic Ice Sheet (EAIS) and the West Antarctic Ice Sheet (WAIS), includes 90% of the global ice volume and is therefore the largest potential source for future sea level rise: a complete melting would result in a sea level rise of about 60 m (Lythe et al., 2001; Vaughan et al., 2003). The larger and more homogeneous EAIS is mainly located above the sea level and contains, alone, ice for approximately 53.3 m of potential sea level rise (Siegert, 2008). The more unstable and sensitive WAIS has a lower elevation than the EAIS. Also, due to the fact that most of its base is grounded below sea level, it is more affected by changes in atmospheric and oceanographic conditions. In case of a complete meltdown, the EAIS would lead to a global sea level rise of 3.3 m or even up to 5 m (Hillenbrand et al., 2013). After a study by Joughin and Alley (2011), an annual sea-level rise of 0.28 to 0.56 mm yr^{-1} would occur only from mass loss of the WAIS. While Pine Island Glacier and Thwaites Glacier drain ~40% (by volume) of the WAIS together, PIG has the largest discharge (66 Gt yr^{-1}) of all WAIS ice streams (Payne et al., 2004).

Fig. 6 illustrates a model of the Antarctic ice sheet with all its various components. Schoof (2007) describes an ice sheet as follows: "Continental ice sheets, such as those covering Greenland and Antarctica, generally behave as thin viscous films spreading under their own weight, subject to mass gain and loss at their surface owing to snowfall and melting".
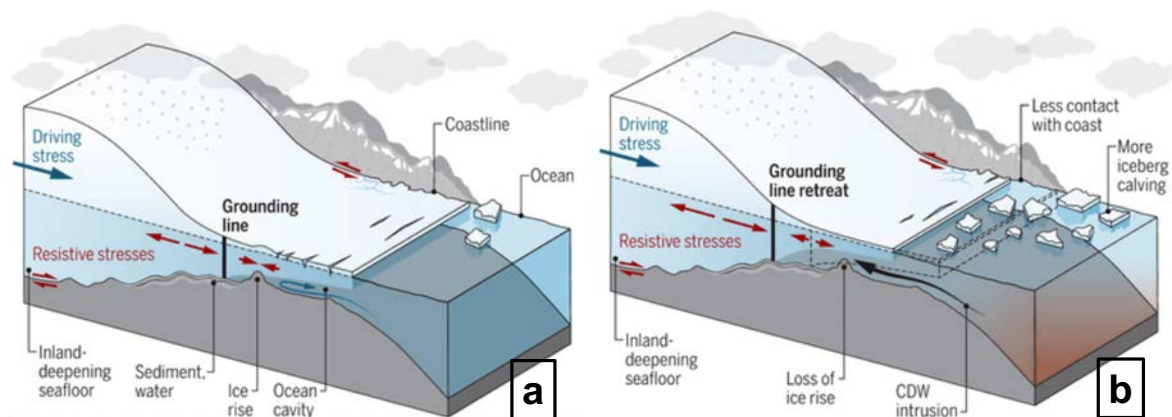
Fig. 6: Conceptual model of a West Antarctic ice sheet (a) and its retreating grounding line with warm water intrusion flowing into ice shelf cavities; the model illustrates a situation comparable with that of the ice shelf from Pine Island Glacier. Modified after Hulbe (2017).

It follows that a marine ice sheet is a highly active and dynamic system. Not only it has a below sea level ice mass grounded on bedrock (Fig. 7), but also a floating extension, called ice shelf.

The fact that a marine ice sheet needs to couple with the floating ice shelve at the grounding line (Schoof, 2007) marks the difference with respect to a land-based ice sheet.
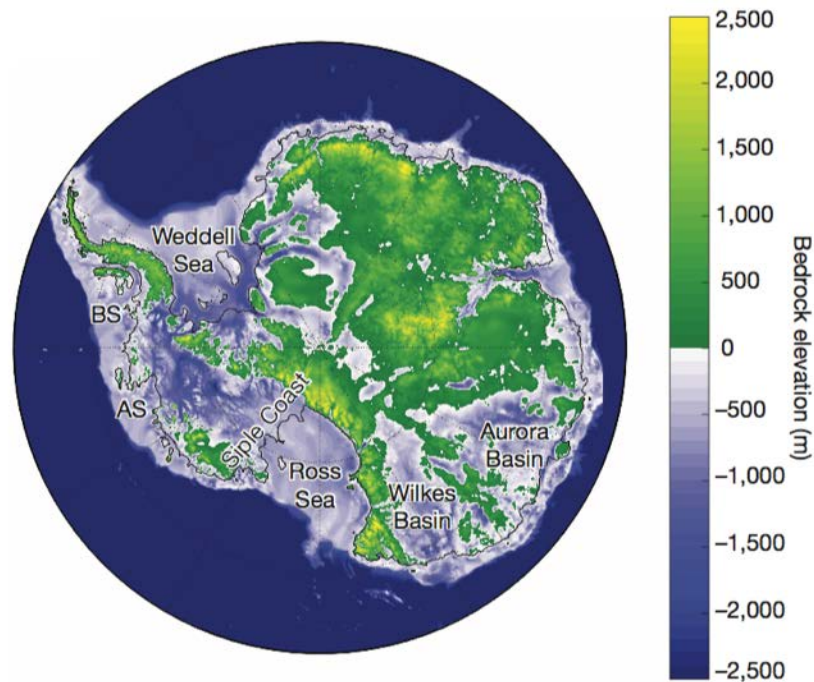
Fig. 7: Bedrock elevations of Antarctica: most part of the WAIS sits on bedrock hundreds to thousands meters below sea level. Bellingshausen Sea (BS); Amundsen Sea (AS). From DeConto and Pollard (2016).

The grounding line of an ice sheet is the transition boundary, where the ice detaches from the bed becomes a floating ice shelf. The grounding line may also be called grounding-zone, since its sensitivity to changes in oceanic tides causes it to oscillate back and forth. The delineation of an ice sheet grounding line is critical to ice sheet mass calculations, numerical modelling of ice sheet dynamics, ice-ocean interactions, oceanic tides and subglacial environments (Rignot et al., 2011).

Already in 1981 T.J. Hughes called the glaciers draining the ASE sector "the weak underbelly of the West Antarctic ice sheet". This is especially true if we consider the fast ice thinning occurring in the sector (Fig. 8), which can be monitored by using repeat satellite altimetry observations with the ICESat laser altimetry system (Pritchard et al., 2009).
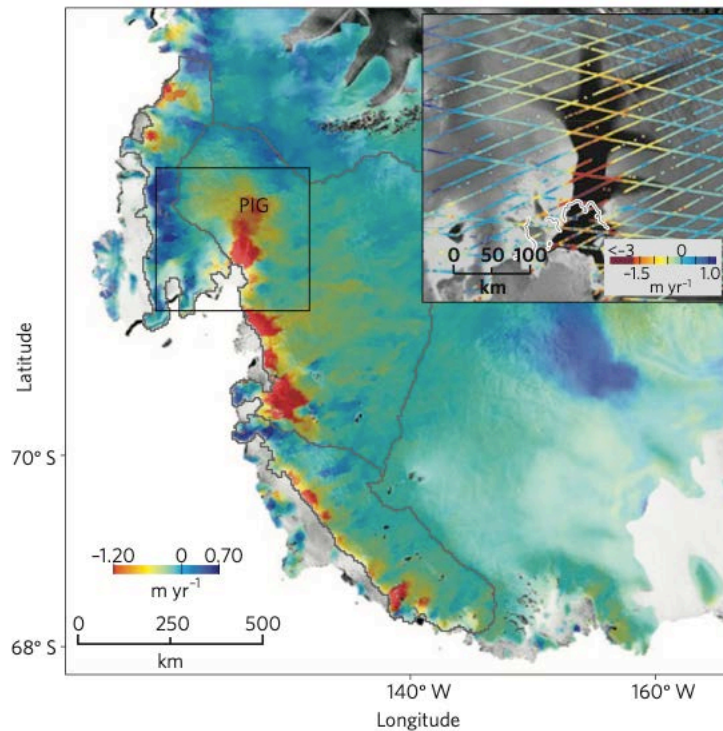
Fig. 8: Rate of elevation change at Amundsen Sea sector of the WAIS monitored by satellite altimetry. Original from Pritchard et al. (2009), modified by Joughin and Alley (2011).

3.3.   The West Antarctic Ice Sheet since the LGM

As Schoof (2007) claims, steady grounding lines cannot be stable on reverse bed slopes. This is what causes the ice retreat of the WAIS to seem unstoppable. Studying past ice sheet behaviour is crucial to gaining knowledge about mechanisms that regulate the stability of the WAIS. Any retreat in ice thickness at the grounding line leads to a higher ice thickness at the grounding-zone. This results in an accellerated ice flow at the grounding line (and, as a consequence, in more ice discharge). Moreover, both a thinning of inland ice and a further grounding line retreat are set in motion (Lowe and Anderson, 2002; Nitsche et al., 2007). This process leads to the fear of Hulbe (2017), which is, at the same time, the title question of her article: Is ice sheet collapse in West Antarctica unstoppable?

The retreat of the WAIS in the sector of the Amundsen Sea is not a recent geological phenomenon. In fact, the ice sheet has been subject to an ongoing decline since shortly after the Last Glacial Maximum (LGM; Lowe and Anderson, 2002).

Larter et al. (2014) have taken into account data from airborne geophysical as well as from marine surveys and radiocarbon and cosmogenic surface exposure dates, to then formulate a number of conclusions concerning the behaviour of the past ice sheet, among which are: 1) the grounding line advanced to or at least was close to the continental shelf edge of the Amundsen-Bellingshausen sector during LGM (23-19 ka BP; 9); 2) at this point, at least three major ice streams flowed across the shelf into the Amundsen Sea. By early Holocene time, ice retreated close to its modern configuration. The formation of grounding-zone wedges in the so-called "bottle neck" area of the Pine Island Trough indicate that the grounding line retreat has been interrupted for several thousand years. The highest ice retreat rates on the inner shelf parts of the Pine Island Trough appear to verify the marine ice sheet instability hypothesis from Schoof (2007).
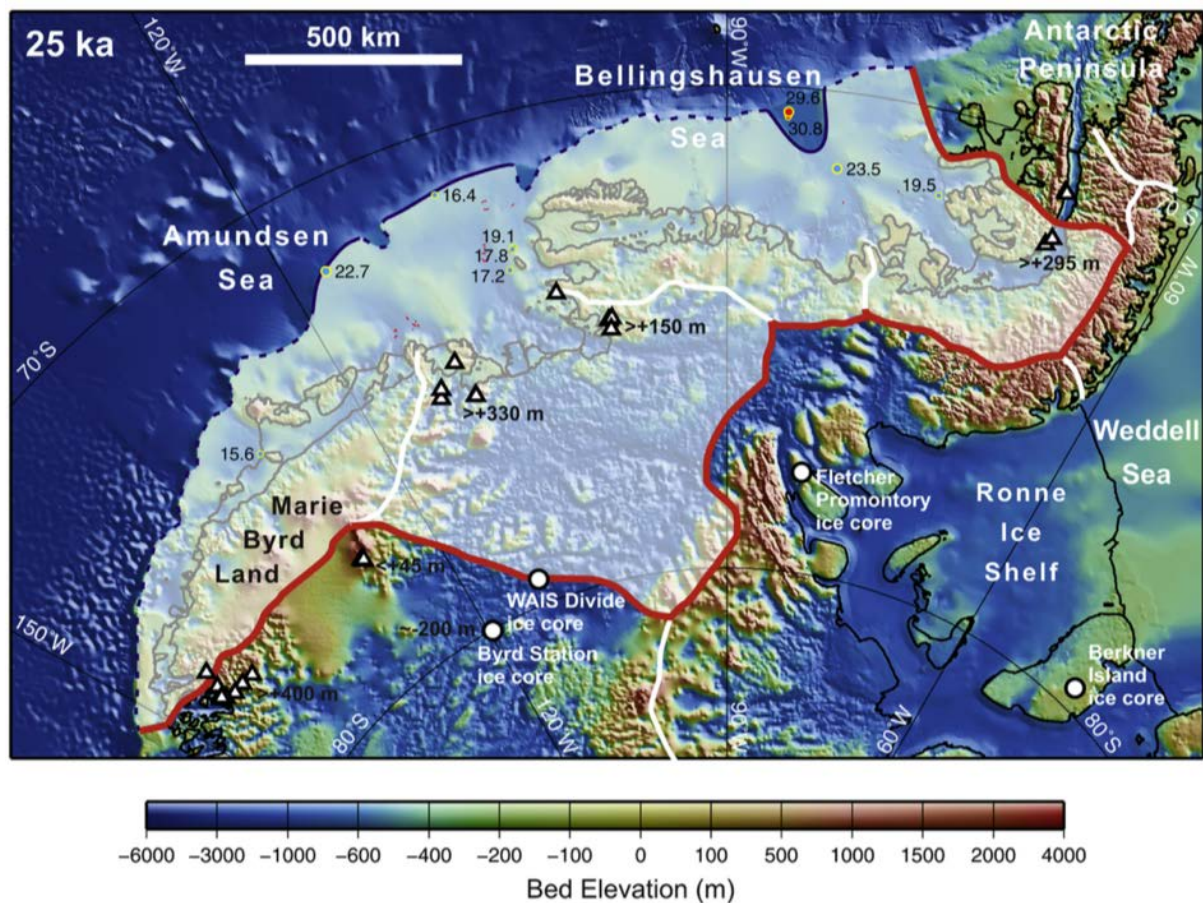
Fig. 9: Reconstruction of the WAIS for 25 ka BP (only for the Amundsen-Bellingshausen sector) overlaid on Bedmap2 ice sheet bed and bathymetry. Extent of ice sheet (semi-transparent white fill). Ice margin (dark blue line, dashed where less certain). Sector boundary follows the main ice drainage divides (thick red line). Other major ice divides (thick white lines). From Larter et al. (2014).

3.4.   Oceanographic Setting in West Antarctica

A brief description of the oceanographic setting can offer an introductory explanation for West Antarctica Ice Sheet's high sensitivity to climate and temperature changes.

Antarctica's climate is undergoing a changing or varying process with a direct influence on the oceanographic setting of the WAIS. A crucial role, not only for the climate, but also for the ice system of WAIS, is played by the Antarctic Circumpolar Current (ACC).

In response to strong westerlies, the tilt of the isopycnals of the ACC is supposed to thermally isolate Antarctica (Fig. 10) by blocking warm subtropical surface waters. The same isopycnal tilt sets the northern limit for seasonal sea ice formation. Also included in the Acc is the reatively warm Upper Circumpolar Deep Water (UCDW). The lack of physical boundaries along its flow path prevents the development of zonal pressure gradients driving meridional flow. The ACC circulates eastward around the globe (Martinson, 2011).
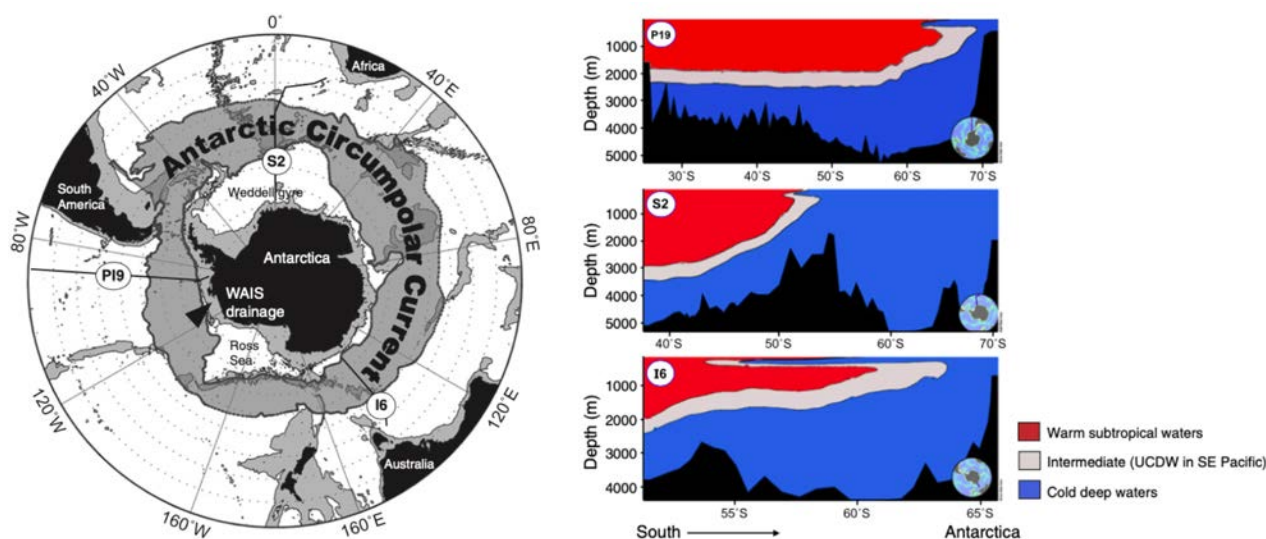
Fig. 10: Oceanographic setting. Left: Eastward flowing Antarctic Circumpolar Current (ACC; shaded gray). The black arrow roughly indicates Pine Island Bay. Right: temperature sections of selected profiles (marked in the left picture) show that ACC prevent warm subtropical waters (red) from reaching Antarctic continental margin; UCDW slips along the tilted isopycnals. Modified after Martinson (2011).

However, the ACC circulates very close to the Amundsen Sea Embayment. This causes depressions in the shelf break to allow the warm water masses of the UCDW to flow onto the continental shelf. The intruding water masses are considered to be a few degrees above the in situ freezing point. If the these water masses then reach the base of the ice shelves (which is also favoured in case of the Amundsen Sea Embayment due to the narrow shelf sloping towards the continent) or the underside of the floating ice shelves, this can trigger an increased ocean-driven melting which, again, can contribute to high rates of mass loss (Assmann et al., 2013; Kimura et al., 2017; Martinson, 2011).

3.5. Sedimentation studies along the Pacific continental margin of West Antarctica

Since the initial onset of Antarctic glaciation, sediment transport and deposition processes along the south Pacific margin of West Antarctica have been strongly affected by past ice sheet advance-retreat cycles. Thus, the study of sedimentary architecture and characteristics provides constraints for paleo-ice dynamic models.

A continuous seismic transect, identified in a study by Lindeque et al. (2016) as stratigraphically linking seismic key horizons from Amundsen Sea to Ross Sea, lead to the establishment of a Cretaceous to Eocene pre-glacial sequence (79-34 Ma), an Eocene to mid-Miocene transitional sequence (34-15.5 Ma) and a mid-Miocene to Quaternary full glacial climate sequence (15.5-0 Ma). The study interprets the top transitional sequence boundary as the onset of the full glacial regime and intensified ice sheet advances onto the distal shelves. In the Amundsen Sea basin, sediments of up to 3.9 km in thickness have accumulated. Further on, the data suggests Paleocene-Eocene bottom-current activity and a late Eocene shelf grounding of the WAIS.

By modelling sediment isopach grids along the pacific margin on the basis of seismic reflection data and correlations with ocean drilling sites, Scheuer et al. (2006) suggest that the onset of sediment accumulation on the continental rise, supplied by frequent advances of the grounding ice on the shelf, occurred at about 10 Ma. The thickest glacially dominated sediment depositions were found in front of major drainage outlets of West Antarctica and [in front of?] a depression on the inner and middle shelves off PIB.

A major sedimentary characteristic along the continental rise of the Amundsen Sea are levee-drift deposits that were shaped by recirculating ocean bottom currents out of glaciogenic debris. Due to a more dynamic ice sheet since 4 Ma, high amounts of material were transported via western Pine Island Trough (amongst other troughs), leading to continued drift deposits (Gohl, 2015; Uenzelmann-Neben and Gohl, 2014).

## 3.6.	Glacially controlled processes on the Amundsen Sea Embayment

At the LGM, the Amundsen Sea Embayment was completely covered with ice. Since then, the ice retreated roughly 500 km from the shelf edge towards south and left behind a marked seabed to be studied (Larter et al., 2014).

The ice sheet left records of its previously glaciated seafloor behind. Bathymetry of Pine Island Bay revealed the most outstanding features on the continental shelf. The Pine Island Trough merges from deep and rugged inner shelf troughs originating from Pine Island Glacier, Thwaites Glacier and Smith Glacier (Nitsche et al., 2007).

Pine Island Trough has remained in the same position since early glacial advances. The eastern and western extensions on the outer shelf have remained in the same position as well. The reason for that is, most likely, that Pine Island Trough has been constrained by the eastern West Antarctic Rift System basin flank and shallow basement structures along tectonic lineaments (Gohl et al., 2013).

Troughs on the inner shelf are incised with systems of subglacial meltwater channels (Lowe and Anderson, 2002). Nitsche et al. (2013) went on to suppose that meltwater volumes currently generated underneath Pine Island and Thwaites Glaciers could not have produced this complex setting of channels and basins if discharged continuously. Most likely, this large network generated over several glacial cycles by episodic flow events caused by storage and release of meltwater through subglacial lakes. However, knowledge about the influence of subglacial lakes on ice sheet dynamics is sparse. In a distinct sediment facies of a basin in the Pine Island Bay, Kuhn et al. (2017) found for the first time sedimentological and geochemical evidence for a subglacial lake and its transition to a glaciomarine environment during the last deglaciation.

Through high resolution bathymetric data, linear morphological features of the inner Pine Island Bay are visible and available to be mapped. Drumlin-shaped ridges, glacial lineations, channels and the orientation of small basins indicate pathways of paleo-ice streams, therefore allowing to identify the direction of ice retreat and paleo-ice flow (Fig.11; Nitsche et al., 2013).
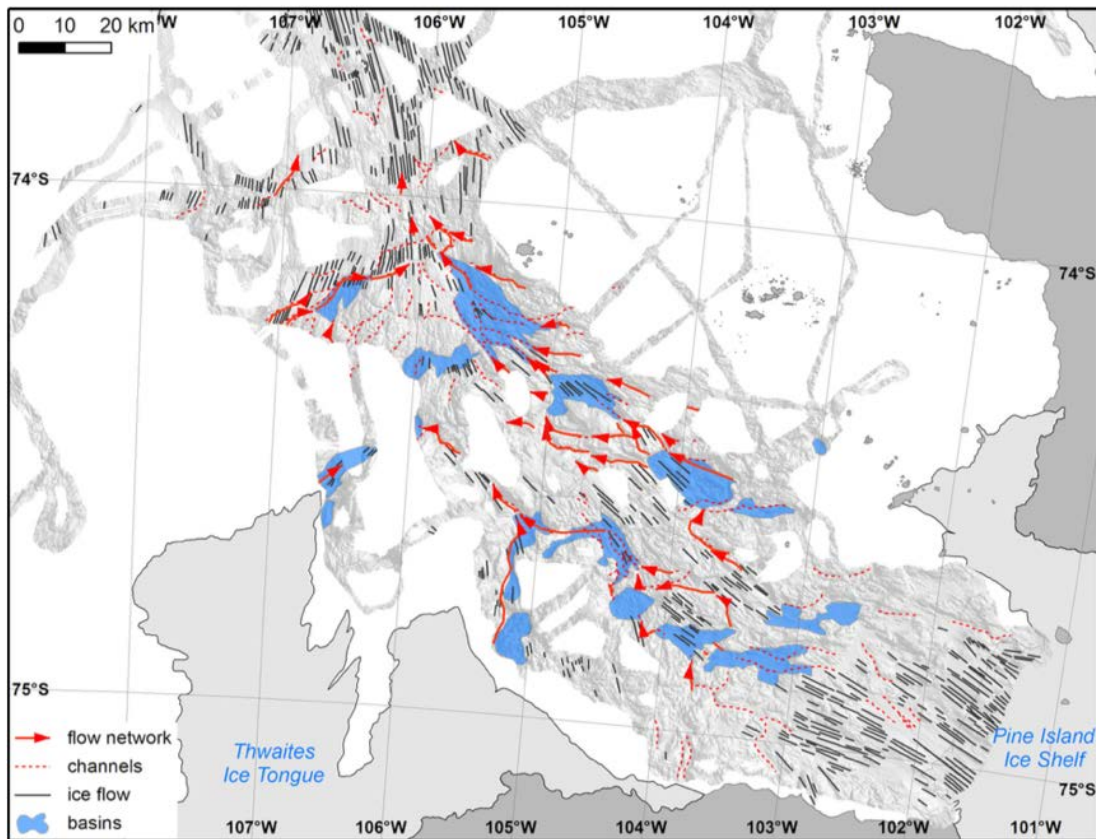
Fig. 11: Lineations indicating ice flow (black lines), minor (dotted red lines) and major meltwater channels (red lines with arrows). The extent of swath bathymetry data is shown as grey shaded area. Light and dark grey shaded areas represent ice shelves and land. From Nitsche et al. (2013).

The diversity of this ice retreat is highlighted in a study on multichannel seismic reflection data of the Pine Island Trough from Uenzelmann-Neben et al. (2007). The study reveals that in the Late Quarternary the ice retreat in the Pine Island Bay was not uniform, as eastern PIB was subject to a different glacial development than western PIB. While in the western PIB topography is strongly incised by channels and cavities that discharged into a glacial trough, topography appears to be much smoother in the eastern part of PIB. Sedimentary layers of ≤400 ms TWT in thickness can be observed in contrast to western PIB, where only sediment depositions of only 75 ms TWT can be observed in wider channels. This is supposed to be related to a much larger drainage area of from PIG and TG. Their much greater thickness (than, for example, Cossgrove Ice Shelf in the eastern PIB) led to larger basal melting and, therefore, to increased meltwater production. High amounts of meltwater are in close relation to more erosion and the creation of troughs.

Further reasons for the unstable retreat of the ice are connected to the complex topography of the continental shelf. While the ice sheet seems to be lubricated for an increased ice stream flow velocity on soft sediments, ice flow velocity decreases on outcropping bedrock. Topographic

highs can slow down the ice retreat. This has been shown by Klages et al. (2013) upon presentation of the first detailed survey of an inter-ice stream ridge in the Pine Island Bay. Large-scale ribbed moraines, hill-hole pairs, terminal moraines and crevasse-squeeze ridge, completely unusual for adjacent ice-stream troughs, were among the identified features. The acknowledgment of these features made it possible to reconstruct slower ice flow on the inter-ice stream ridge.

4. Data & Methods

The present study bases on different types of data acquired on expedition PS104 with RV Polarstern to the Amundsen Sea, West Antarctica, which took place between 6 February and 19 March 2017. The harbour of Puntas Arenas, Chile, was both port of departure and port of destination. Among the main purposes of the expedition were, on the one hand, the drilling of a series of sediment cores (with the MARUM-MeBo70 drill device) of different stratigraphic sequences of the Amundsen Sea Embayment, which should provide further insights in the development of the WAIS, and, on the other hand, the carrying out of seismic surveys to be linked to the sediment cores. Moreover, bathymetric and Parasound data has been acquired throughout the expedition to deliver additional scientific data.

4.1.   Seismic Data

Expedition PS104 focused, among other things, on gaining information about glacially controlled sedimentary processes of small sedimentary basins offshore from Pine Island Glacier. Knowledge about the characteristics and orientation of the sediment layers in the basin and the course of the underlying crystalline basement was acquired through a standard 2D multi-channel seismic reflection method. The method involves a seismic signal source producing an acoustic signal, which is sent out towards the seafloor and reflected by geological interfaces. The reflected acoustic signal is detected and recorded by a receiver, a seismic cable called "streamer". The streamer transmits the information in real time to the ship – a sketch of the setup from Gohl (2017) is shown in Figure 1. The streamer also records the time period between the generation of the signal and the detection of the returned signal. This time period is called "two-way traveltime" (TWT) and is usually indicated in milliseconds (ms).
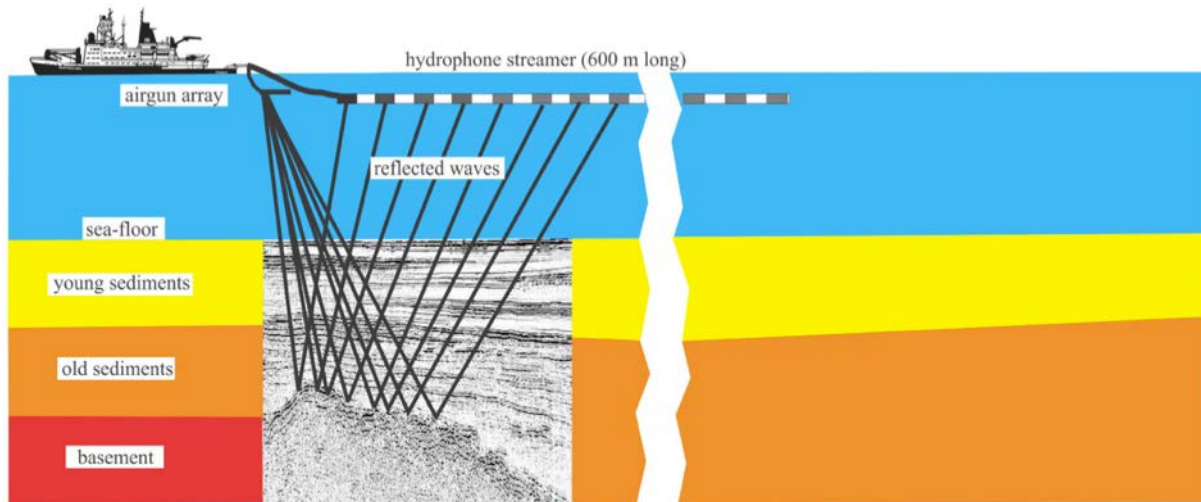
Fig. 12: Sketch of the setup of a 2D reflection seismic survey. From Gohl (2017).

Configuration of the seismic source

During the expedition, a cluster of two *GI Guns* was towed 20 m behind RV Polarstern at a constant depth of 2 m; each *GI Gun* consists of two independent airguns. The so called "Generator" airgun generates a primary pulse and the "Injector" airgun controls the oscillation of the produced bubble from the first airgun. In order to produce an almost bubble-free signal, the "Generator" had been set up with a volume of 0.72 l (45 in^3), while the "Injector" had been set up with a volume of 1.68 l (105 in^3) and triggered with a delay of 30 ms (33 ms). The guns were triggered every 10 s (~25 m shot interval) at a nominal pressure of 190 bar. The respective record length was 4 s and the sampling rate was 1 ms (Gohl, 2017).

Recording system

For the acquisition of the abovementioned seismic profiles, a 96-channel, 600 m long analogue streamer from *Prakla-Seismos* was used and floated behind the ship at around 2 meters of water depth. This streamer had been coupled to a set of four seismic recorders (*Geode* from Geometrics; 24-channel each) on board. The recorders converted the analogue signal into a digital signal (A/D conversion) and passed the digitized data on to the host computer. The data was then stored into SED-D files via the *Seismodule Controller Software* from Geometrics (Gohl, 2017).

Since the precision of the timing system between seismic sources and recording systems is crucial, an electric trigger-clock system was used to synchronize the firing signal of the source with the time-control of the seismic data system. A GPS clock from Meinberg, mounted on the upper deck of RV Polarstern, provided UTC date and time (Gohl, 2017).

Seismic Profiles

Main goal of this work is the processing and subsequent analysis of seven seismic profiles recorded during cruise PS104 (Tab. 1).

Tab. 1: List of the seven seismic profiles recorded during cruise PS104. Modified after Gohl (2017).

PROFILE NO. AWI-...	Start / End	DATE [UTC]	TIME (UTC)	LATITUDE	LONGITUDE	PROFILE LENGTH [nm]
20170001	start	16.02.17	02:31:00	-74.99214	-101.53341	17.5
	end	16.02.17	06:07:00	-74.86551	-102.58550	
20170002	start	16.02.17	06:23:00	-74.86841	-102.54579	5.7
	end	16.02.17	07:33:00	-74.94156	-102.30299	
20170003	start	16.02.17	07:33:00	-74.94156	-102.30299	4.9
	end	16.02.17	08:34:00	-74.88998	-102.06321	
20170004	start	16.02.17	08:43:00	-74.89320	-102.03080	7
	end	16.02.17	10:09:00	-75.01497	-102.02154	
20170005	start	16.02.17	10:30:00	-75.01442	-102.02183	8.8
	end	16.02.17	12:18:00	-74.93179	-101.56008	
20170006	start	16.02.17	12:44:00	-74.93179	-101.55372	3
	end	16.02.17	13:21:00	-74.96753	-101.40987	
20170007	start	16.02.17	13:44:00	-74.95726	-101.41303	6.8
	end	16.02.17	15:07:00	-75.04366	-101.78682	

Three more seismic profiles, which have already been entirely processed, also contribute to the results of the present study: the profiles recorded during expedition ANT-XXVI/3 to the Amundsen Sea in 2010 (AWI-20100123, AWI-20100124 and AWI-20100125). Though these profiles refer to the same isolated sedimentary basin, the data quality appears to be significantly lower if compared to the recorded profiles from 2017.

Data Quality

However, the quality of the seismic data acquired during cruise PS104 is not unflawed either. The streamer, which should normally float at a constant depth below the sea surface, was hanging down in the most distal areas, which led to an increased ghost presence in the data. Ghosts are defined as multiples, which develop through reverberating seismic energy from sea surface between seismic sources and receivers (Yilmaz, 1987). Another reason for reduced seismic data quality are the geological conditions of the survey area, which will be described in more detail in the results.

4.2.   Parasound Data

While seismic data is used for imaging the deeper parts in the sediment body, Parasound data gives a better resolution of the uppermost tens of meters of the sediment layers below the seafloor and the seafloor topography itself. Use of the parametric echosounder *Teledyne Reson Parasound System DS3 (P70)* (Gohl, 2017) ensured the acquisition of high-resolution sediment echosounding data during cruise PS104.

The system utilises the parametric effect, which generates additional frequencies through non-linear acoustic interaction of finite amplitude waves. If two sound waves of a certain frequency are simultaneously emitted, an additional secondary signal of the difference frequency is also generated. During the expedition, the primary low frequency was set to 18 kHz and the energy was transported within a beam of an angle of only 4.5°. The primary high frequency can be varied between 18.5 and 24 kHz, which would lead to difference frequencies between 0.5 to 6 kHz. However, the primary high frequency was set to 22 kHz, leading to a secondary low frequency of 4 kHz. The secondary signal component travels within the emission cone of the 18 kHz beam. Therefore, the footprint of the system is much smaller than it would have been with a conventional system emitting the 4 kHz signal from the start. This leads to a significantly improved lateral and vertical resolution of the data (Gohl, 2017).

In order to permanently acquire bathymetric and Parasound data, the echosounding system has operated throughout nearly the whole cruise. Onboard, the system was controlled with the software *Hydromap Control* and the data was stored in ASD and PS3 formats for both SLF and PHF signal through *Parastore*. Moreover, the data was converted to SGY format with the ps32sgy software (created by Hanno Keil, University of Bremen). The *Kingdom®* software from IHS was used to ensure visualization and quality control. Navigation data was filed in UKOOA format by using the *Postprocessor* Matlab script written by Florian Riefstahl from the AWI, Bremerhaven (Gohl, 2017).

4.3.   Bathymetry Data

High-resolution bathymetric mapping is crucial to gain morphological knowledge from the shelves of the Amundsen Sea Embayment. During cruise PS104, the hull-mounted *Teledyne*

Reson Hydrosweep DS3 multibeam echosounding system was used for the acquisition of swath bathymetric data (Gohl, 2017).

The multibeam echosounding system has acquired data throughout nearly the whole cruise. While the system was managed with *Hydromap control*, the software package *Hypack 2016a* made the immediate visualisation of the ongoing data acquisition possible. The formats ASD and HSX were used for data storage with *Parastore* and *Hypack 2016a*. The processing and cleaning of the data shown in the upcoming section has been carried out with the *CARIS Hips and Sips* software (Gohl, 2017). For usage in this work, the Alfred-Wegener-Institut provided a 100 m grid of the Amundsen Sea in the georeferenced TIF format by the bathymetry section. Unfortunately, the high-resolution 25 m grid from cruise PS104 had not been completely processed yet, so that the 100 m grid was the grid with highest available resolution.

4.4.   Software tools

In accordance with the different kinds of data used in this work, several software tools were employed during the working process. The complete processing of the seismic reflection data was carried out with *Echos™* from the software package *Paradigm® 17*, a product from *Emerson E&P Software*. The seismic interpretation, including detection and definition of seismic units and horizons, has being completed with *Integrated Canvas*, which is also included in *Paradigm® 17*. All figures in this work relating to the seismic reflection data were produced with this software package. The illustration of the defined horizons and the generation of grids from the sedimentary basin have been carried out with *Basemap* from *Paradigm® 17*.

The open source geographic information system software *QGIS 3.10* was used for geographic maps and the visualization of the bathymetric data.

The *Kingdom®* software from *IHS™ Markit Ltd.* was used for the visualization and creation of figures referring to the Parasound data.

The editing of the figures has been carried out using the open source software *GIMP 2.10* and the beta-version of *Inkscape 1.0*.

5. Seismic data processing

The aim of seismic data processing is to improve the data quality as to obtain a possibly clear subsurface image below the seafloor. The present chapter will briefly explain all processing steps in the seismic processing software *Echos* in the order of application, as well as the reason of application supported by theoretical background. The seismic processing is organised through a so-called jobflow or flowchart, which shows the order of single modules applied on the data.

The jobflow can, of course, be very different between one seismic profile and another, dependent on the geological background of the survey or on the desired results of the processing. For this reason, a standard jobflow that works for all seismic data does not exist. Beyond that, a single jobflow is not enough for one seismic profile, which is why the processing is divided in several steps. For instance, it can be very useful to split the jobflow before and after stacking, since the stacking of seismic data can be a very time-consuming and demanding process for the computer. It is, therefore, advisable to first perform all processing steps prior to stacking in one jobflow; to then create a specific jobflow for the stacking; and to eventually proceed to one more jobflow containing processing modules, which need to be applied after the stacking.

In order to check the processing progress and its success, it can be helpful to compare interim results with a one-channel profile.

Preprocessing

Of course, before the actual processing starts, the raw seismic data needs to be prepared. This preprocessing of the data has already been completed during the expedition, on board of RV Polarstern. The main steps of the preprocessing are the definition of the survey geometry and sorting the data.

For the definition of the survey geometry it is crucial to use the marine navigation data of the research vessel. This allows to assign the coordinates of shot points and the receiver locations correctly, and to store them on trace headers. If this is done inaccurately, the whole processing outcome is at risk of being endangered. Afterwards, the sorting of the data and the binning of traces follow. Data from several shots and receivers are combined into a single gather and sorted by their common depth-points (CDP). Fig. 13 shows the principle of CDP sorted data. Here, the binning was set to 25 m, meaning that one CDP is 25 m away from the next CDP. This process can already increase data quality due to noise-reduction.
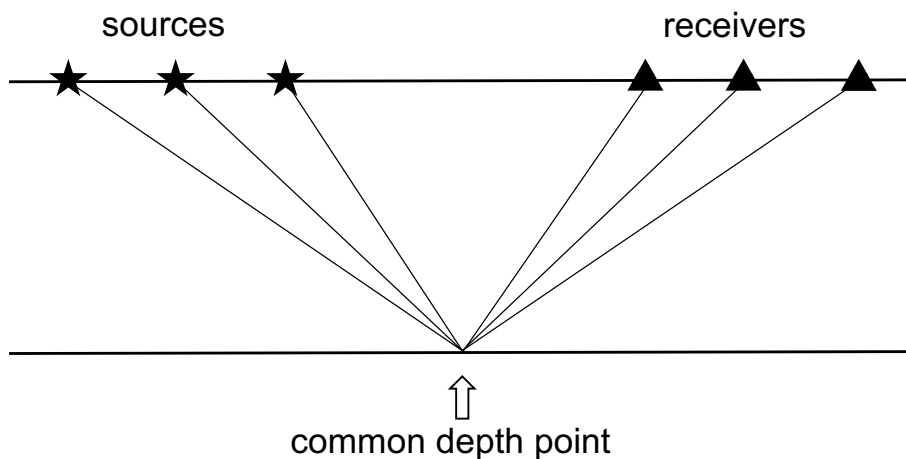
Fig. 13: Principle of CDP-sorted data.

Data input/output

The first input of the CDP-sorted data from the hard disk is carried out with the module *DSKRD*. The module *DSOUT*, which stores the processed or semi-processed seismic profile in the internal database of the software, is employed to save the data. Any further read in of the profile is then completed with the module *DSIN*.

Edit

One of the first steps of the processing is to eliminate defective traces. Using the module *EDIT*, dead traces can be eliminated just by selecting the channel numbers. In the case of the data presented here, the traces of channels number 18, 28, 57, 59, 60, 74, 75, 76, 77, 78, 79 have been removed due to malfunction during data acquisition.

Filter

The most common frequency filter used during seismic data processing is a bandpass filter. With the module *FILTER*, all different types of filter can be applied. Even though filtering is mentioned at the very beginning of this seismic processing, the filter was applied several times throughout the whole processing, since several of the steps, e.g. the stacking or migration, can produce new noise in the data. That is why it is recommended to incorporate the bandpass filter at various points during the jobflow.

The aim of this type of filter is to remove disturbing noise from the data, thus improving the signal-to-noise ratio. The occurrence of noise in the seismic data can have different origins. On the one hand, noise can be created during data acquisition due to natural reasons (such as wave action and wind); on the other hand, it can occur due to ship movement or even noise from the seismic sources (the airguns) themselves. Finally, as mentioned above, noise can also be generated through the seismic processing.

Four frequencies need to be determined for the application of the filter. In the seismic data, all frequencies smaller than the lowermost frequency (F1) and higher than the upper frequency (F4) are suppressed. All frequencies between the determined frequencies (F2 and F3) pass through the filter in their entirety and constitute the main frequency signal. Between F1 and F2 as well as between F3 and F4, the frequencies are attenuated (Paradigm® 17 Manual).

The average power spectrum can be of use for the determination of the main source signal. The software allows to specify a certain area in the data where the power spectrum shall be applied. The area was selected to be inside the sedimentary basin, as this is the most interesting part for the results. As Fig. 14 shows, the main source signal is roughly between 40 and 55 Hz.

Fig. 14: Average power spectrum from the internal sedimentary basin of profile AWI-20170001 with an applied bandpass filter (F1=10, F2=15, F3=200, F4=250), showing the main signal between 40 and 55 Hz.

A series of filter tests was carried out next, in order to find the filter best designed to fit the data. As an example of the filter tests, Fig. 14 shows how, with a closer gate of the passing frequencies (F2=50 and F3=80), the spike of the average power spectrum becomes more defined, since the smaller spikes at both sides nearly disappear. However, even if the spectrum is more defined, it is clear to see that the data has changed at the same time: especially the

reflections beneath the seafloor are more present and even seem to overlap underlying reflections, which is an unwanted side effect.
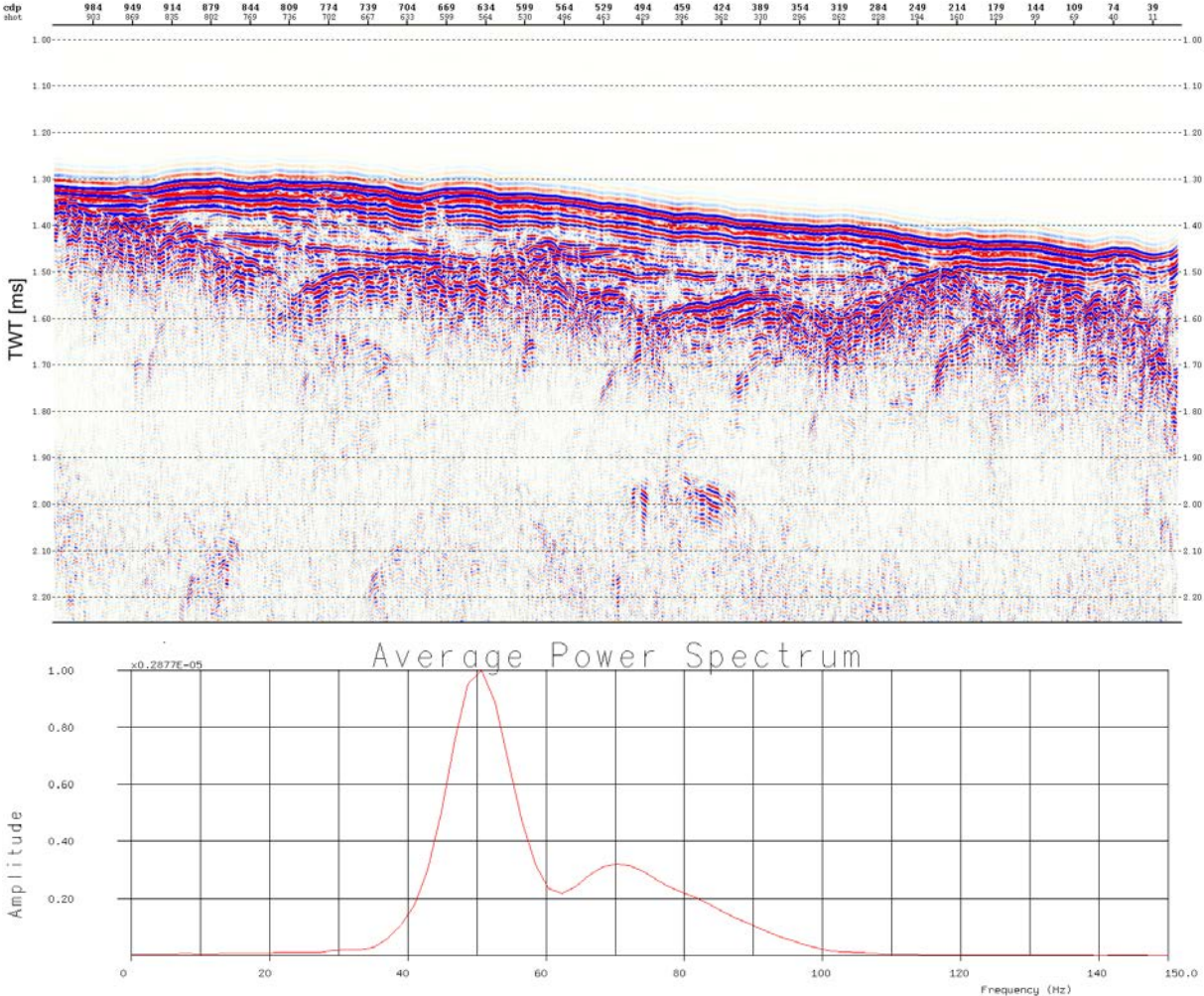
Fig. 15: Test of a bandpass filter (F1=35, F2=50, F3=80, F4=120) on profile AWI-20170001 with the average power spectrum from the internal basin.

Completion of the filter tests led to the decision to let a wide frequency band pass the gate. The final configuration of the bandpass filter is illustrated in Fig. 16. The following frequencies were eventually chosen: F1=10, F2=15, F3=200, F4=250. Thanks to these parameters, it was possible to achieve good results with significantly reduced noise. Since the quality of the original data was not optimal, the filter tests were an important step.
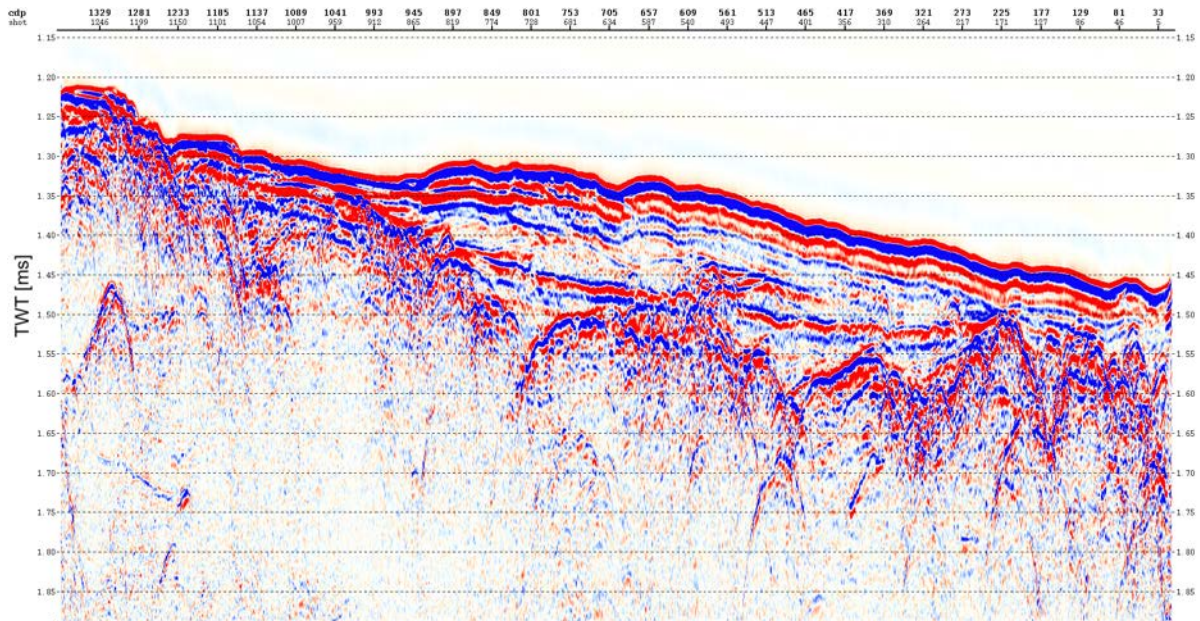
Fig. 16: Final configuration of the bandpass filter (F1=10, F2=15, F3=200, F3=250) after a row of filter test.

Velocity analysis and normal moveout correction

The most important and time-consuming step during seismic processing is the velocity analysis. Velocity analysis is vital for the correction of the normal moveout, as well as for the migration. The so-called two-way traveltime (TWT) is the time that the seismic wave needs to travel from the seismic source (S) to the acoustic reflector (D) and then back to the receiver G (Fig. ??). The vertical projection at surface of the depth point D is the midpoint M.
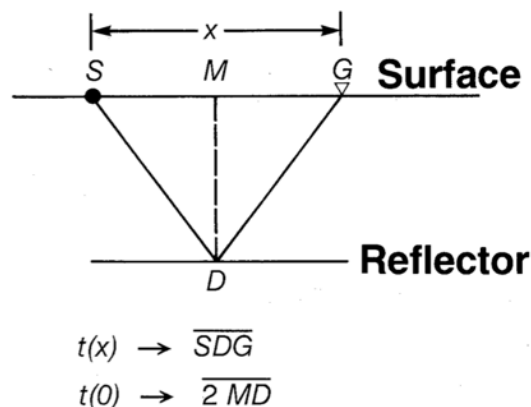
Fig. 17: NMO geometry; S=seismic source, G=receiver, D=acoustic reflector. From Yilmaz (1987).

The following equation describes the TWT as a function of offset (x), which is the distance from the source to the receiver (Yilmaz, 1987):

36

$$t^2(x) = t^2(0) + x^2/v^2,$$

where v is the velocity of the medium above the reflector and $t(0)$ is twice the traveltime of the path MD.

Since the offset to the next hydrophone at the streamer that records the same acoustic interface is bigger, the signal needs more time to arrive. This delay creates a hyperbola in the CDP gather and needs to be corrected. This so-called normal moveout is defined by the difference between the two-way traveltime at a given offset $t(x)$ and the two-way zero-offset time $t(0)$. Mathematically, the normal moveout is expressed by the equation (after (Yilmaz, 1987):

$$\Delta t_{NMO} = t(x) - t(0) = t(0)\left\{\left[1 + \left(\frac{x}{v_{NMO}t(0)}\right)^2\right]^{1/2} - 1\right\}$$

However, a velocity model has to be defined prior to the correction of the normal moveout. After the normal moveout, if the velocity analysis is done correctly, the hyperbola is supposed disappear.

The interactive picking module *VELDEF* was used for the velocity analysis in *Echos*. Fig. 18 illustrates an example of profile AWI-20170001. The screen is divided in two parts through the function *Compute Coherency*. On the left side lies the CDP gather, while on the right side lies the semblance, a quantitative measure of the coherency. The first strong seafloor presenting hyperbola is initially picked in the CDP gather. Each pick should approximately correlate with a high in the semblance window. For the next picks, it is important to keep in mind that, in general, seismic velocity increases with depth due to physical properties of the subsurface, e.g. pore pressure.
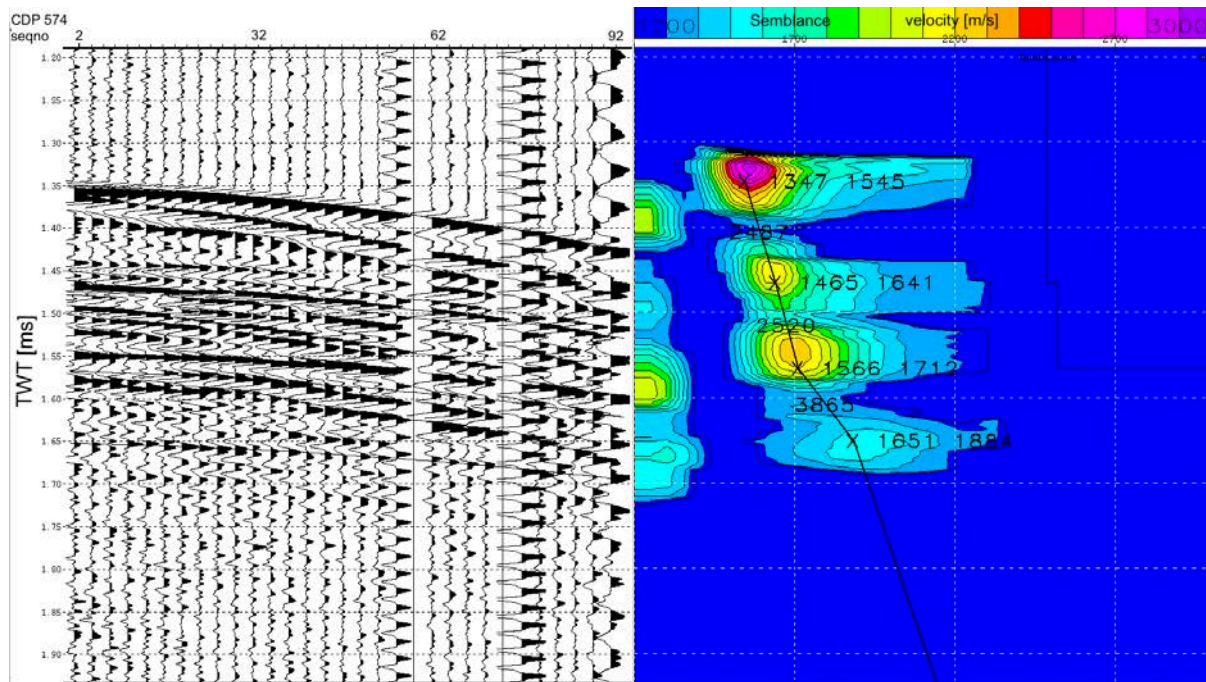
Fig. 18: Interactive picking window for velocity analysis. In this case profile AWI-20170001 CDP 574.

In this case, the velocity of the seafloor is 1545 m/s, whereas the underlying reflectors had velocities of 1641 m/s, 1712 m/s and 1884 m/s. To ensure that the picking calculates properly, an additional pick had to be made in the semblance window, in greater depth with higher velocity.

Naturally, a specific velocity model had to be defined for every seismic profile. Optionally, in the module it is possible to already determine whether the velocity analysis should be the carried out with a specific increment. This means that for an increment of, for instance, 30, the picking window jumps from CDP 30 to CDP 60 to CDP 90 and so on. In this case there was no preset increment, but the picking was done roughly every 20 to 40 CDPs, depending also on the quality of the CDP (not every CDP is suitable to be picked). Generally, it can be added that the more picks, the more precise the velocity model will be in the end. Zones like the relatively steep basin flanks may require smaller increment.

With the function *Apply NMO*, the current CDP gather is NMO corrected (Fig. 19) and conveys a first impression on whether the velocities have been picked successfully, even though the permanent NMO correction for the whole profile has to be carried out with a specific module in the jobflow. The necessary module is self-explanatorily called *NMO*.
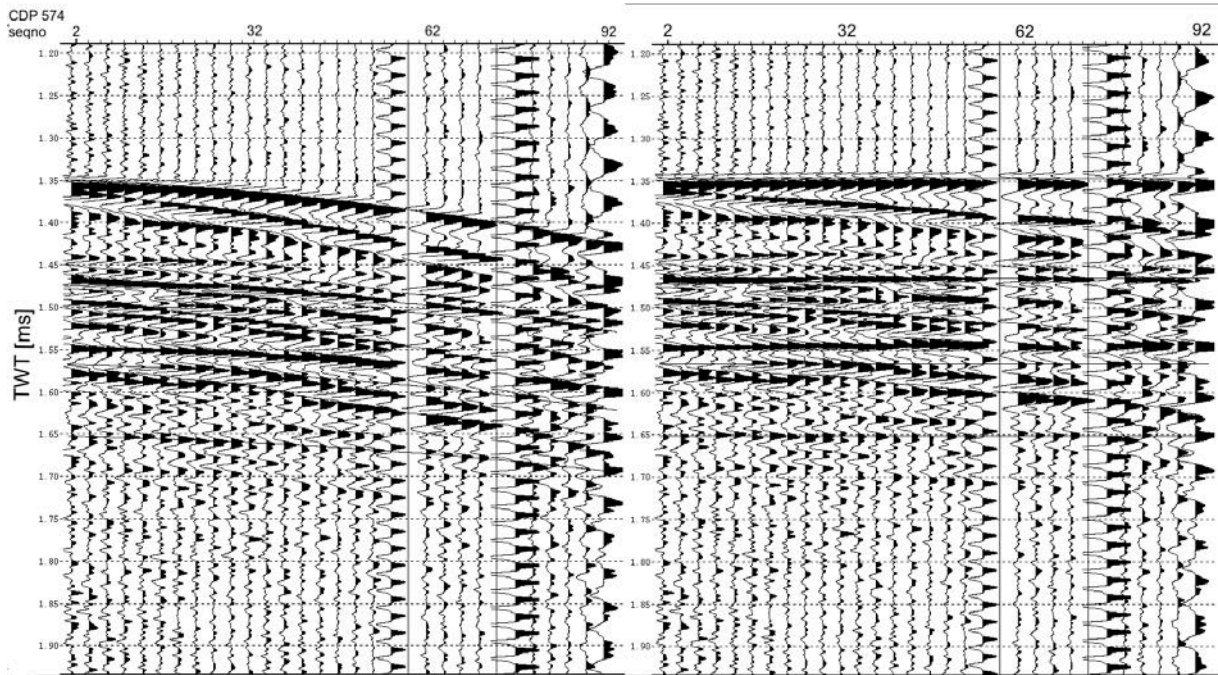
Fig. 19: CDP 574 of profile AWI-20170001 before (left) and after(right) applied NMO correction.

Mute

The module *MUTE* is applied to the data in order to remove all noise from the water column above the seafloor. This module has been applied once before the stacking with the ulterior motive that less data leads to a less time-consuming process; and once after the migration, as the migration produces, again, noise above the seafloor. Fig. 20 illustrates the interactive picking window on the left side and the same profile with the muted water column on the right side.
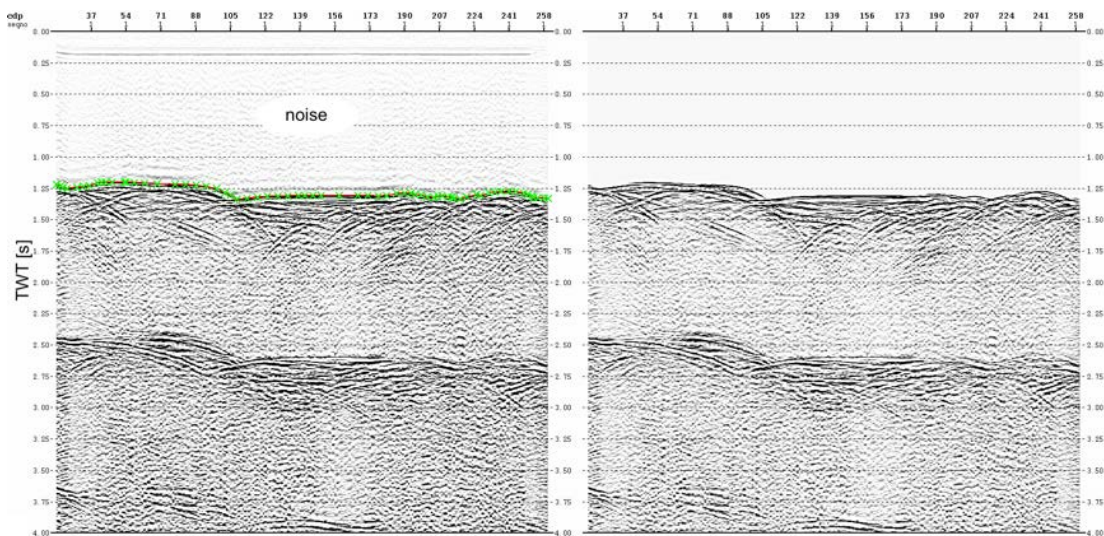
Fig. 20: Profile AWI-20170006 – on the left with the interactive picking window of the MUTE-module before application, and on the right after the application.

Karhunen-Loeve transform

This step of the processing involves the application of another module for multiple attenuation. The module *KLTRANS* was therefore added to the jobflow after the NMO correction. The concept behind the Karhunen-Loeve transform (K-L transform) is that it is possible to decompose a two-dimensional data set into a number of components (so-called eigenimages). The transform starts with the first eigenimage, which has the highest degree of correlatable events, continuing with eigenimages of a lesser degree of correlatble events, until the eigenimage with the least degree of correlatable events. The mentioned flat events and multiples have the highest correlation from trace to trace, meaning that they will map in the first eigenimage of the K-L transform.

After the NMO application to the CDP gathers using primary velocities, the primaries will be flattened, which is why they show the highest degree of correlation from trace to trace in the CDP gathers. The primaries will now map into the first eigenimage of the transform (Yilmaz, 2001). The module has been applied with its default configuration.

Spherical divergence correction

The module *GAIN* is used to correct the spherical divergence. As traveltime increases through the subsurface, the seismic signal progressively loses energy. Gain is a time-variant scaling, applied to seismic data to strengthen weak signals (Yilmaz, 1987). This module requires the previously created velocity model.

In addition to this module, an automatic gain control display window can be selected in the seismic profile via the *Section Attributes Panel* (AGC), in order to manually weaken or strengthen the reflectors by giving a number of decibels (dB) to be applied.

Stacking

After the application of all previously explained modules, the CDP-sorted data was stacked, meaning that all traces of the same CDP have been layered one on top of the other to receive one single trace. For seismic profiles with a high number of CDPs, this process can require a significant amount of time. In the case at hand, the longest profile has roughly 1300 CDPs, which only takes a few minutes to process. The module *STACK* was configured to perform mean iterative stacking.

Migration

The last big step of the seismic processing is the migration. A migration of the stacked seismic data was carried out to depict reflection events at their true subsurface positions and to collapse diffraction hyperbolas. In this way, migration increases spatial resolution and should result in an image as close as possible to a geologic cross section (Yilmaz, 1987). An example of diffraction hyperbolas is shown in Fig. 21.
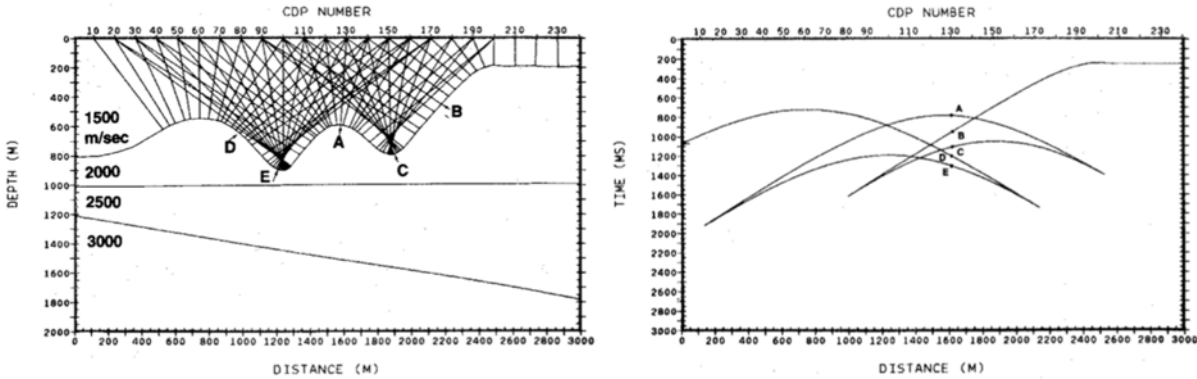
Fig. 21: Diffraction hyperbolas: the left picture depicts the reflection pattern of a dipping reflector, while the right picture visualises the appearance of the five marked points in the seismic data and their untrue subsurface location. From Yilmaz (1987).

Diffraction hyperbolas have represented a large issue in the processing of the data at hand, and they often occurred in connection with so-called bowties. These hyperbolas often arise concurrently with sharp edges in the seismic profile, plenty of which can be found in the seismic data profiles object of this study, as they have been recorded in a sedimentary basin with relatively steep flanks. To further improve the data quality, module *MIGFX* was applied to the data to perform a finite-difference migration. Fig. 22illustrates a part of profile AWI-20170001 before and after the migration. Although not all hyperbolas could be collapsed, data quality significantly improved.

6. Results

In this chapter are presented the results of the seven processed seismic profiles AWI-20170001, AWI-20170002, AWI 20170003, AWI-20170004, AWI-20170005, AWI-20170006 and AWI-20170007, sections from Parasound data and grids of the main units identified I the seismic profiles. Additionally, already processed profiles AWI-20100123, AWI-20100124 and AWI-20100125 will be presented as well.

Although the seismic processing was challenging, the results appear to be highly satisfactory, providing intriguing insights into the sub seafloor. Conspicuous units have been identified in all profiles and, when possible, also linked to the correspondent units of other profiles. The approach for every profile has been that of identifying the seafloor and the acoustic basement at first. While picking the seafloor was quite straightforward, the identification of the basement proved to be significantly more challenging. For most of the profiles, the basement was not represented by one continuous reflector, but by reflectors presenting large gaps or chaotic reflectors. In these cases, it is surely useful to develop a sense for the geometry and orientation of the sedimentary basin. An average velocity of 2000 m/s for sediments was used for calculating bed thickness etc.

The Parasound data do not deliver a good enough penetration in the upper tens of meters of the seafloor to identify seismic units from the profiles, and yet the data reveal much information about seafloor topography, morphological features and sediment depositions. The results of the seismic profiles are enriched with findings from the Parasound data to provide supplementary insights.

The identified units represent significant reflectors in the sediment body. For clarity, the profiles are listed in Tab. 2 together with all occurring units respectively, as many reflectors can only be tracked in some of the profiles, but not through the whole sedimentary basin.

Tab. 2: Overview of the seismic profiles with ocurrig units, respectively.

AWI-20170001	PIG-u1, PIG-u2, PIG-u3, PIG-u4, PIG-w1, PIG-w2
AWI-20170002	PIG-w1, PIG-w2
AWI-20170003	PIG-u1, PIG-u2, PIG-3, PIG-u4, PIG-A, PIG-B
AWI-20170004	PIG-u1, PIG-u2, PIG-u3, PIG-u4
AWI-20170005	PIG-u1, PIG-u3, PIG-u4
AWI-20170006	PIG-ne1, PIG-ne2
AWI-20170007	PIG-u4, PIG-e1, PIG-e2
AWI-20100123	PIG-u1, PIG-u2, PIG-u3, PIG-u4
AWI-20100124	PIG-u1, PIG-u3, PIG-u4
AWI-20100125	PIG-u1, PIG-u2, PIG-u3, PIG-u4

Thin green lines in the seismic profiles indicate locations, where other profiles cross. Small dots in colours on the green lines indicate locations of crossing units from other profiles. Most of the profiles are strongly enhanced in the vertical sense to better resolve the sedimentary basin, even if this can be misleading at a first glance. In general, all profiles are oriented from west to east. Enlarged versions of these profiles without marked units can be found in the appendix chapter. Two colour versions of each profile are available in the appendix. An average velocity of 1500 m/s was used for calculations of the depth of the seafloor, while an average velocity of 2000 m/s was used for the calculations of bed thickness.

6.1. Processed seismic reflection data from cruise PS104

AWI-20170001

Profile AWI-20170001 (Fig. 22) has been made out for the main profile of this analysis. With roughly 35 km, it is not only the longest profile, but also the profile which crosses the basin in the direction of ice retreat and represents the longitudinal axis. The water depths of the seafloor roughly range from 1250 ms of TWT at the northwestern boundary of the basin to 1460 ms of TWT in the southeast. In general, the seafloor is constantly sloping downward except for one observed structure, which will be explained after the description of the single units. In contrast to a smooth and continuous seafloor, the acoustic basement is very rugged and incised, but follows a downward sloping trend overall. In the NW of the profile, the basement follows quite closely the seafloor until CDP1250, where it abruptly decreases to roughly 1500 ms TWT. The

highest sediment bed thickness is then found at a with sediment filled incision in the basement at CDP 810 with roughly 300 ms of TWT (~225m).

The profile can be divided in two different parts: an eastern part of the basin and a smaller western part. Both can be divided through a strong reflection named PIG-w2. In the eastern main basin, 4 different main units were found: PIG-u1, PIG-u2, PIG-u3 and PIG-u4. In this case, the term unit does not describe a real horizon, but a significant reflector. The units all have in common that they are subparallel to each other and that they slightly slope downwards in eastern direction. The PIG-u1 is interrupted by chaotic reflections between CDP 550 and 600. The unit is terminated by a small basement high at CDP 220 and is no longer traceable behind it. At its western termination, PIG-u1 starts at a basement high at CDP 910. From this basement-high, PIG-w2 develops in western direction towards surface, representing a boundary between the two parts of the basin. The next significant reflector which could be picked is PIG-u2. PIG-u2 onlaps on PIG-w2 on its western termination and on PIG-u1 on its eastern termination. The following two subparallel identified units are PIG-u3 and PIG-4. Both units onlap at their western end on PIG-w2. PIG-u3 ends in the east together with PIG-u1 at the basement high at CDP 910, but continues shortly after, thus marking a continuous reflector above incised basement. PIG-u4 is not interrupted by this basement high and follows the basement until the end of the profile in the east. PIG-u4 is considered to be the first identifiable unit under a pack of strong reflectors below the seafloor. The high amplitude reflectors between the seafloor and PIG-u4 are reverberated acoustic waves from the seafloor.

The western part of the basin, divided by PIG-w2, is much more chaotic, with less continuous reflectors. One unit could be identified here: PIG-w1. This reflector slightly dips downwards in western direction and is the only traceable reflector in this part of the disturbed basin.

The main morphological feature identified in this profile is a formation beginning at CDP 940 and is located under the seafloor. Against the trend, the seafloor suddenly rises slightly until CDP 880. The ice distant side is relatively "steep"-rising, while on the eastern side the structure seems to thin out. This formation most probably indicates a grounding-zone wedge (GZW) with a thickness of roughly 30 ms of TWT (~30 m). This formation can be resolved even better in the Parasound data (Fig. 22b). The longitudinal extension of the GZW is not fully clear, but it is roughly estimated to 5000 m.

Another significant appearance can be found at the western flank of the basin, when the basement rises closely to the seafloor (Fig. ??a). The seafloor developed several platforms on its rise, with a potential thin layer of sediments.

Furthermore, three faults in the middle part of the profile could be identified between CDP 760 and 640. The faults are either vertical or they dip in eastern direction.
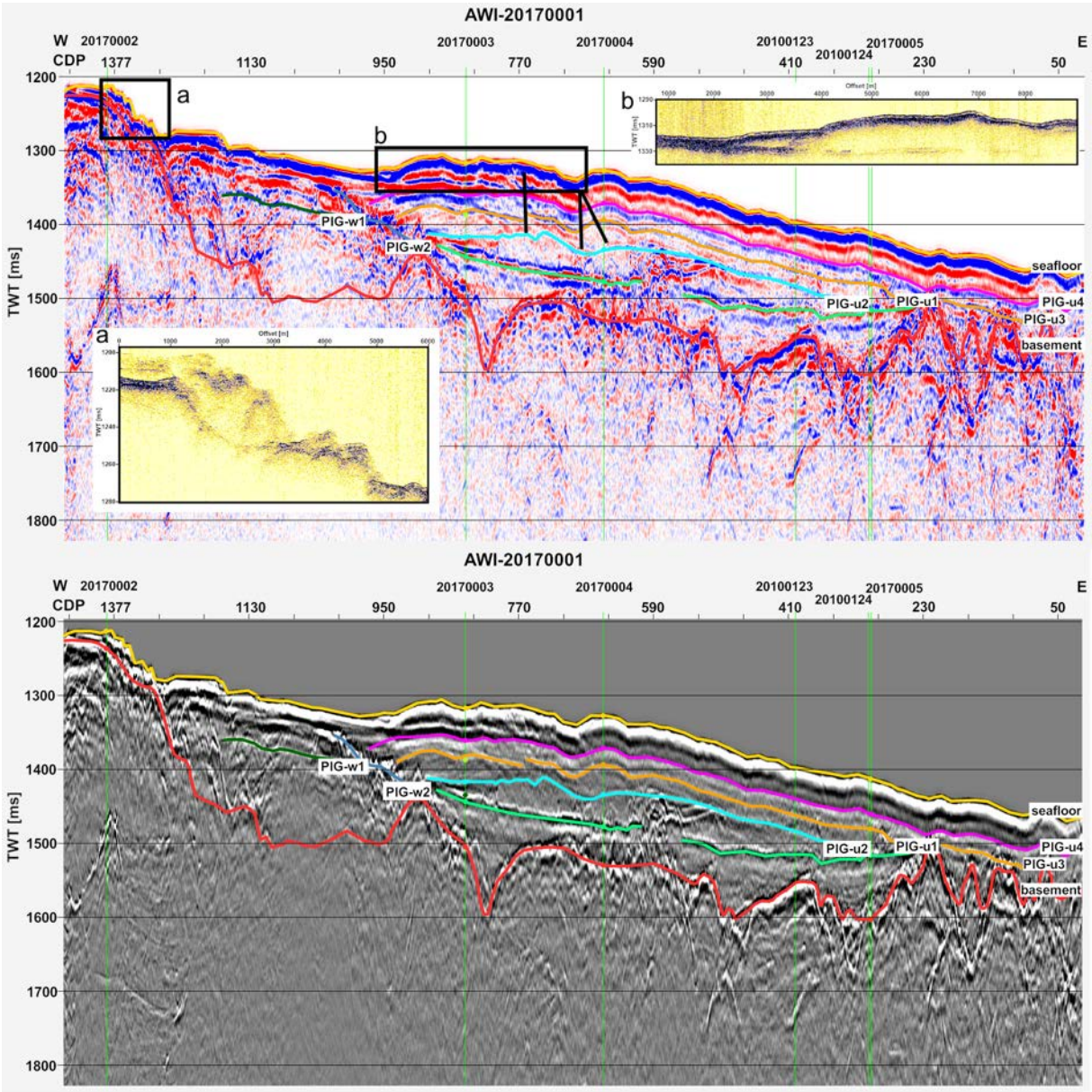
Fig. 22: Processed profile AWI-20170001 with main units.

AWI-20170002

Profile AWI-20170002 (Fig. 23) is oriented from NW to SE and is located on the southwestern part of the basin. The seafloor is relatively uneven, with a lot of small mounds. At the western part of the profile, the basement follows the seafloor really close (10 ms TWT). Afterwards, a small sedimentary basin can be found, separated by basement high at CDP 140 from the bigger

basin. In this very small sub-basin, sediment thickness is of ~80 ms TWT. The basement in the larger basin is wavy and incised at CDP 180 and CDP 240.

This profile is connected with the western part of profile AWI-20170001. Units PIG-w1 and PIG-w2 have been identified again. They represent the only two traceable reflectors in a very chaotic basin. While PIG-w1 is dipping in eastward direction and in contrast to the first profile, PIG-w2 lays horizontally, in nearly constant depth of 70 ms TWT below the seafloor.
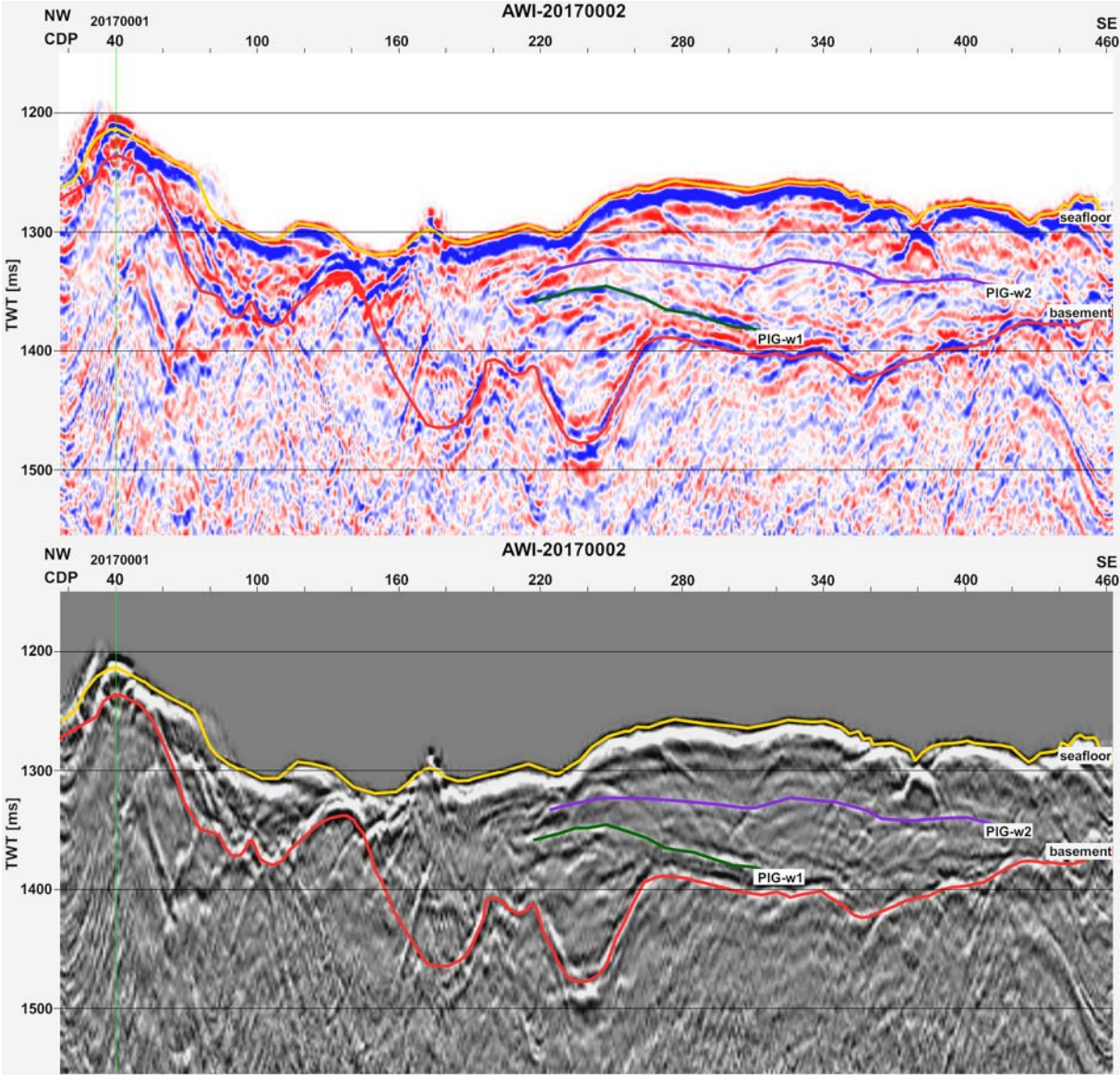
Fig. 23: Processed profile AWI-20170002 with main units.

AWI-20170003

The first profile crossing the basin from SW to NE is profile AWI-20170003 (Fig.24). The seafloor is relatively constant in its depth (at the beginning of the profile in a depth of 1270 ms

TWT, bending downwards in the middle part to 1320 ms TWT and going upwards to 1270 ms TWT). Around CDP 80 are two seafloor incisions and at CDP 165 is one seafloor incision. In the western part, the basement is shallow under the seafloor (~60 ms TWT below) with wavy incisions in the basement. At CDP 120, the basement starts gaining depth until the deepest point of the basin in this profile, at around 1570 ms TWT (total sediment thickness is ~245 m). From this point on, basement rises up until a TWT time of 1400 ms, then dips down until the end of the profile.

Some of the identified units in this profile are already known from the cross profile AWI-20170001 and were used as a support for the identification in this profile. PIG-u1, PIG-u2, PIG-u3 and PIG-u4 have been identified. PIG-u1 and PIG-u2 start in the middle of the basin and corner the high-amplitude reflector PIG-A; which is only ~70 CDP long and lays horizontally in the basin. PIG-u2 lies above PIG-A. A remarkable dome-like structure is found above PIG-u2 with a basal diameter of 1875 m and a height of ~60 m. PIG-u3 lies, in turn, above PIG-u2, but is interrupted by the dome and onlaps on its sides. The uppermost reflector below seafloor is PIG-u4. Significant is that PIG-1-4 all are ascending at the western of the deepest point in the basin. They follow a topographic high in the basement at 1400 ms TWT.
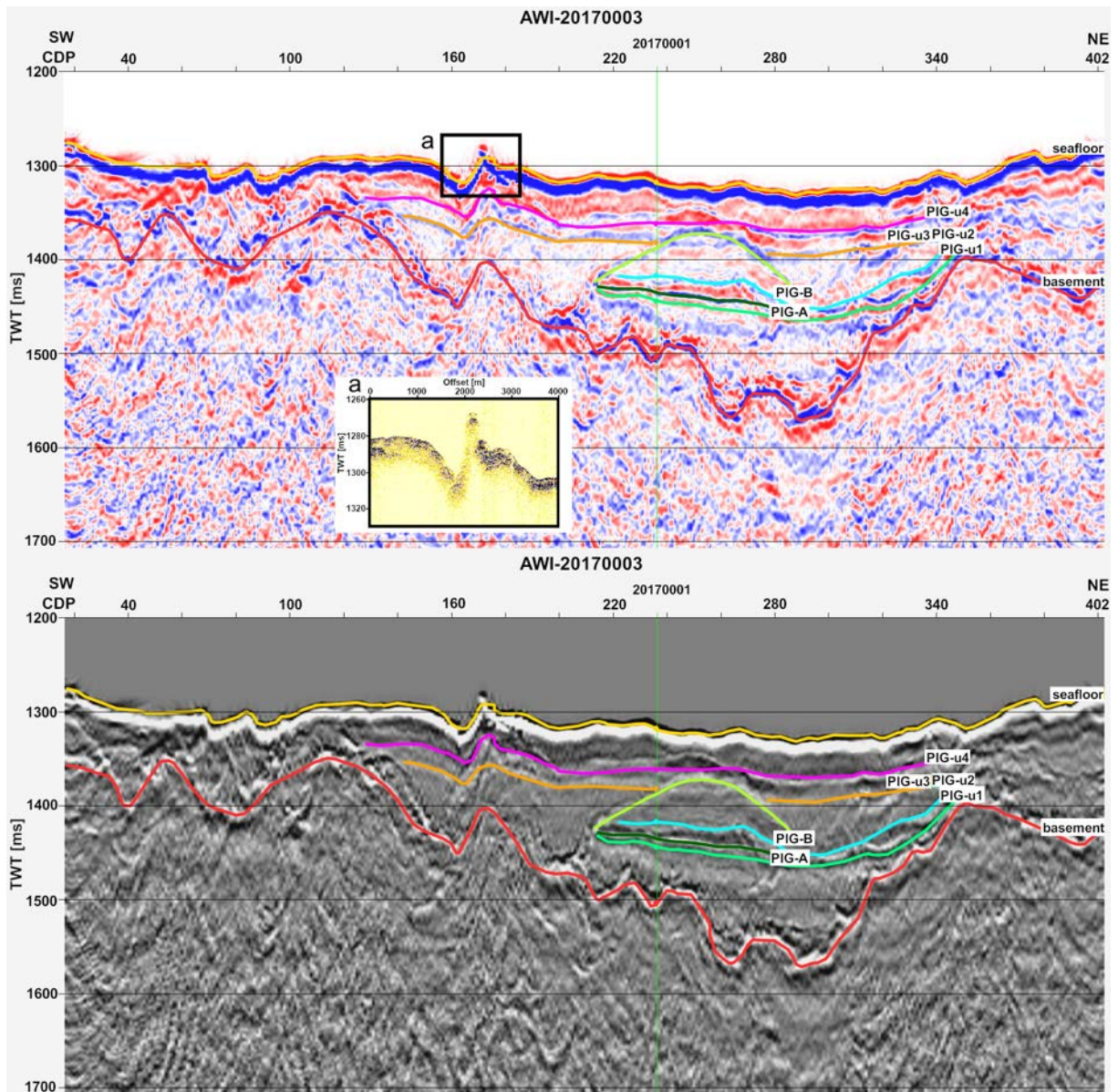
Fig. 24: Processed profile AWI-20170003 with main units.

AWI-20170004

This section is a N to S transverse section through the basin (Fig. 25). The basement has several smaller incisions. In the northern edge area it is possible to find a small sub-basin, which is incised into the basement with a total thickness of ~140m. At CDP100, the basement meets the seafloor and then dips, opening the main basin with "deep" basement incisions. At the end of the basin, the basement advances again closely to the seafloor. Units PIG-u1-4 are found in the basement. PIG-u1, PIG-u2 and PIG-4 terminate onlapping on the seafloor, while PIG-u3 onlaps on PIG-u2. PIG-u2 is interrupted by the basin at around CDP 305. The seafloor at the middle part of the basin varies around a depth of 1325 ms TWT. The basin has a sediment thickness of

around 200 m. The basement comes very close to the seafloor at CDP 460 at the southern end of the basin. Seismic reflectors appear to be very chaotic in that area. After 40 CDPs, another small sub-basin opens up. Units PIG-u3 and PIG-u4 could be tracked. Overall, the reflections in the basement are rather parallel and well visible. Reflectors close to the seafloor are more chaotic, but strong. In the bigger basin in the middle, seafloor is relatively smooth, while seafloor on the flanks is rougher.

Morphologically interesting is a seafloor incision at CDP 360, right at the same location where a basement high can be found. On the western flank of the basin, PIG-u1, PIG-u2 and PIG-u4 onlap on the basement. Two faults were recognised at CDP 340 and CDP 350, close to the incision in the seafloor. Both faults cut through all units and finish at an incision in the basement. These two faults are surrounded by some more small-scale faults.
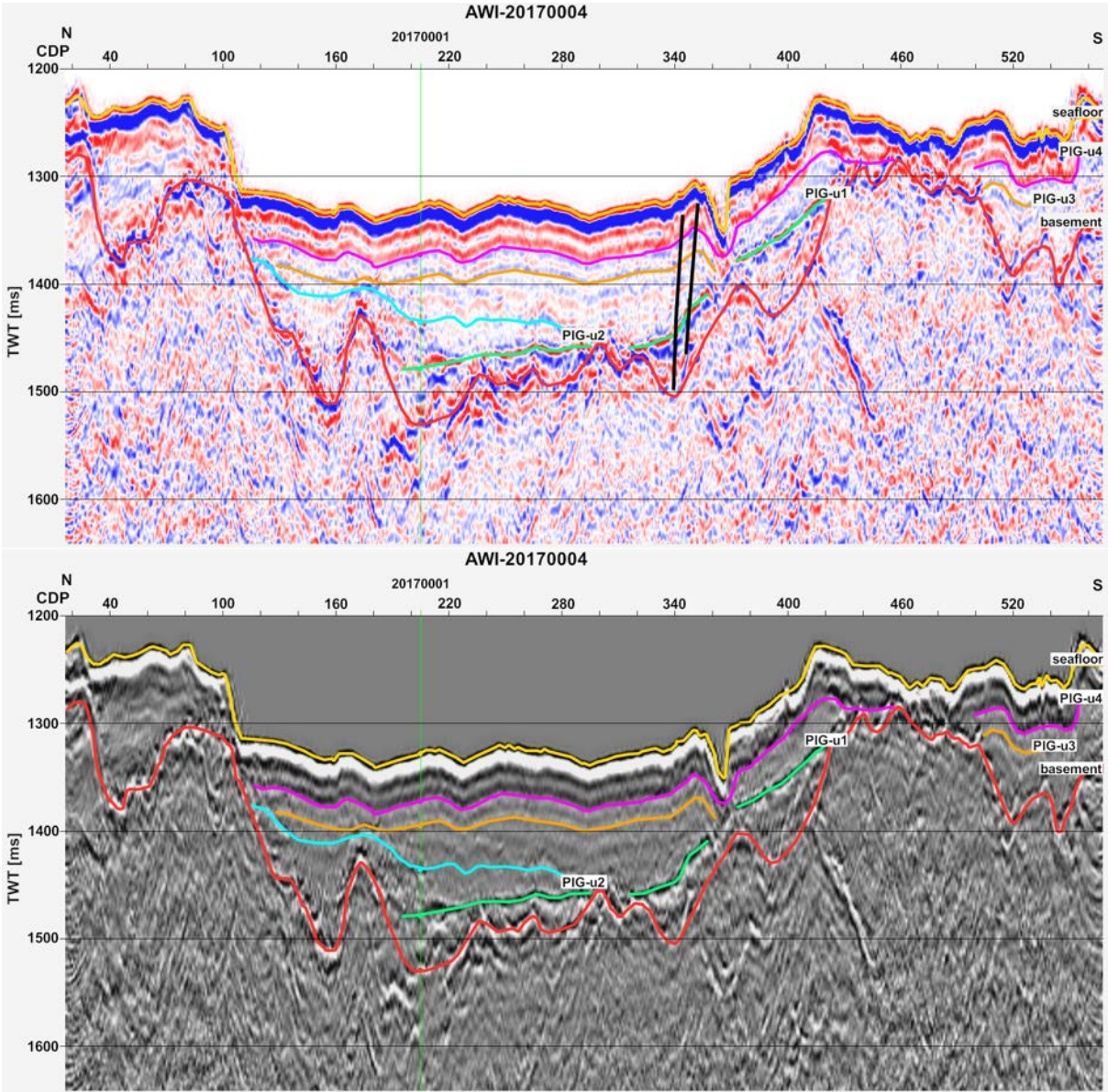

Fig. 25: Processed profile AWI-20170004 with main units.

AWI-20170005

Profile AWI-20170005 (Fig. 26) is a cross section through the basin that is oriented SW to NE. At the southern end of the profile, the seafloor topography is parallel to the basement until a topographic high at CDP 65. Then, the seafloor is dipping downwards into the middle part of the basin. A thin band of sediments appears to be laying on the flank of the basin, between CDPs 60 and 140, since the reflections below the seafloor are relatively clear in this part compared to the following range between CDPs 140 and 240. The basement approaches the seafloor and layers are chaotic. Then, the basement is descending until the deepest incision of the basin (at 1710 ms TWT). At this point, sediment thickness of the basin is roughly 300 m. The basement then ascends at CDP 450, while the seafloor suddenly rises steeply as well for roughly 50 ms TWT in height. After that, sediment thickness amounts to only ~130 m. There is one larger incision at CDP 515, cutting ~100 m into the basement. From CDP 620 on, basement and seafloor are rising on the northwester flank of the basin to a, lying closely together, until seafloor reaches a water depth of 1230 ms TWT (~920 m).

Fig. 26a depicts the Parasoud data between CDP 560 and the end of the profile. Parasound has almost no penetration into the seafloor, except for one small, lower sedimentary basin in front of the rise. This is quite remarkable, since it can be seen from the seismic profile that this small basin is already surrounded by other sediments which, in contrast, don't allow the echosounder to penetrate.

In this profile, PIG-u1, PIG-u3 and PIG-u4 have been identified. While PIG-u1 and PIG-u3 are subparallel and onlap on both flanks of the deeper part of the basin on the basement reflection, PIG-u4 is rather parallel to the seafloor and onlaps on the eastern flank on the basement before the rise.

Interesting is, again, an identified fault at the rise from the deeper part of the basin to the lower part of the basin in the east. The fault is dipping in SW direction and follows the direction of the descending basement from a small topographic high at CDP 445.
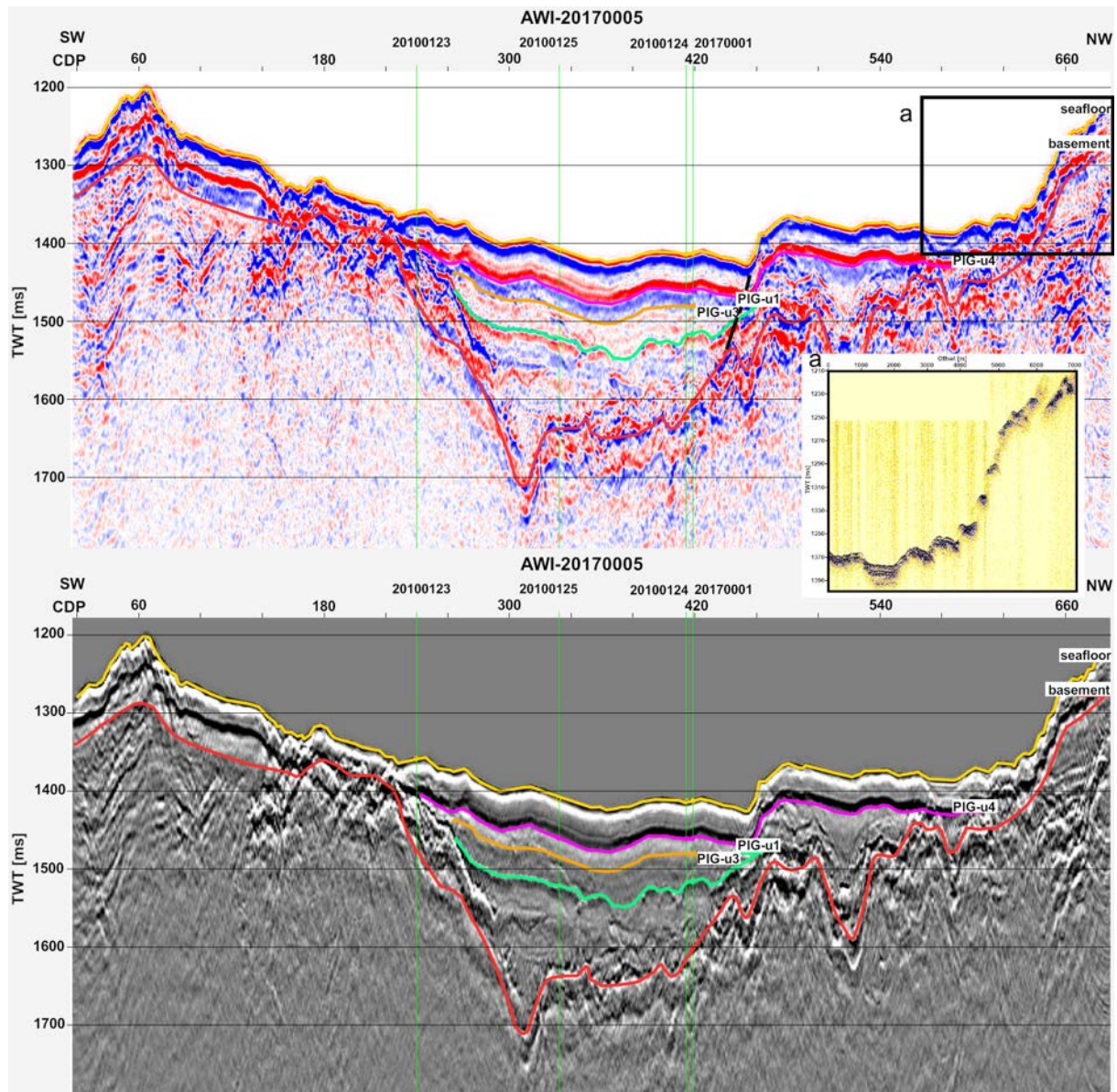
Fig. 26: Processed profile AWI-20170005 with main units.

AWI-20170006

Profile AWI-20170006 (Fig. 27) is oriented from NW to SE and is relatively short. It is located at the northeastern boundary of the basin. At the beginning of the profile, the seafloor is at a water depth of roughly 1200 ms TWT (~900 m water depth), with the basement real close to the seafloor. At CDP 90, the seafloor is steeply descending for ~110 ms TWT (~80 m). The basement drops and opens a sedimentary basin between CDPs 90 and 230. The deepest point of the basin is at CDP 190; the sediment body has a thickness of ~230 ms TWT (~230 m). This basin is relatively chaotic with 2 significant reflections: PIG-ne1 and PIG-ne2. Both reflections rise towards the eastern flank.
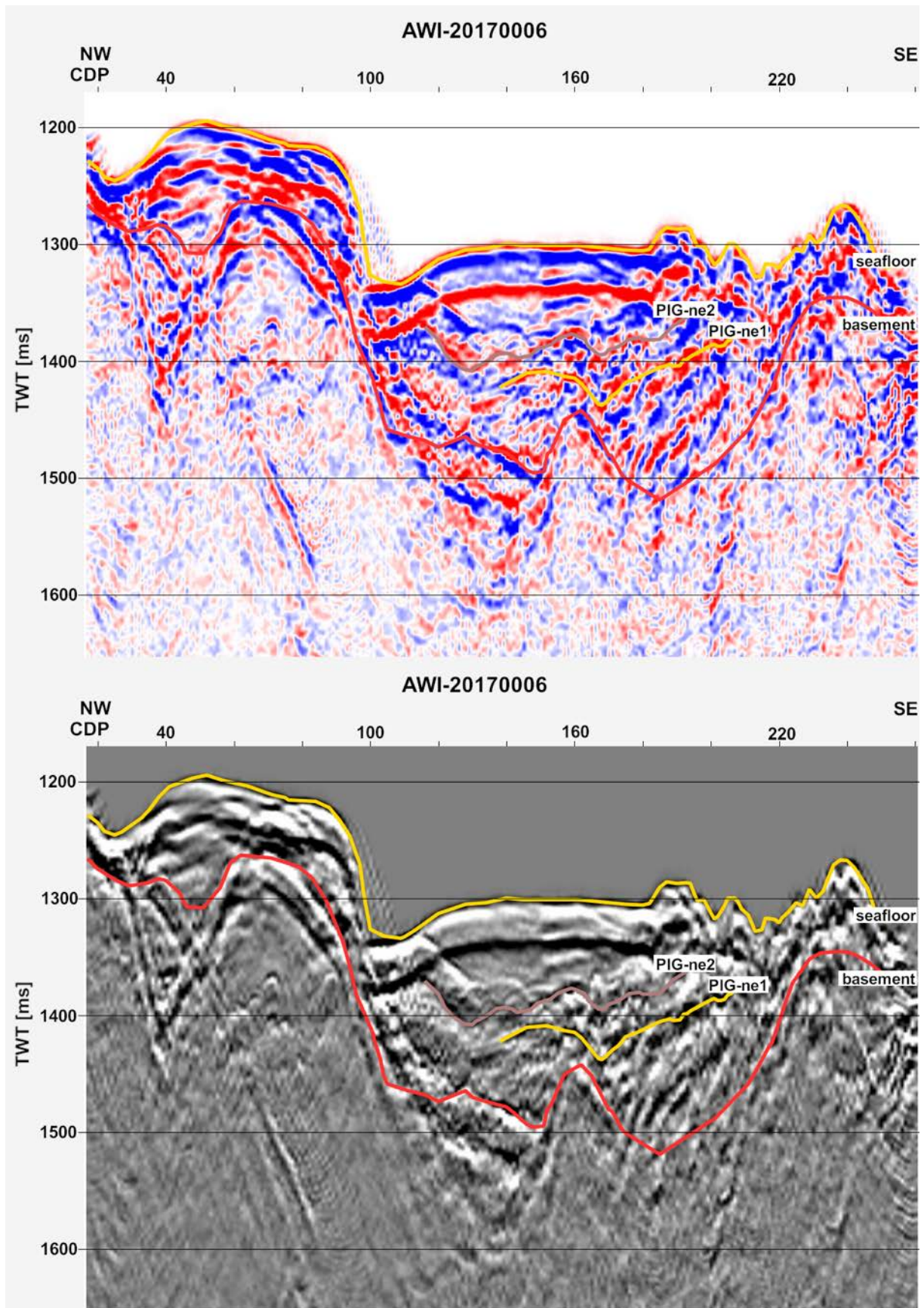
Fig. 27: Processed profile AWI-20170006 with main units.

AWI-20170007

The easternmost profile AWI-20170007 (Fig. 28) is oriented from SW to NE and is the closest profile to the ice shelf front. This profile has rough structure and shows the rugged course of basement and seafloor very well. This profile distinguishes itself from the other profile in some ways. The large basin is not one large middle basin as e.g. in profiles AWI-20170004 and AWI-20170005, but it consists of several small basins separated by "ridges" from the uprising basement. In the SW part of the profile, seafloor and basement are close to each other on the basin flank at ~1280 ms TWT. The opposite basin flank begins at CDP 190 and the seafloor, closely and parallelly followed by the basement, rises until a water depth of ~1275 ms TWT is reached. Below the seafloor, on the flank, seismic reflectors are rough and of a high-amplitude. The profile ends at CDP 35 with another incision in the seafloor and the basement. The middle area of the profile, which presents the isolated basin, has water depths between ~1420 and 1490 ms TWT and is underlaid by sediments. The exceptions are the ridges, which have heights between 15 and 75 ms TWT (15 and 75 m). The highest thickness of sediments can be found at CDP 415 with ~250 m. PIG-u4 could be traced back in this profile. This unit onlaps on the basin flanks and on the "ridges". Further on, two other significant reflections in the sediment body could be found: PIG-e1 and PIG-e2. In a bed of discontinuous reflectors with often chaotic appearances, these identified units are the exception.
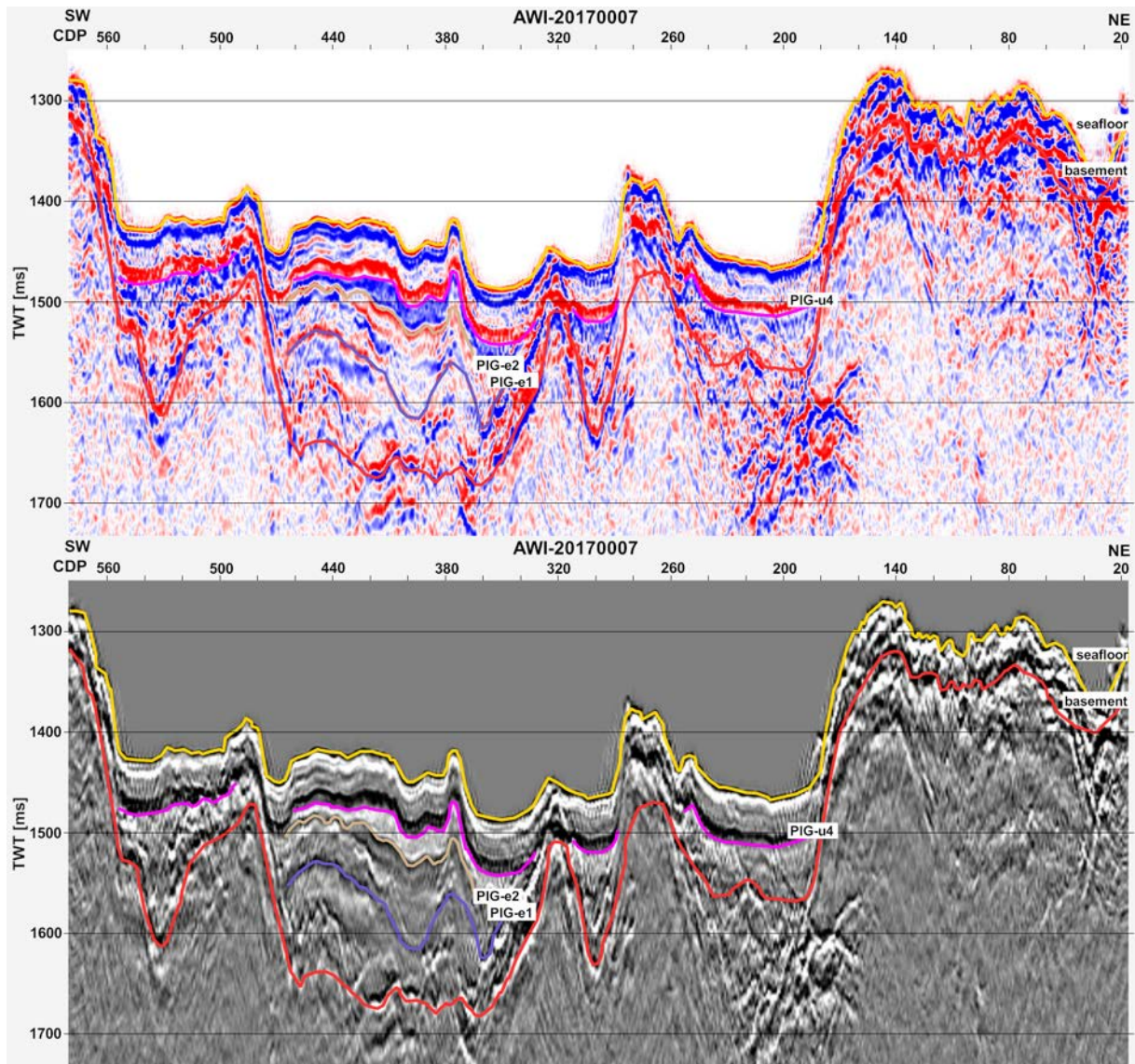
Fig. 28: Processed profile AWI-20170007 with main units.

6.2. Existing seismic profiles from cruise ANTXXVI/3

AWI-20100123

This profile (Fig. 29) is oriented from SW to NE and also represents a cross-section through the basin. From the beginning of the profile until CDP 170, the basement is quite close to the seafloor with one rise in topography at CDP 50. After CDP 170, seafloor and basement separate and the sediment basin opens. Highest sediment thickness of the basin can be found at CDP 255 with 240 ms TWT. Below this basin there are a few incisions in the basement (all between 10 and 80 ms TWT deep). From CDP 420 on, the basement rises, first to a shallower platform with overlying sediments and then (rather parallelly and closely to the seafloor) up to the highest

point of the profile in the NE, at a water depth of 1000 ms TWT. In this profile, units PIG-u1, PIG-u2, PIG-u3 and PIG-u4 have been traced, which all lay subparallel in the sediment body and lean upwards at the sides of the basin.
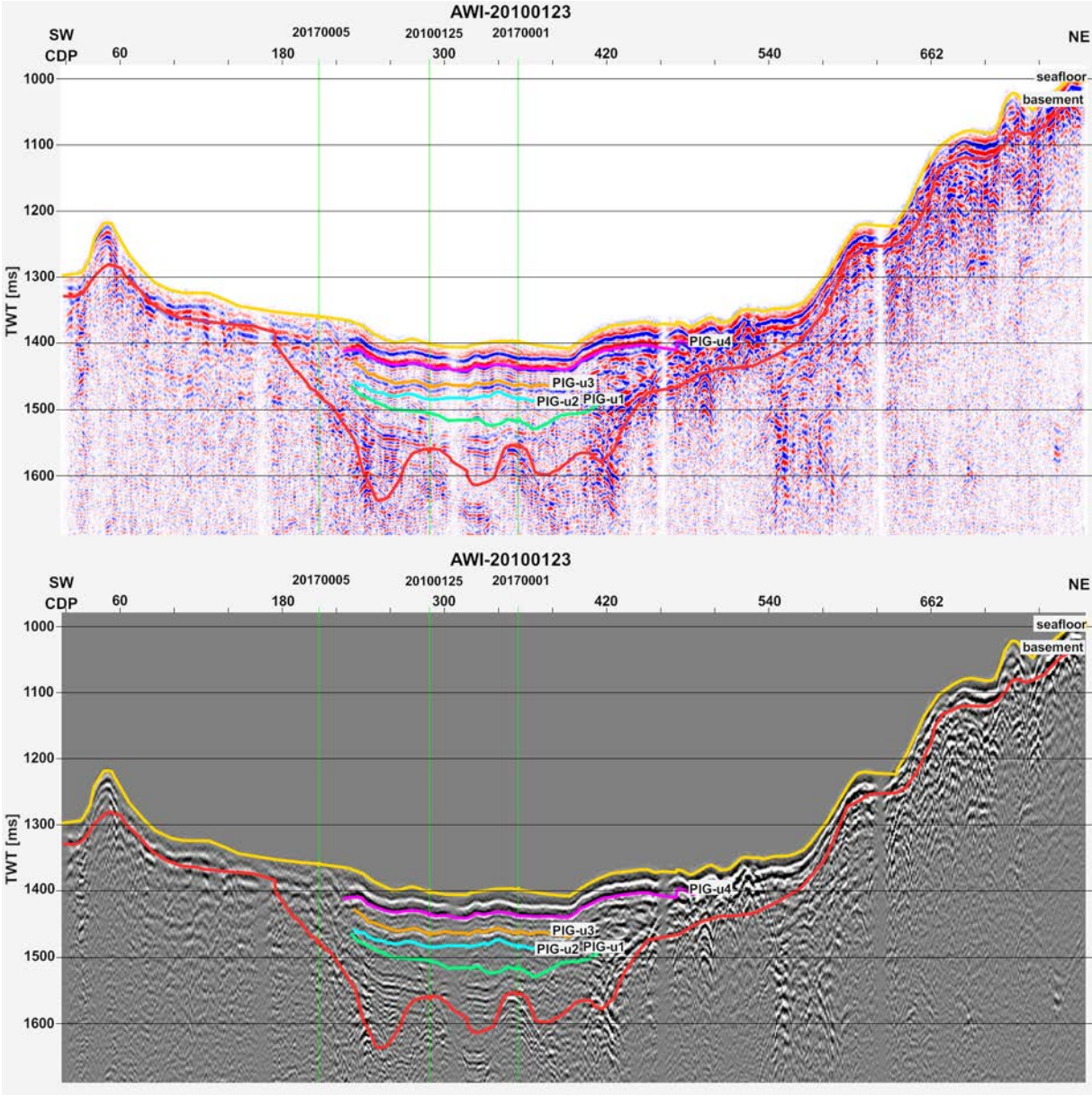
Fig. 29: Already processed profile AWI-20100123 with main units.

AWI-20100124

This profile (Fig. 30) is oriented from N to S and represents the steep flank of the northern boundary of the sedimentary basin. Highest point of the seafloor and of the basin is in the north, at 1050 ms TWT (~790 m) water depth. The appearance of this profile is very similar to profile AWI-20100123, as they are close to each other at the basin flanks. Identified units are PIG-u1,

PIG-3 and PIG-u4. PIG-u2 is missing, since this unit is only present at the inner part of the basin. These units are, again, the only continuous and significant reflectors in a basin with sometimes very strong and chaotic reflections and sometimes very weak reflections. Similarly to profile AWI-20100123, here the basement rises from the inner basin to an upper platform in the basin, before basement and seafloor rise close to each other at the flank.
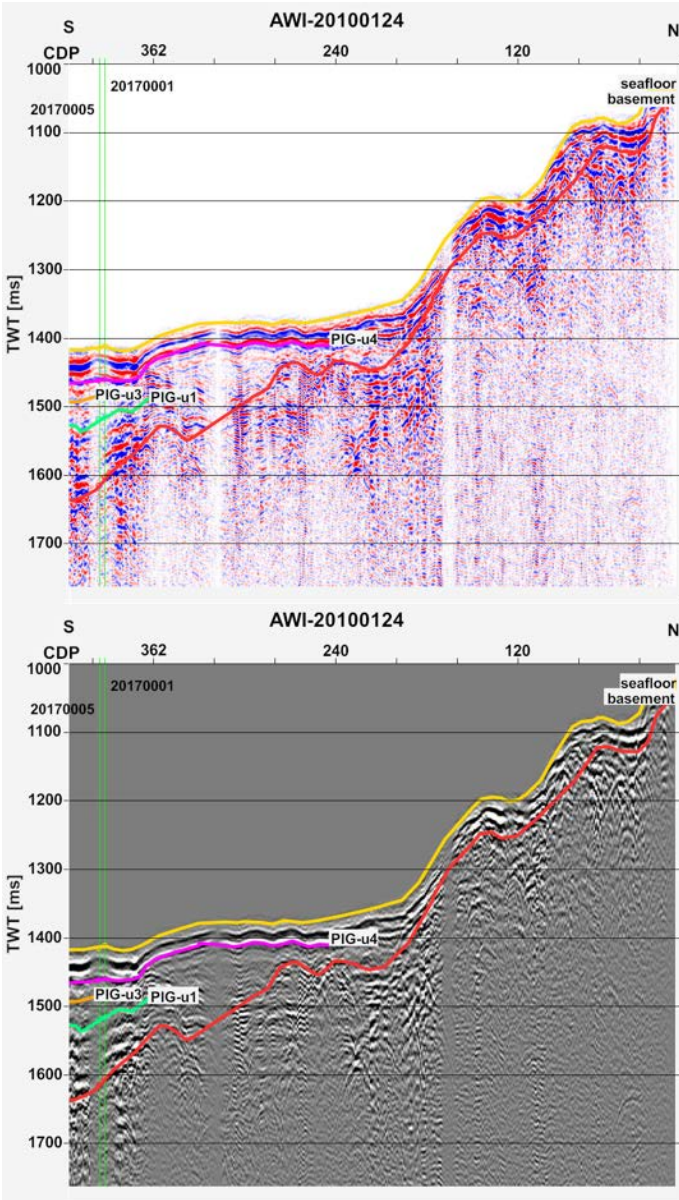
Fig. 30: Already processed profile AWI-20100124 with main units.

AWI-20100125

The last described profile (Fig. 31) is oriented from NW to SE and is located parallelly to profile AWI-20170001. For this reason, the appearances are very similar, even though it has to be noted that data quality from the profile recorded in 2017 is clearly increased. Picking of the basement and the four main units PIG-u1, PIG-u2, PIG-u3 and PIG-u4 was carried out by comparing the profile with the one from 2017. The main units lay more or less parallelly in the sediment body and are slightly dipping downwards in SE direction. The basement also follows a descending trend. Both basement and seafloor are relatively smooth in this profile, as they were in profile AWI-20170001 at the same section. The total sediment cover is slightly increasing in thickness throughout the profile from W to E. The sediment body has a thickness of ~130 m in the west and of ~220 m in the east.
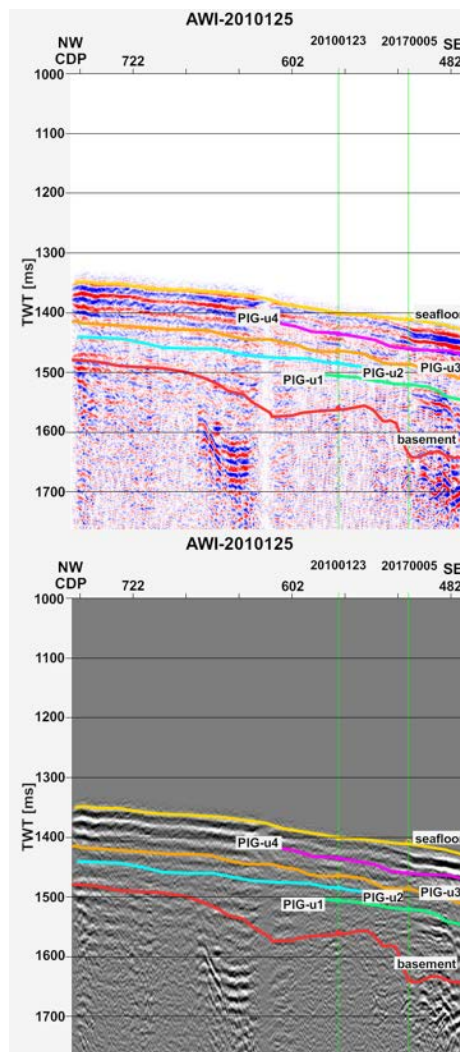
Fig. 31: Already processed profile AWI-20100124 with main units.

6.3.   2D-grids from main units

One of the aims of mapping the horizons in the seismic profiles is to generate 2D grids afterwards. Even though the seismic lines are not suitable for a 3D mapping of the basin, generating 2D grids can provide useful indications on the orientation of the basin and its units. The results can be incorporated into a conceptual model of the sedimentary basin. However, the grids have to be handled with motion, as data points in this grid exist, of course, only where the particular units appear. The minimum curvature interpolation method has been employed for their generation. Unfortunately, the picked units from Ant-20100123, Ant-20100124 and Ant-20100125 could not be included in the generation of these grids, as an issue with the project boundaries occurred: all seismic reflection data at the AWI is organised in surveys/projects in Paradigm, and the geographical boundaries of the ANTXXVI/3 survey appeared to be conflicting with those of the Ant2017 survey. Nevertheless, the results are satisfactory. The coordinate system is referencing to UTM Zone 17 N 81 W – WGS1984.

The grids have been generated for the main units from the basin (PIG-u1, PIG-u2, PIG-u3, PIG-u4) since these are the units which appear most frequently. Two grids in particular have been produced for the seafloor and the basement (Fig. 32). Even though seafloor topography can be resolved significantly better through a bathymetric map, it is interesting to see the results from the picking.
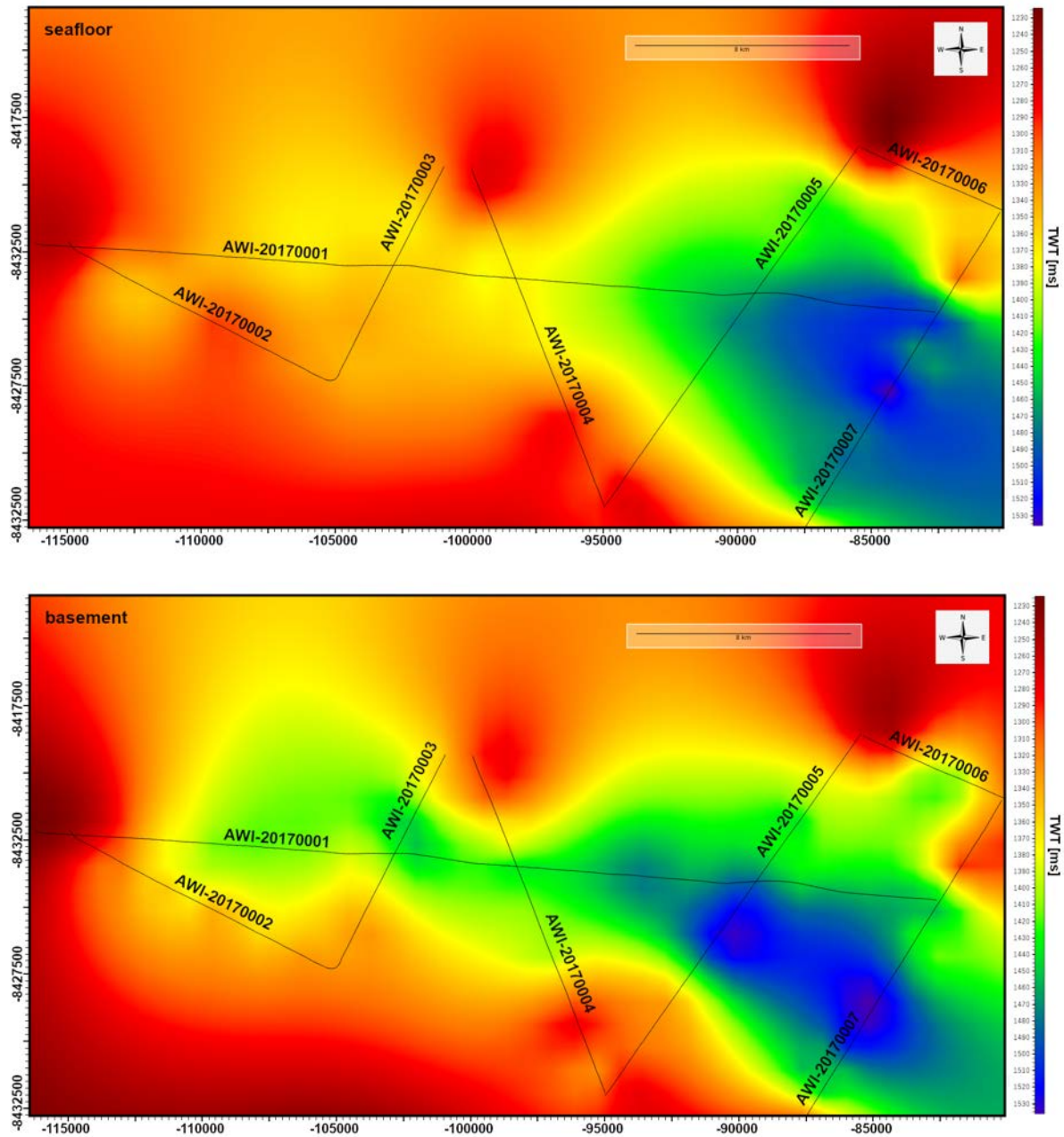
Fig. 32: 2D grids from the identified seafloor (above) amd basement (below) show an obvious descending trend in ESE of the sedimentary basin.

At first glance, the grids of the seafloor share some similarities. The mapped seafloor confirms this impression, which the previous results had already suggested. The sedimentary basin is, indeed, rather isolated, and has a W to E orientation. At the eastern side, the seafloor is at its deepest point and the basin seems to slightly turn in SE direction. But, again, it should be minded that the map does not necessarily represent the real situation.

The grid of the basement is relatively similar to the grid of the seafloor. At the basin flanks, the rise of the basement is even more clear. The change of elevation is higher than it is for the

seafloor, and the isolation of the sedimentary basin is obvious. At both sides of profile AWI-20170006, the seafloor is increased, while the middle part seems to be a lower passage. The seafloor has two depressions in SE. These depressions were visible as sharp incisions in the basement.

The maps of the four main units (Fig. 33) identified in the seismic reflection are, naturally, far from the real situation in more than one way. The conspicuousness of these units was that they were only trackable in the inner parts of the basin, laying horizontally in their sediment bed and mostly onlapping on the uprising basement at the flanks. Still, the dipping trend from W to E is unambiguous.

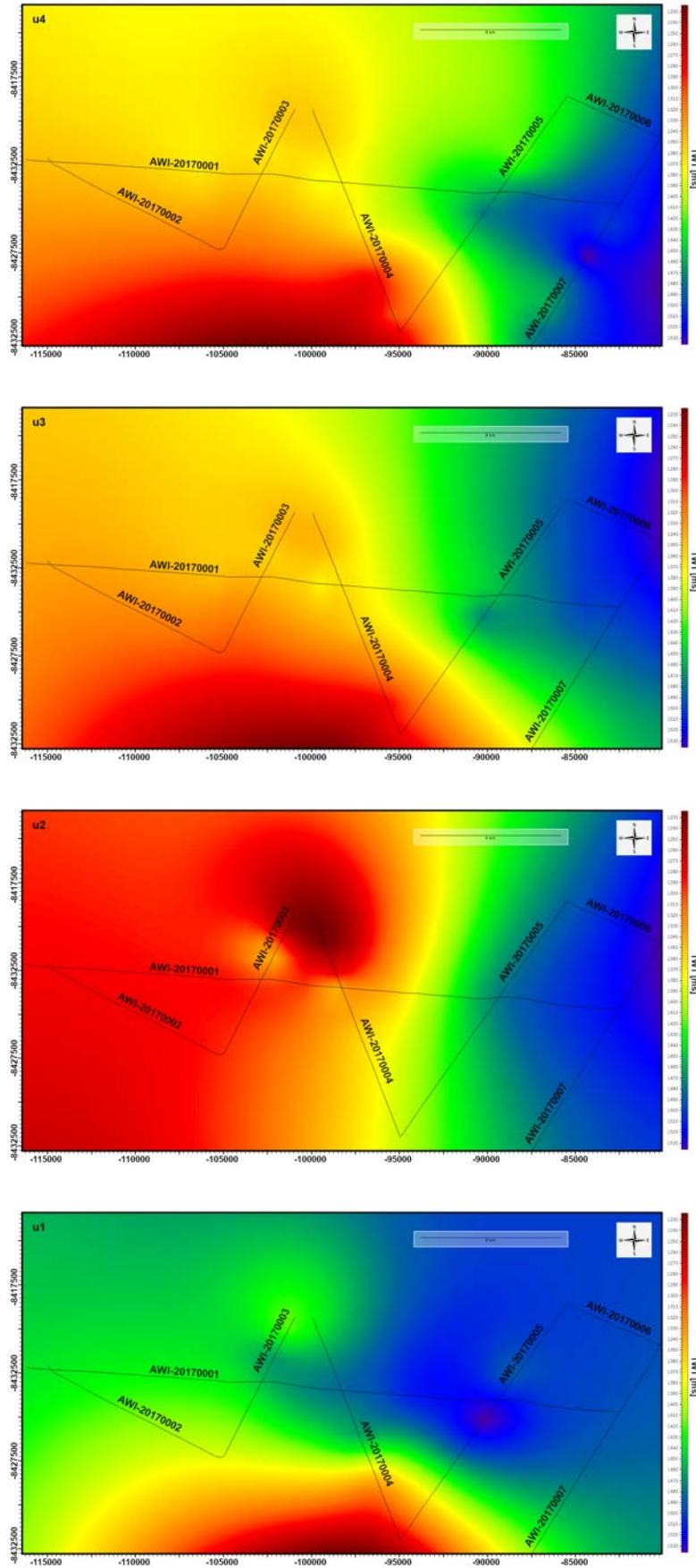*Fig. 33: 2D grids from the identified main units (PIG-1, PIG-2, PIG-3, PIG-4;in the order of their appearance) show their orientation in the sedimentary basin.*

7. Discussion

The results provide a significant amount of information, thus inspiring a joint discussion about the sedimentary basin and its role for the ice retreat.

The results of the seismic reflection data, the Parasound data, the grids and the bathymetric maps have been taken into account for the application on a conceptual model of (part of) the isolated sedimentary basin. Its aim is to provide as much of a graphical access to the geological setting of the basin as possible and to illustrate the orientation in the basin.

The model (Fig. 34) is a pseudo three-dimensional geological block diagram and though it is not completely true to scale, distances have been accurately based on the real situation in order for the model to be as precise as possible. The representation depicts a clipping of the NE part of the basin. The cross section on the right is based on a clipping profile AWI-20170001, which is oriented from NW to SE. The NW part of the profile is not visible. The model begins just before the grounding zone wedge at CDP ~1010. The length of the profile is roughly 25 km. The cross section on the left side is based on clipping profile AWI-20170003, which is oriented from SW to NE. The SW-most part of the profile is not visible and the profile begins at CDP ~185. The length of this profile in the model is roughly 5.5 km. The proportions indicate that this profile is not true to scale; also, likely the profile is also vertically exaggerated. The model shows the main orientation of basement, seafloor and the identified main units, as well as their position in the sediment bed. The morphology of the seafloor is outlined and illustrates the main features found in the sedimentary basin: a GZW, lineations, a ridge with a close-by fault zone and channels. The general trend increasing water depth in SE direction is as obvious as the rugged basement and the basement flanks. Each feature of the model is discussed in the following analysis.
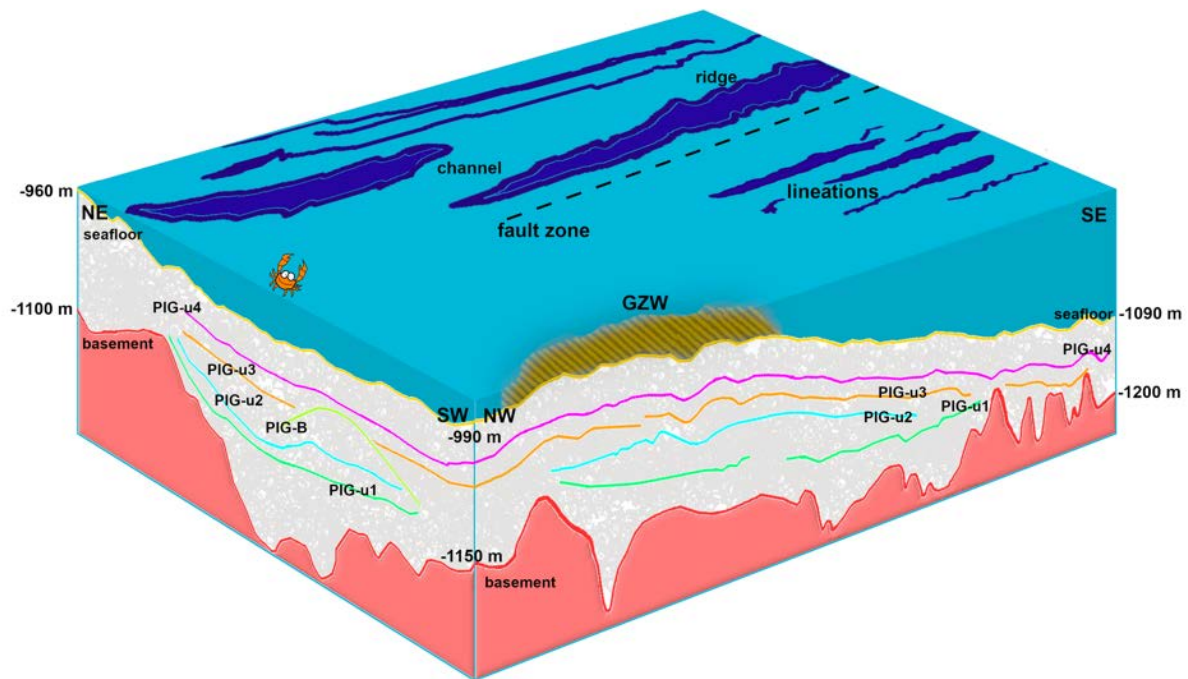
Fig. 34: Conceptual model of the isolated sedimentary basin. The left cross section represents a clipping of profile AWI-20170003 and the left cross section represents a clipping of profile AWI-20170001. The model shows morphological features on the seafloor, in the sedimentary basin and at the basement interface.

7.1. Grounding-zone wedge

Evidence for a grounding-zone wedge has been found in profile 20170001. The GZW becomes even more visible in the Parasound data, where an even reflection is visible below the wedge for the range of the GZW. This is remarkable, since the Parasound data for the sedimentary basin in general show almost no penetration into the seafloor.

Batchelor and Dowdeswell (2015) draw up an inventory for high-latitude GZWS, describing GZWs as "[…] asymmetric sedimentary depocentres which form through the rapid accumulation of glacigenic debris along a line-source at the grounding zone of marine-terminating ice sheets during still-stands in ice sheet retreat". GZWs indicate constraint vertical space under the floating ice shelf beyond the grounding zone. The wedge-shaped deposits are mainly composed of glacial diamict or till, which form at the grounding zone with high sediment flux. Thus, GZWs can indicate fast flowing ice streams. Diamict and till can either be emplaced directly from sedimentary beds at the grounding zone or be transported across the grounding line by subglacial meltwater channels. In their study, the researchers included all

found asymmetric wedges of sediment that are at least 1 km long and 10 m thick (Batchelor and Dowdeswell, 2015; Dowdeswell et al., 2008).

One characteristic feature of GZWs is their asymmetric appearance in ice flow direction with a steeper ice-distal side (Dowdeswell and Fugelli, 2012). This surely served as an identification feature in this case. Taking the sub-seafloor images as a starting point, the GZW seems to have a thickness of ~34 m at its thickest point and a length of at least ~5000 m. Dowdeswell and Fugelli (2012) compared several GWZs from Greenland and found at that the steeper ice-distal slope have angles between 1.8° and ~4°. However, the slopes of the ice proximal side are less steep and have angles between 0.3° and 0.7°. The GZW from the study area considered in the present study has significantly lower angles. The angle of the ice-distal slope is ~0.42° (the slope has a length of ~4600 m until the highest point with a height of ~34 m). The angle of the ice-proximal slope has not been calculated, as it is not clear where the end of the GZW lies. However, here the angle is very likely to be even lower. Though the hypothesis that this formation is, in fact, a GZW, seems more and more plausible, to be totally certain a sediment core would need to be collected, preferably from the point with the highest thickness of the wedge. In the literature it is often mentioned that till in the GZW represents a chaotic pattern in seismic reflection data (e.g. Batchelor and Dowdeswell (2015)). This cannot be seen in the seismic data at hand, as the uppermost layers cannot be resolved due to the mentioned multiples generated by reverberating seismic waves.

Close to the study area discussed in this thesis, Klages et al. (2015) mapped three GZWs at the cross-shelf Abbot Trough in the western Amundsen Sea, north of the inner PIB. The GZWs were found at the Abbot-Cosgrove paleo-ice stream. They were described as wedges with gently dipping slopes on the ice-proximal side and steeply deeping, sinuously-shaped ice-distal sides with lineations on top of the wedge. The GZWs have sizes of from $\geq \sim 25$ km–≥ 11 km–14 m to ~28 km–≥ 35 km–100 m. In the main Pine Island Trough, in the middle and outer shelf, five GZWs have already been mapped (e.g. Graham et al. (2010)). Klages et al. (2015) suggested that three of them could correlate with GZWs from Abbot Trough (since they have similar latitudes) and therefore indicate a stepped retreat in both troughs. The study involved the use of bathymetric grids with 35 m cell size, and the GZWs were very clearly visible. In the bathymetric grid with 100 m cell size, it is unfortunately impossible to resolve the wedge from the sedimentary basin. Klages et al. (2015) refer to the publication from Larter et al. (2014), where the authors described the morphological setting at the location from GZW5 in the PIT as a "bottle neck". This expression perfectly fits the setting of the analysed sedimentary basin as

well. The NW part of the basin is clearly much narrower than the SE main part of the basin at the position where the grounding zone wedge formed. Finally, it can be said that the GZW provides clear evidence for a standstill of the grounding zone in the sedimentary basin at this area. Most likely, only at this point of the ice front there was enough sediment available for the creation of a GZW.

7.2.　　Meltwater flow

Bathymetric maps, seismic reflection data and Parasound data indicate large drainage network in the Pine Island Bay. This network consists of many small but deep basins, which are usually connected through channels. Part of this network is the studied sedimentary basin. However, not only the sediment in the basin and the outcropping bedrock at the basin flanks are strongly incised, but the basement under the sediments is as well. As the model illustrates, the basement has deep incisions into bedrock. These incisions are most likely channels of former meltwater flow. The deepest incision was found in profile AWI-20170004 with ~90 m; most of the incisions cut between 20 and 50 m into the basement. However, it seems disputable that these deep incisions in the basement are just the result of meltwater flow. Also, the question about why the channels are at the same exact position as the deep basement incisions and not somewhere else is still open. One hypothesis could be that meltwater found its way in already existing weak points in the basement, which could have originated much earlier, maybe even during phases of tectonic activity. The meltwater then had starting points for initial scouring and eroding of the basement. Another theory, elaborated by Lowe and Anderson (2002), implies that some basins in PIB had initially eroded into the bedrock and have been later modified by meltwater flow.

Nitsche et al. (2013) mapped large parts of the drainage network in the Pine Island Trough to reconstruct flow directions. Most large channels are abundantly NW of the studied basin, while a few smaller channels can be found in and around the basin. The authors suggest that it is unlikely that large basins were completely filled meltwater, while it is more likely that they were partially filled with meltwater at the bottom and with ice above (Nitsche et al., 2013). While the existence of subglacial lakes harbouring meltwater is proven (e.g. Kuhn et al. (2017)), it still would not be sufficient to create a drainage network of this size.

7.3.   Sediments in the basin

The sediment inside the basin is mostly horizontally layered and units often onlap on the basin flanks at uprising basement. The in some cases over 300 m thick strata clearly point to a basin-wide vertical deposition. The most challenging questions are: how/why did the sediments end up in the basin? And when did they deposit there?

A hint of the characteristics of the sediments is that Parasound had no significantly low penetration in the seafloor in almost every profile, while at the GZW there was penetration of up to 35 m. One reason for this lack of penetration could be the compactness of the sediments as the ice sheet was laying on top, reducing hollow spaces and pores in the sediment, leading to less pore volume. The GZW, instead, is not as compressed, since the ice was not overriding. Observations on the low Parasound penetration in consolidated sediment have been made before. Nitsche et al. (2013) confirm presence of minimum thickness of unconsolidated sediments. The hard substrate of the outcropping basement at the sides of the sedimentary basin shows no penetration of Parasound at all. Nitsche et al. (2013) observed, for the area object of their study, that some basins and channels are characterised by significant channel infill (<5m), and that others are completely abandoned from unconsolidated sediments. This corresponds with the characterisation of the present study area. While a channel with sediment infill can be found in profile AWI-20170005, a channel without sediment infill can be observed in profile AWI-20170003. At the GZW, Parasound cannot resolve any internal structure, but a contrast in impedance is visible below the GZW in the Parasound data (cf. results of profile AWI-20170001). The assumption, then, is that most of the sediments which can be penetrated correspond to sands, silts and muds and have not been overridden by ice. Therefore, their origin is post-glacial. Turbidity currents or other mass wasting mechanisms could have contributed to the deposition of sediments in deeper basins by eroding and transporting material from shallower shelf areas or other channels (Nitsche et al., 2013).

During expedition PS104, several sediment cores have been taken with the MeBo70 seabed drill rig. One drill site in the studied basin was located at the crossing point of profile AWI-20170001 and AWI-20170005. The initial coring results describe the sediment core (drill depth 23.95 m, core length 23.75 m and core recovery 7.78 m) as consisting of brown and olive muds, sands and grey-olive diamictons (Gohl et al., 2017). First results at the AWI, Bremerhaven, showed that dateable microfossils are quite sparse. A comparable experience was made Kellogg and Kellogg (1987) as well, when they recovered one piston core DF85-107 close to the study area and two further piston cores. They characterized the core by very low abundances of

foraminifera and of both marine and non-marine diatoms, as well as by the absence of Radiolaria. Usually, core tops and cores were consisting of only a few specimens per sample or less.

Concerning the age of the sediments, it can be said that the upper sediment layers have most likely been eroded by the oscillating glacier. The question remains, whether the sediment were deposited pro-glacially or post-glacially as a result of meltwater flows. Death et al. (2006) modelled iceberg trajectories, sedimentation rates and meltwater input to the Norwegian-Greenland Sea from the Eurasian Ice Sheet during LGM. For the Norwegian Channel fan, the meltwater sedimentation rate is 24 mm kyr^{-1}, while the sedimentation rate from icebergs contributing to the Bear Island fan is 48 mm kyr^{-1}. A higher meltwater sedimentation rate was calculated from Knies et al. (2000) for the much smaller Franz Victoria Trough with 4-21 cm kyr^{-1}. Obviously, these locations differ completely from the West Antarctica location. Even though the meltwater sedimentation rate was one dimension bigger, it would never come close to >300 m thick sediment deposition due to meltwater in the isolated sedimentary basin of PIB. The significant structure PIG-B within the sediments of profile 20170003, also illustrated in the model, could indicate former ice flow at a point in time where there was less sediment deposited in the basin. It could possibly represent a sediment "ridge" with ice flow to both sides of the formation. A possible reason for the resistance against erosion could be the internal compactness of these consolidated sediments. The longitudinal axis has presumably the same direction of ice advance and retreat. However, this consideration is based on mere speculation, since this structure only appears in this single profile and no further indications of it were found in the basin.

At the beginning of profile AWI-20170001, a smaller basin is separated from the main basin through an increase of basement elevation; unit PIG-w2 represents the border between both parts of the basin. In the smaller basin, reflections show a chaotic pattern. In the results, platforms located on the western flank of the smaller basin have been described. These two features together could indicate that, during a phase of extension of the glacier (or just due to oscillation of the grounding zone), sediments from the basin could have been reworked and maybe even partially pushed up on the outcropping basement flank by the ice sheet. With a subsequent retreat of the ice sheet, most parts of the sediments lapsed back into the basin, unlayered and chaotic. A smaller fraction of the sediments, however, could have remained on the platforms, since the Parasound data indicate a quite thin cover of sediments.

7.4. Ice retreat

The number of paleogeological studies on the extent and subsequent retreat of the WAIS in the Amundsen Sea sector has remarkably increased during the last decade. There are several scientific clues for the retreat history of the WAIS on the outer and middle shelf since the LGM. However, the retreat history is unclear as far as the innermost shelf area is concerned. The closest location where ice retreat was dated is located close (NW) to the studied sedimentary basin and indicates that the ice retreat was largely complete with the beginning of Holocene at roughly 10 kyr B.P. at this point (Hillenbrand et al., 2013; Nitsche et al., 2013).

Evidence for interrupted ice retreat was found in the studied basin. The above explained GZW indicates a standstill of the grounding zone. In general, inner PIB is due to its outcropping hard, crystalline bedrock, an area with higher bed friction that slows down ice stream flow significantly. However, high amounts of subglacial meltwater can lubricate the paleo-ice stream bed and facilitate increased flow velocities over rugged bedrock, assuming that meltwater volume is sufficiently abundant to flow within both major channels and non-channelised areas. If meltwater flow had been limited to channels only, the shear stresses of bedrock should have been higher, forcing the ice flow to slacken off (Bell, 2008; Nitsche et al., 2013).

The form of the sedimentary basin, lineations and ridges on the seafloor, the orientation of the GZW and the downward sloping seafloor follow all the present retreat direction of the PIG.

Recent observations identified the incursion of relatively warm Circumpolar Deep Water beneath the Pine Island Glacier ice shelf (PIGIS). This intrusion is, amongst other factors, to hold accountable for a large mass imbalance of PIG and the reason for a reduced buttressing-effect of the grounded ice sheet, which resulted in increased ice flux (Muto et al., 2016; Pritchard et al., 2009).

Muto et al. (2016) dedicated a study to the investigation of seafloor topography and sediment distribution beneath PIGIS with an autonomous underwater vehicle and aerogravity data. They confirmed that the submarine ridge beneath PIGIS extends over the whole width (~45 km) of the ice shelf with no major deep troughs crossing it. This submarine ridge (height ~350 to 400 m) marks the transition from a thick sedimentary basin around the 2009 grounding line to a region, which includes the study area, where crystalline bedrock crops out and sediments are sparse. On the ice-proximal side of the ridge, models indicated that the sedimentary basin is up to 800 m thick and that ice could flow easily over it by sliding or sediment deposition (as opposed as the study area). Most likely, the ice retreat of PIG stabilized at the submarine ridge

as a pinning point. Based on this observation, Muto et al. (2016) support the hypothesis that further ice retreat was forced by changes in ocean circulation.

7.5. Origin of the basin

The origin of small sedimentary basins on the ASE is, for the most part, still unknown. In the seismic reflection profiles, evidence was found that tectonics could have played a role. At basin flanks of profiles AWI-20170004 and AWI-20170005, faults have been detected. In the model, the seafloor is marked by a dashed black line, which can possibly be interpreted as a fault zone. Said fault zone is parallel and close to a ridge of bedrock. In the seismic data, it is possible to see that the fault zone, the basement rise-up and the ridge stand in close connection. Tectonic activity could have initiated the creation of the basin and paleo-ice streams and/or meltwater flow could have scoured the basin further.

Another theory would be that the basin developed through an interaction between ice extension, ice retreat, ice stream flow and meltwater flow.

8. Conclusion

The investigation of an isolated sedimentary basin in the eastern Amundsen Sea provided powerful knowledge about the glacial history of the innermost Pine Island Bay, offshore Pine Island Glacier. Seismic reflection data from the RV Polarstern expedition PS104 (2017) paired with bathymetric and Parasound data revealed interesting characteristics of the subseafloor, sedimentation characteristics and the retreat history of the WAIS. Additionally, three seismic profiles recorded in 2010 during expedition ANTXXVI/3 were included in the interpretation of the study area. Identified units in the seismic reflection data enabled the creation of 2D-grids and of a conceptual model of the sedimentary basin. The characteristics of the seafloor and the crystalline bedrock play a major role in the interpretation of the region.

Besides seafloor and basement, several units in the basin have been identified. The most representative units are PIG-u1, PIG-u2, PIG-u3 and PIG-u4. They could be tracked in most seismic profiles of the basin and showed the depositional regime. The four units mostly lay parallelly to subparallelly in a horizontal orientation in the sediment body, with uprising course at the basin borders onlapping onto the basement. The basin is defined and surrounded by outcropping bedrock, which, in general, is not covered by sediments. Seismic reflection profile AWI-20170001 is equivalent to the longitudinal axis of the basin and shows a relatively smooth and homogeneous seafloor surface. However, the basement is rugged and incised (channels, scoured by meltwater flow). The basin dips in southern direction (direction of the grounding zone) and sediment cover gets thinner. The profiles, which cross the main profile and run more or less parallelly to the ice retreat, show very deep incisions (up to 90 m, but mostly 25 m to 60 m) into the basement and relatively steep basin flanks. The highest points in the seismic profile can be found in profile AWI-20170005, where they rise from a water depth of ~1070 m in the central part of the basin to a water depth of ~900 m at the flanks. Sediment cover reaches its maximum thickness with up to 300 m of sediments in the same profile. Normal faults have been identified at steep basin flanks, which could imply tectonic activity at some point of the origination process of the basin.

The most prominent formation in the study area is a grounding zone wedge, which is located on the seafloor of profile AWI-20170001. With Parasound data, its maximum height of ~34 m and length of at least 5000 m could be determined. The ice-distal, steeper slope of the GZW has an angle of ~0,42°. The GZW indicates glacier standstill at this part. The outcropping bedrock around the basin most probably decreased the ice flow velocity due to the high basal friction (Nitsche et al., 2013).

It can be suggested that the sediments in the basin have been strongly consolidated during a time when the ice sheet was grounded in the basin. Evidence for this suggestion was, amongst other things, that Parasound had no penetration in most parts of the basin, but it penetrated the grounding zone wedge and a small post-glacial channel in the sedimentary basin, which both represent less consolidated depositions.

All in all, the investigation of the sedimentary basin was successful. The seismic processing was not straightforward due to several ghosts from side reflections in the sedimentary basin, but in the end it was possible to obtain well interpretable seismic profiles. A starting point for future work in the study area would be to resolve the GZW in a bathymetric map, in order to confirm the discovery. Further on, sediment cores from the consolidated sediments in the basement and the internal structure of the GZW would provide useful information for further classification of the sedimentary basin in the retreat history of the Pine Island Glacier. An age determination for the sediments would also be extremely important to better understand the depositional regime. Of course, the spatial resolution of the basin would be highly improved if more seismic lines were added to carry out a real 3D survey in the sedimentary basin.

9. Literature

Abrahamsen, E., 2012, Oceanographic conditions beneath Fimbul Ice Shelf, Antarctica.

Assmann, K. M., Jenkins, A., Shoosmith, D. R., Walker, D. P., Jacobs, S. S., and Nicholls, K. W., 2013, Variability of Circumpolar Deep Water transport onto the Amundsen Sea Continental shelf through a shelf break trough: Journal of Geophysical Research: Oceans, v. 118, no. 12, p. 6603-6620.

Batchelor, C. L., and Dowdeswell, J. A., 2015, Ice-sheet grounding-zone wedges (GZWs) on high-latitude continental margins: Marine Geology, v. 363, p. 65-92.

Dalziel, I. W. D., 1992, ANTARCTICA; A TALE OF TWO SUPERCONTINENTS?: Annual Review of Earth and Planetary Sciences, v. 20, no. 1, p. 501-526.

Dalziel, I. W. D., and Lawver, L. A., 2001, The Lithospheric Setting of the West Antarctic Ice Sheet: The West Antarctic Ice Sheet: Behavior and Environment, p. 29-44.

Death, R., Siegert, M. J., Bigg, G. R., and Wadley, M. R., 2006, Modelling iceberg trajectories, sedimentation rates and meltwater input to the ocean from the Eurasian Ice Sheet at the Last Glacial Maximum: Palaeogeography, Palaeoclimatology, Palaeoecology, v. 236, no. 1, p. 135-150.

DeConto, R., and Pollard, D., 2016, Contribution of Antarctica to past and future sea-level rise: Nature, v. 531, p. 591-597.

Dowdeswell, J. A., and Fugelli, E. M. G., 2012, The seismic architecture and geometry of grounding-zone wedges formed at the marine margins of past ice sheets: Bulletin of the Geological Society of America, v. 124, no. 11-12, p. 1750-1761.

Dowdeswell, J. A., Ottesen, D., Evans, J., Cofaigh, C. Ó., and Anderson, J. B., 2008, Submarine glacial landforms and rates of ice-stream collapse: Geology, v. 36, no. 10, p. 819-822.

Gohl, K., Tectonic and sedimentation processes of West Antarctica and the southern Pacific and their relationship to glacial history2015.

Gohl, K., Freudenthal, T., Hillenbrand, C.-D., Klages, J., Larter, R., Bickert, T., Bohaty, S., Ehrmann, W., Esper, O., Frederichs, T., Gebhardt, C., Küssner, K., Kuhn, G., Pälike, H., Ronge, T., Simões Pereira, P., Smith, J., Uenzelmann-Neben, G., van de Flierdt, C., and PS104, t. S. T. o. E., 2017, MeBo70 Seabed Drilling on a Polar Continental Shelf: Operational Report and Lessons From Drilling in the Amundsen Sea Embayment of West Antarctica: Geochemistry, Geophysics, Geosystems, v. 18, no. 11, p. 4235-4250.

Gohl, K., Uenzelmann-Neben, G., Larter, R. D., Hillenbrand, C.-D., Hochmuth, K., Kalberg, T., Weigelt, E., Davy, B., Kuhn, G., and Nitsche, F. O., 2013, Seismic stratigraphic record of the Amundsen Sea Embayment shelf from pre-glacial to recent times: Evidence for a dynamic West Antarctic ice sheet: Marine Geology, v. 344, p. 115-131.

Gohl, K. a. o. c. p., 2017, The Expedition PS104 of the Research Vessel POLARSTERN to the Amundsen Sea in 2017: Reports on Polar and Marine Research, v. 712.

Graham, A. G. C., Larter, R. D., Gohl, K., Dowdeswell, J. A., Hillenbrand, C.-D., Smith, J. A., Evans, J., Kuhn, G., and Deen, T., 2010, Flow and retreat of the Late Quaternary Pine Island-Thwaites palaeo-ice stream, West Antarctica: Journal of Geophysical Research: Earth Surface, v. 115, no. F3.

Hillenbrand, C.-D., Kuhn, G., Smith, J. A., Gohl, K., Graham, A. G. C., Larter, R. D., Klages, J. P., Downey, R., Moreton, S. G., Forwick, M., and Vaughan, D. G.,

2013, Grounding-line retreat of the West Antarctic Ice Sheet from inner Pine Island Bay: Geology, v. 41, no. 1, p. 35-38.

Hughes, T. J., 1981, The weak underbelly of the West Antarctic ice sheet: Journal of Glaciology, v. 27, no. 97, p. 518-525.

Hulbe, C., 2017, Is ice sheet collapse in West Antarctica unstoppable?: Science, v. 356, no. 6341, p. 910.

Joughin, I., and Alley, R. B., 2011, Stability of the West Antarctic ice sheet in a warming world: Nature Geoscience, v. 4, no. 8, p. 506-513.

Kellogg, D. E., and Kellogg, T. B., 1987, Microfossil distributions in modern Amundsen Sea sediments: Marine Micropaleontology, v. 12, p. 203-222.

Kimura, S., Jenkins, A., Regan, H., Holland, P. R., Assmann, K. M., Whitt, D. B., Van Wessem, M., van de Berg, W. J., Reijmer, C. H., and Dutrieux, P., 2017, Oceanographic Controls on the Variability of Ice-Shelf Basal Melting and Circulation of Glacial Meltwater in the Amundsen Sea Embayment, Antarctica: Journal of Geophysical Research: Oceans, v. 122, no. 12, p. 10131-10155.

Klages, J. P., Kuhn, G., Graham, A., Hillenbrand, C. D., Smith, J., Nitsche, F., Larter, R. D., and Gohl, K., 2015, Palaeo-ice stream pathways and retreat style in the easternmost Amundsen Sea Embayment, West Antarctica, revealed by combined multibeam bathymetric and seismic data: Geomorphology, v. 245.

Klages, J. P., Kuhn, G., Hillenbrand, C. D., Graham, A. G. C., Smith, J. A., Larter, R. D., and Gohl, K., 2013, First geomorphological record and glacial history of an inter-ice stream ridge on the West Antarctic continental shelf: Quaternary Science Reviews, v. 61, p. 47-61.

Knies, J., Nowaczyk, N., Müller, C., Vogt, C., and Stein, R., 2000, A multiproxy approach to reconstruct the environmental changes along the Eurasian continental margin over the last 150 000 years: Marine Geology, v. 163, no. 1, p. 317-344.

Kuhn, G., Hillenbrand, C.-D., Kasten, S., Smith, J. A., Nitsche, F. O., Frederichs, T., Wiers, S., Ehrmann, W., Klages, J. P., and Mogollón, J. M., 2017, Evidence for a palaeo-subglacial lake on the Antarctic continental shelf: Nature Communications, v. 8, no. 1, p. 15591.

Larter, R. D., Anderson, J. B., Graham, A. G. C., Gohl, K., Hillenbrand, C.-D., Jakobsson, M., Johnson, J. S., Kuhn, G., Nitsche, F. O., Smith, J. A., Witus, A. E., Bentley, M. J., Dowdeswell, J. A., Ehrmann, W., Klages, J. P., Lindow, J., Cofaigh, C. Ó., and Spiegel, C., 2014, Reconstruction of changes in the Amundsen Sea and Bellingshausen Sea sector of the West Antarctic Ice Sheet since the Last Glacial Maximum: Quaternary Science Reviews, v. 100, p. 55-86.

Lawver, L. A., and Gahagan, L. M., 2003, Evolution of Cenozoic seaways in the circum-Antarctic region: Palaeogeography, Palaeoclimatology, Palaeoecology, v. 198, no. 1, p. 11-37.

Lindeque, A., Gohl, K., Henrys, S., Wobbe, F., and Davy, B., 2016, Seismic stratigraphy along the Amundsen Sea to Ross Sea continental rise: A cross-regional record of pre-glacial to glacial processes of the West Antarctic margin: Palaeogeography, Palaeoclimatology, Palaeoecology, v. 443, p. 183-202.

Lowe, A. L., and Anderson, J. B., 2002, Reconstruction of the West Antarctic ice sheet in Pine Island Bay during the Last Glacial Maximum and its subsequent retreat history: Quaternary Science Reviews, v. 21, no. 16, p. 1879-1897.

Lythe, M., Vaughan, D., and Consortium, B., 2001, BEDMAP: A new ice thickness and subglacial topographic model of Antarctica: Journal of Geophysical Research, v. 106, p. 11335-11352.

Martinson, D., 2011, Antarctic circumpolar current's role in the Antarctic ice system: An overview: Palaeogeography Palaeoclimatology Palaeoecology - PALAEOGEOGR PALAEOCLIMATOL, v. 335.

Matsuoka, K., Skoglund, A., and Roth, G., 2018, Quantarctica [Data Set]. Norwegian Polar Institute.

Nitsche, F. O., Gohl, K., Larter, R. D., Hillenbrand, C. D., Kuhn, G., Smith, J. A., Jacobs, S., Anderson, J. B., and Jakobsson, M., 2013, Paleo ice flow and subglacial meltwater dynamics in Pine Island Bay, West Antarctica: The Cryosphere, v. 7, no. 1, p. 249-262.

Nitsche, F. O., Jacobs, S. S., Larter, R. D., and Gohl, K., 2007, Bathymetry of the Amundsen Sea continental shelf: Implications for geology, oceanography, and glaciology: Geochemistry, Geophysics, Geosystems, v. 8, no. 10.

Payne, A. J., Vieli, A., Shepherd, A. P., Wingham, D. J., and Rignot, E., 2004, Recent dramatic thinning of largest West Antarctic ice stream triggered by oceans: Geophysical Research Letters, v. 31, no. 23.

Pritchard, H., Arthern, R., Vaughan, D., and Edwards, L., 2009, Extensive dynamic thinning on the margins of the Greenland and Antarctic Ice Sheets: Nature, v. 461, p. 971-975.

Rignot, E., Mouginot, J., and Scheuchl, B., 2011, Antarctic grounding line mapping from differential satellite radar interferometry: Geophysical Research Letters, v. 38, no. 10.

Scheuer, C., Gohl, K., and Eagles, G., 2006, Gridded isopach maps from the South Pacific and their use in interpreting the sedimentation history of the West Antarctic continental margin: Geochemistry, Geophysics, Geosystems, v. 7, no. 11.

Schoof, C., 2007, Marine ice-sheet dynamics. Part 1. The case of rapid sliding: Journal of Fluid Mechanics, v. 573, p. 27-55.

Siddoway, C. S., 2007, Tectonics of the West Antarctic rift system: new light on the history and dynamics of distributed intracontinental extension, 2007-1047-KP-09.

Siegert, M. J., 2008, Antarctic subglacial topography and ice-sheet evolution: Earth Surface Processes and Landforms, v. 33, no. 4, p. 646-660.

Storey, B. C., Dalziel, I. W. D., Garrett, S. W., Grunow, A. M., Pankhurst, R. J., and Vennum, W. R., 1988, West Antarctica in Gondwanaland: Crustal blocks, reconstruction and breakup processes: Tectonophysics, v. 155, no. 1, p. 381-390.

Uenzelmann-Neben, G., and Gohl, K., 2014, Early Miocene glaciation in the Amundsen Sea, Southern Pacific: a Study of the distribution of sedimentary sequences.

Uenzelmann-Neben, G., Gohl, K., Larter, R., and Schlüter, P., 2007, Differences in ice retreat across Pine Island Bay, West Antarctica, since the Last Glacial Maximum: Indications from multichannel seismic reflection data: Short Research Paper USGS Open-File Report Short Research Paper, v. 084.

Vaughan, D., Marshall, G., Connolley, W., Parkinson, C., Mulvaney, R., Hodgson, D., King, J., Pudsey, C., and Turner, J., 2003, Recent Rapid Regional Climate Warming on the Antarctic Peninsula: Climatic Change, v. 60, p. 243-274.

Veevers, J. J., 2012, Reconstructions before rifting and drifting reveal the geological connections between Antarctica and its conjugates in Gondwanaland: Earth-Science Reviews, v. 111, no. 3, p. 249-318.

Yilmaz, Ö., 1987, Seismic Data Processing, Society of Exploration Geophysicists.

-, 2001, Seismic Data Analysis, Society of Exploration Geophysicists.

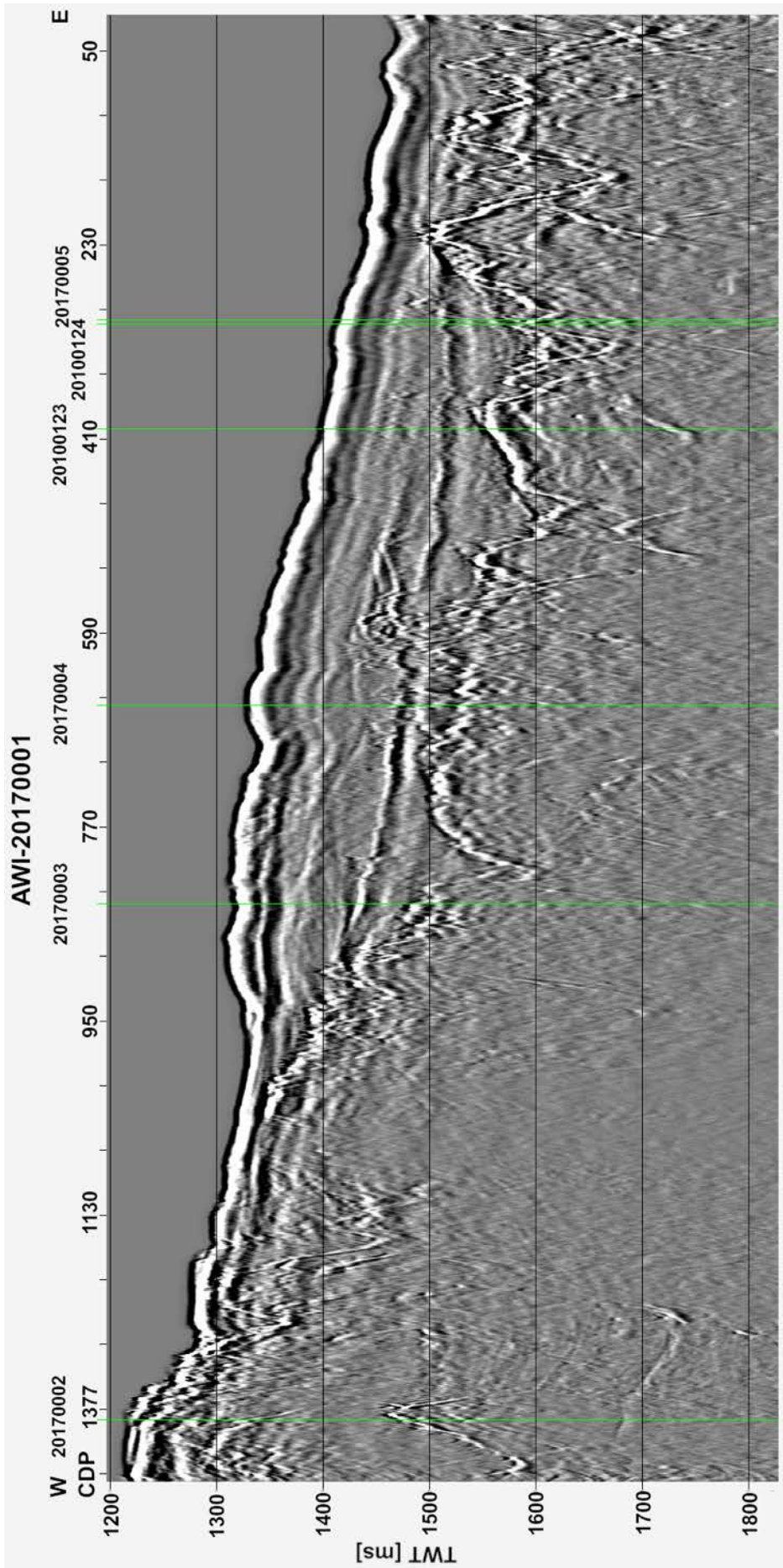Paradigm ® 17 Manual. Paradigm Ltd. Houston. Accessed June 2020

10. Appendix
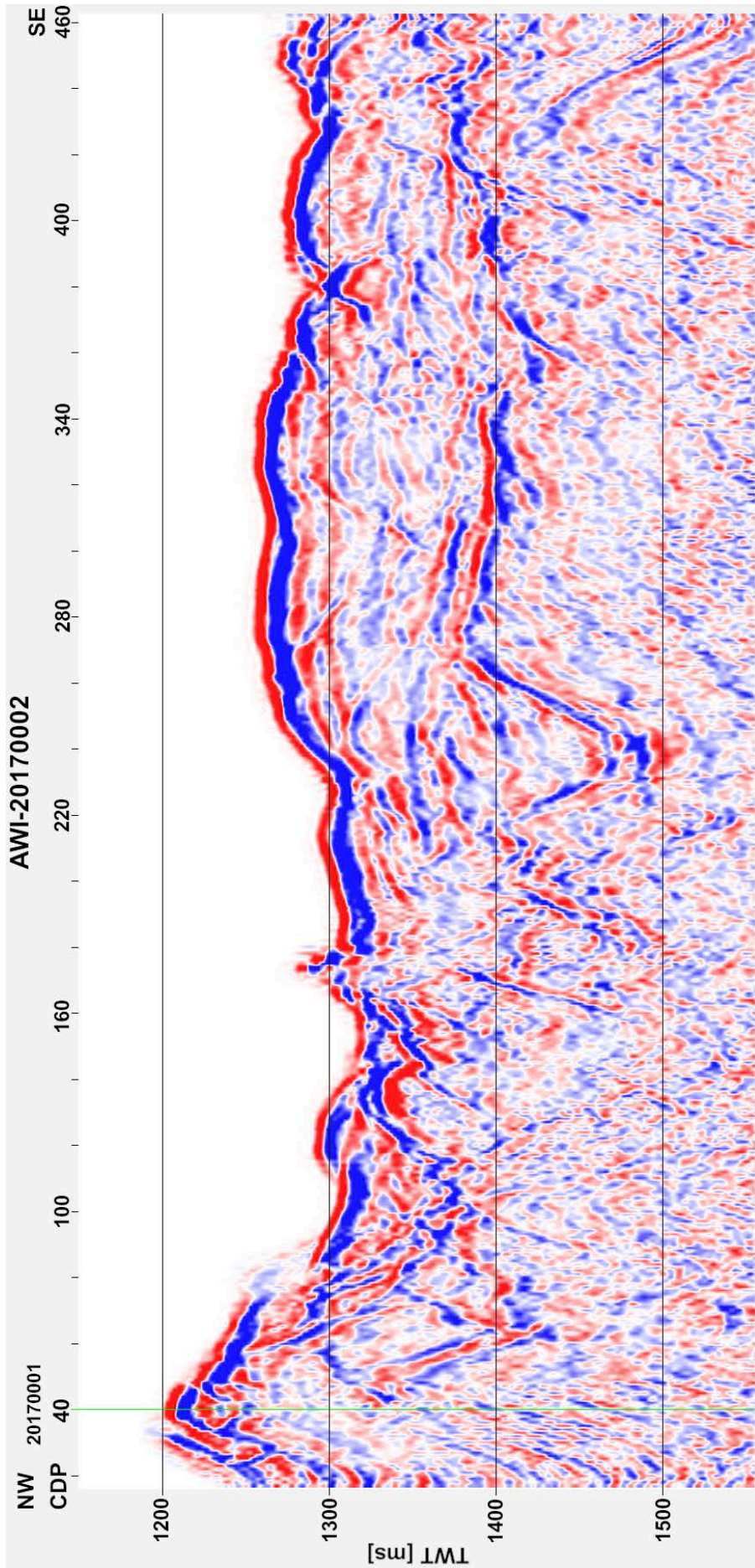
10.1. Enlarged results of the seismic processing
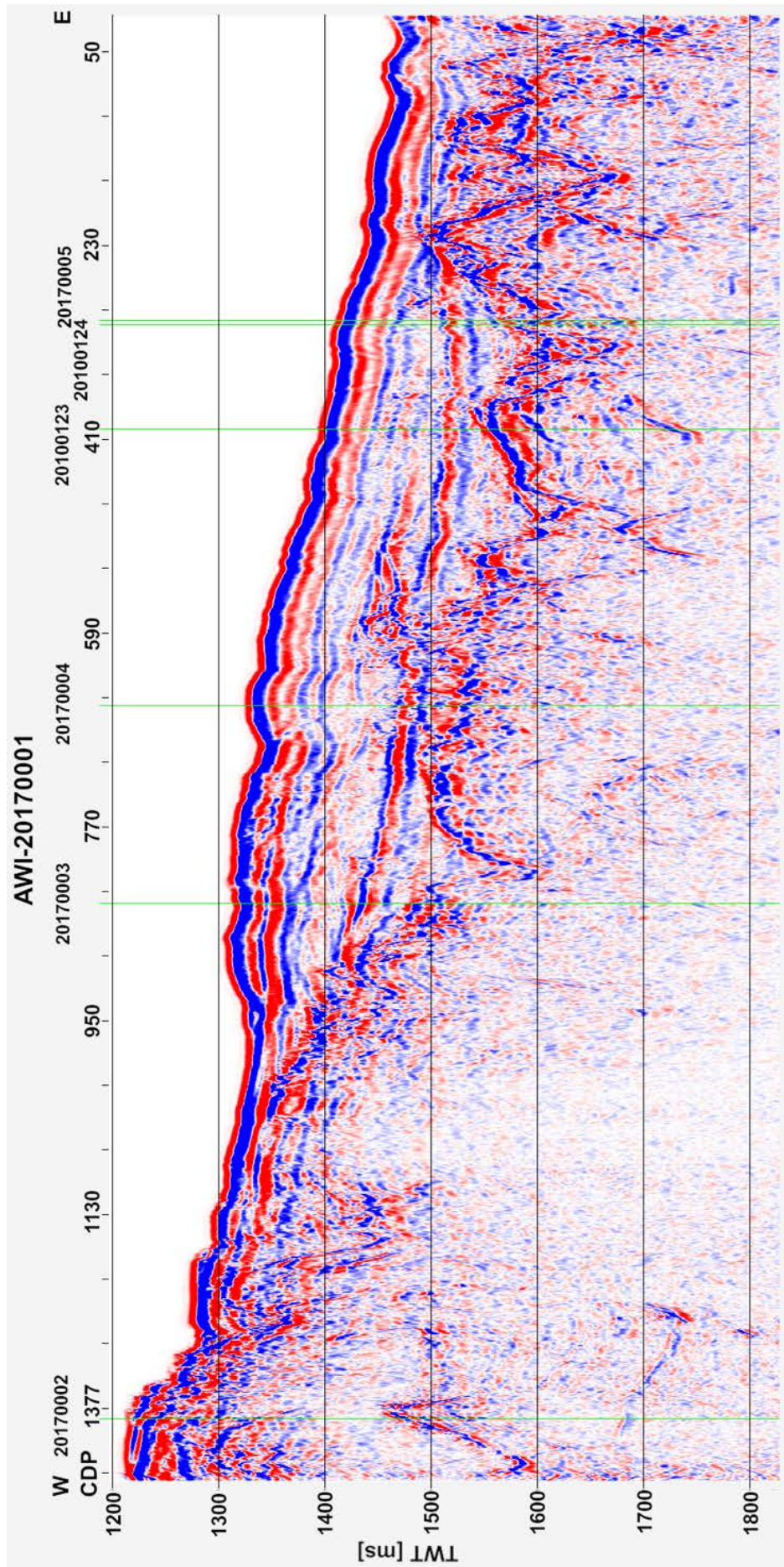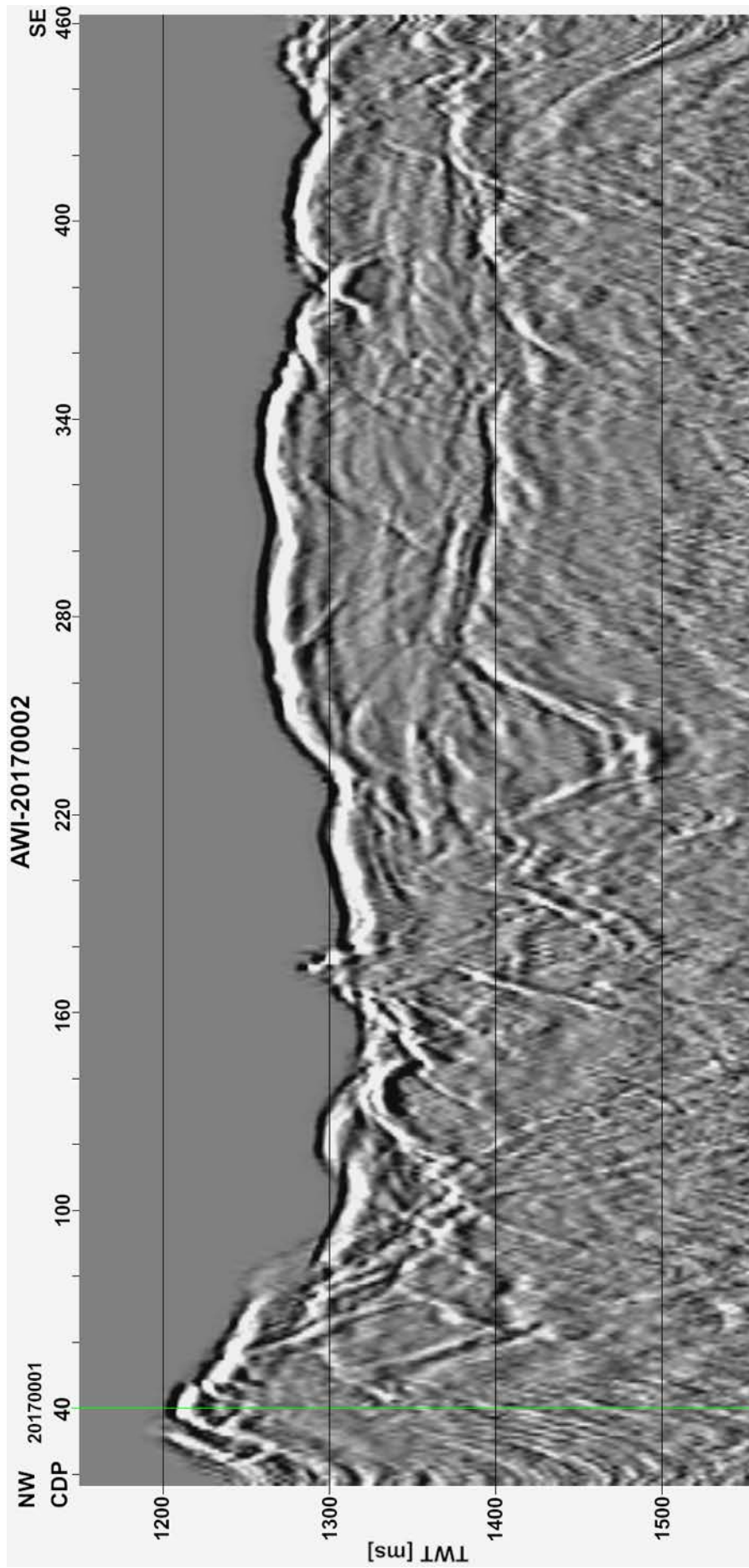
A. 1: Processed seismic profile AWI-20170001.

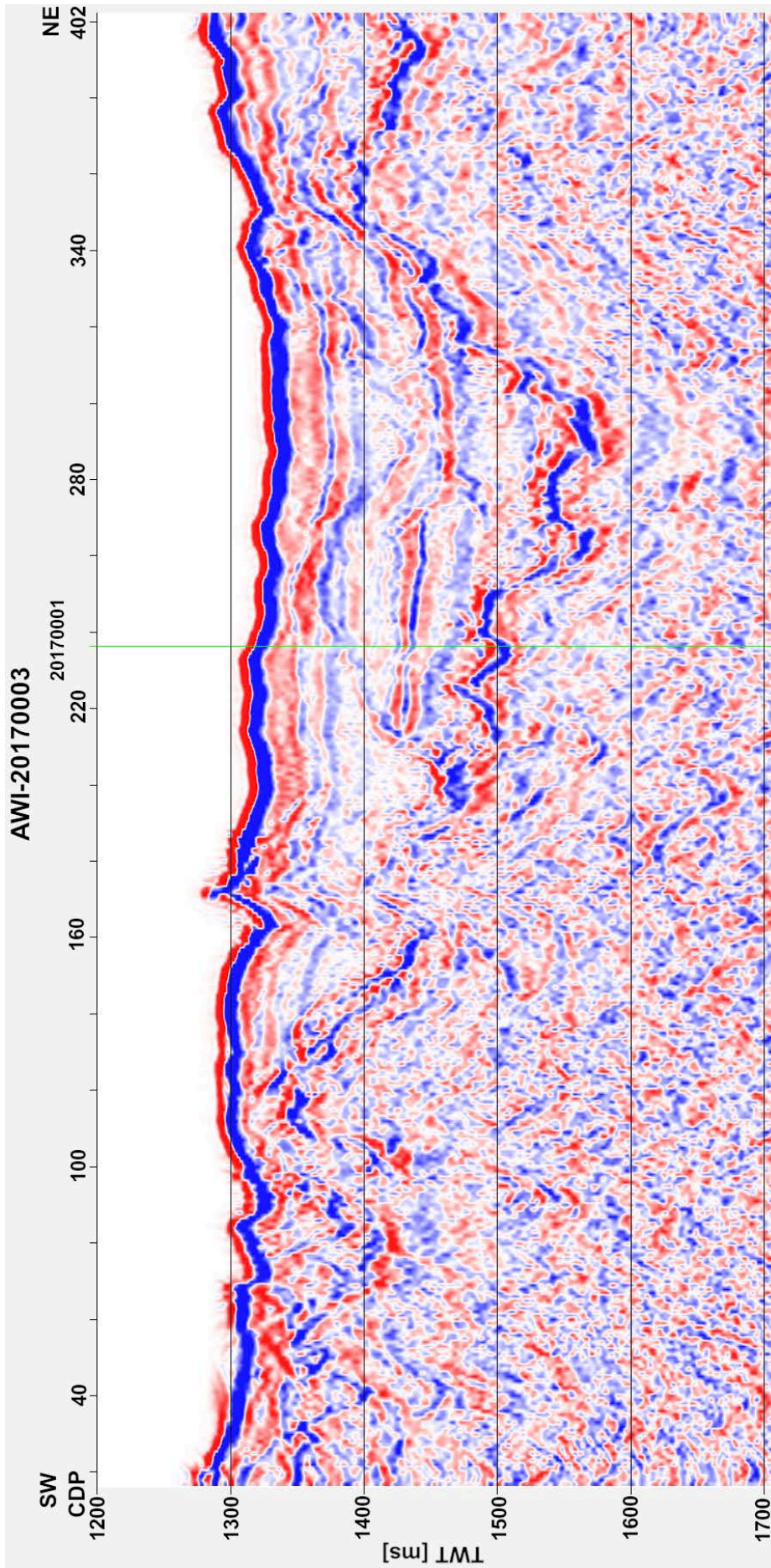*A. 2: Processed seismic profile AWI-20170001.*

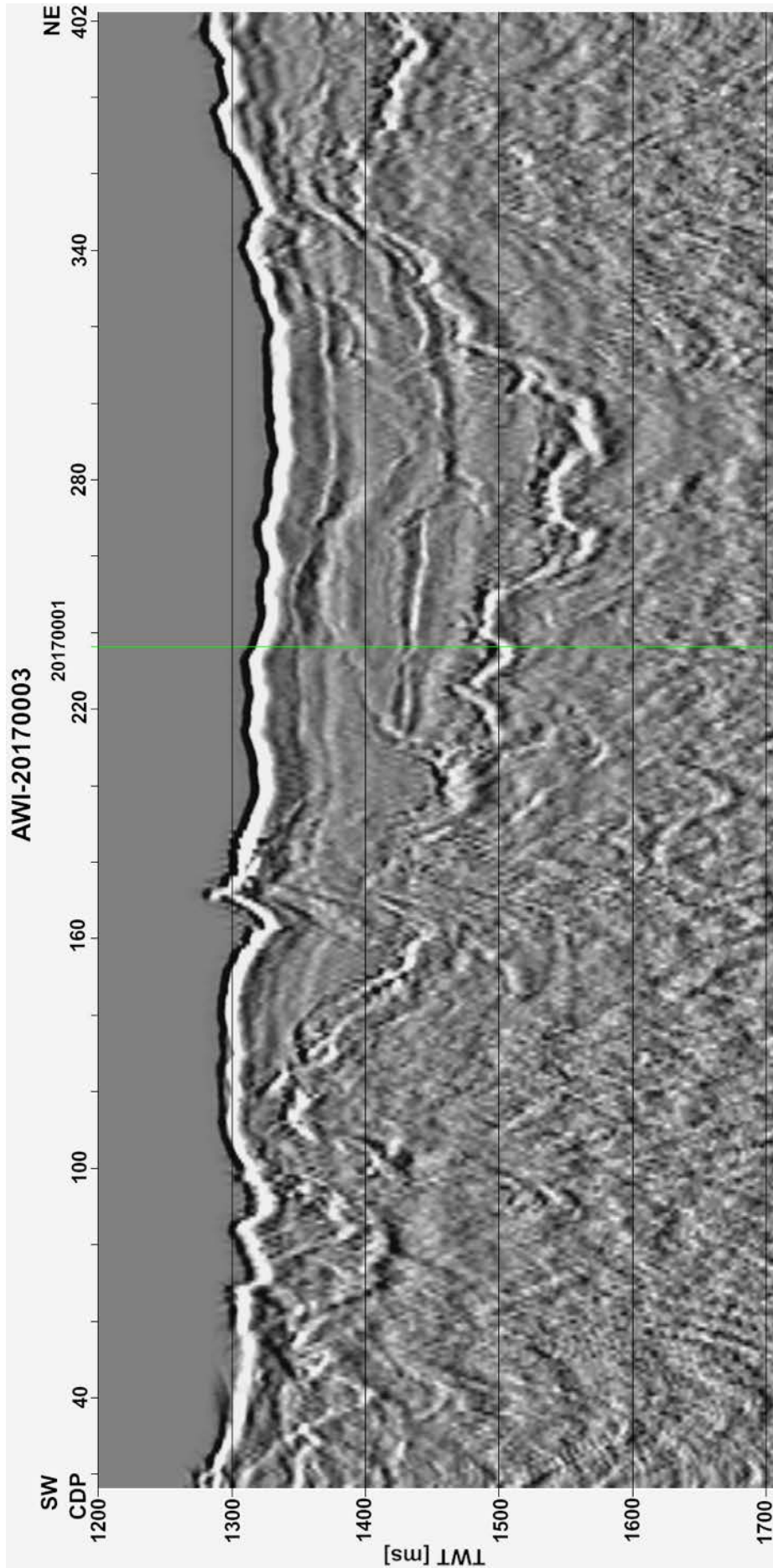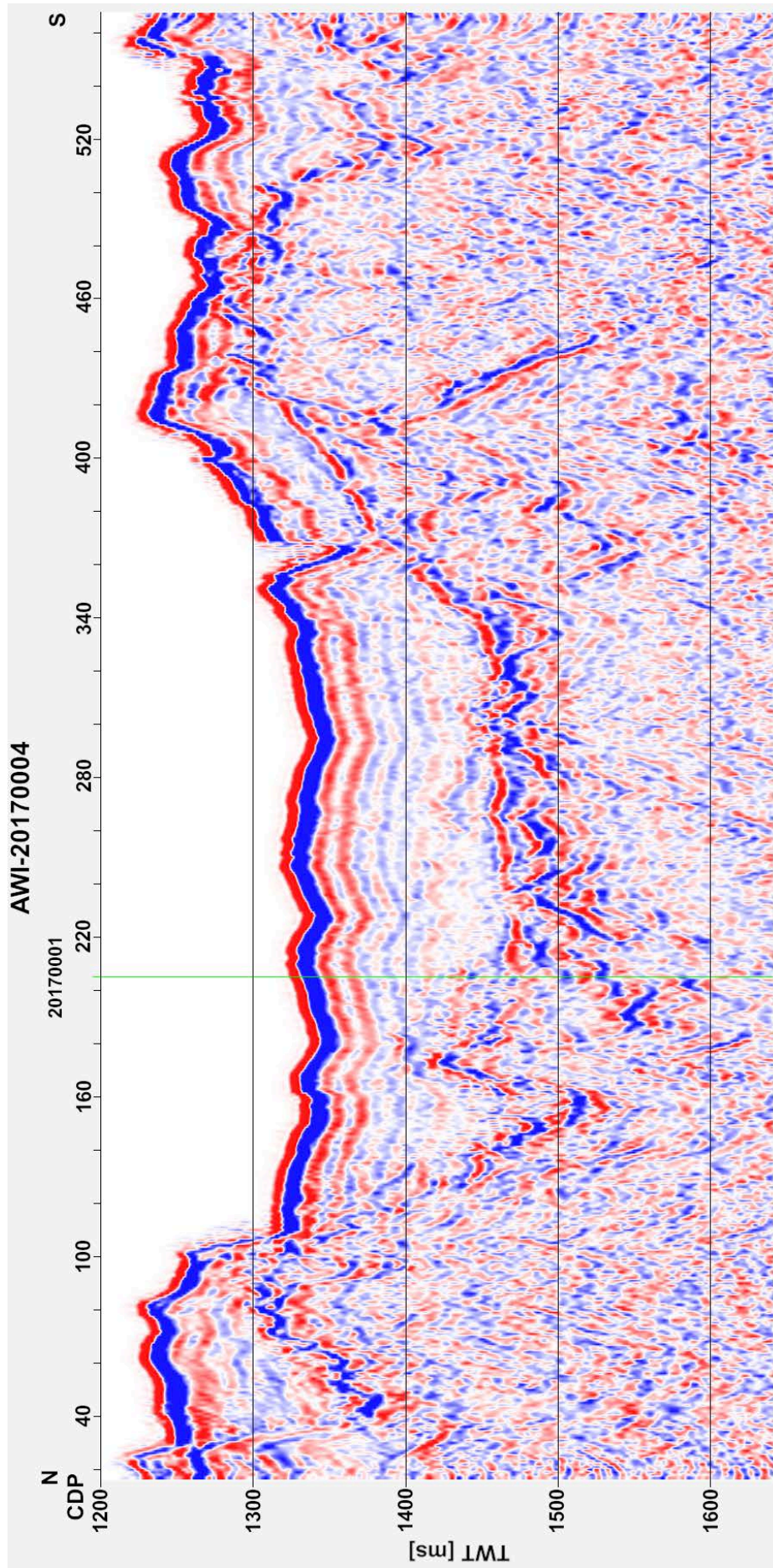*A. 3: Processed seismic profile AWI-20170002.*
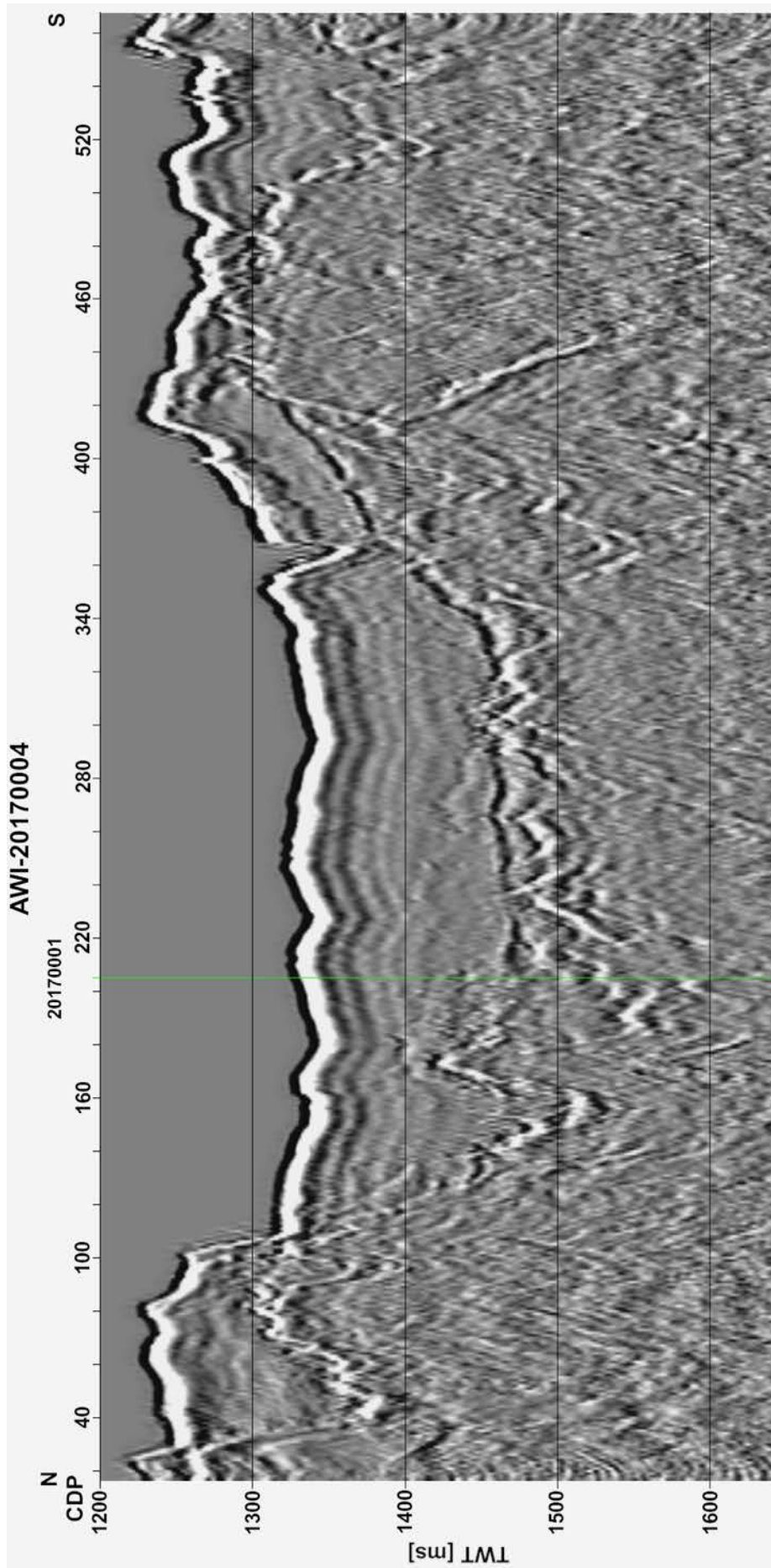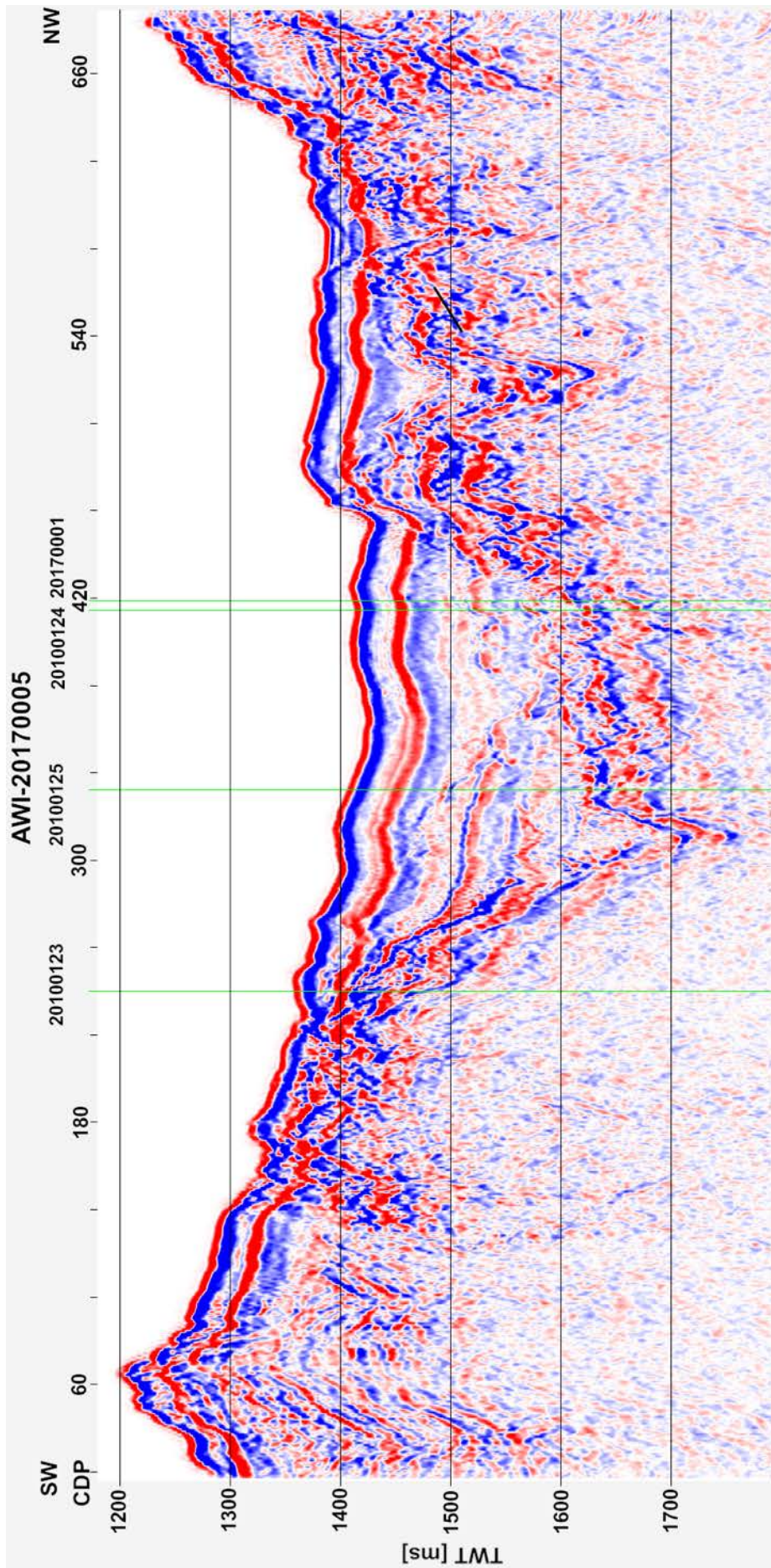
A. 4: Processed seismic profile AWI-20170002.

A. 5: Processed seismic profile AWI-20170003.
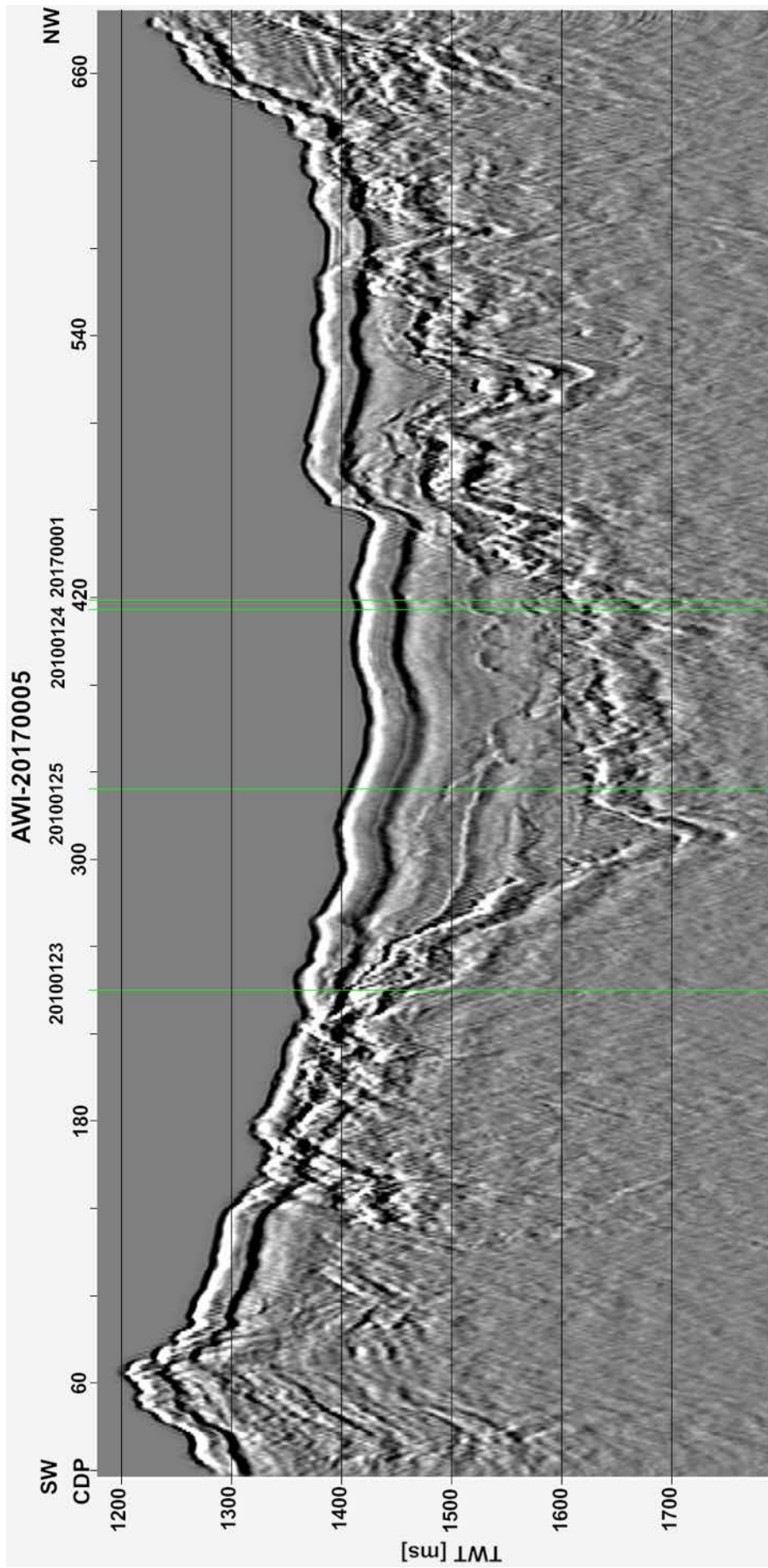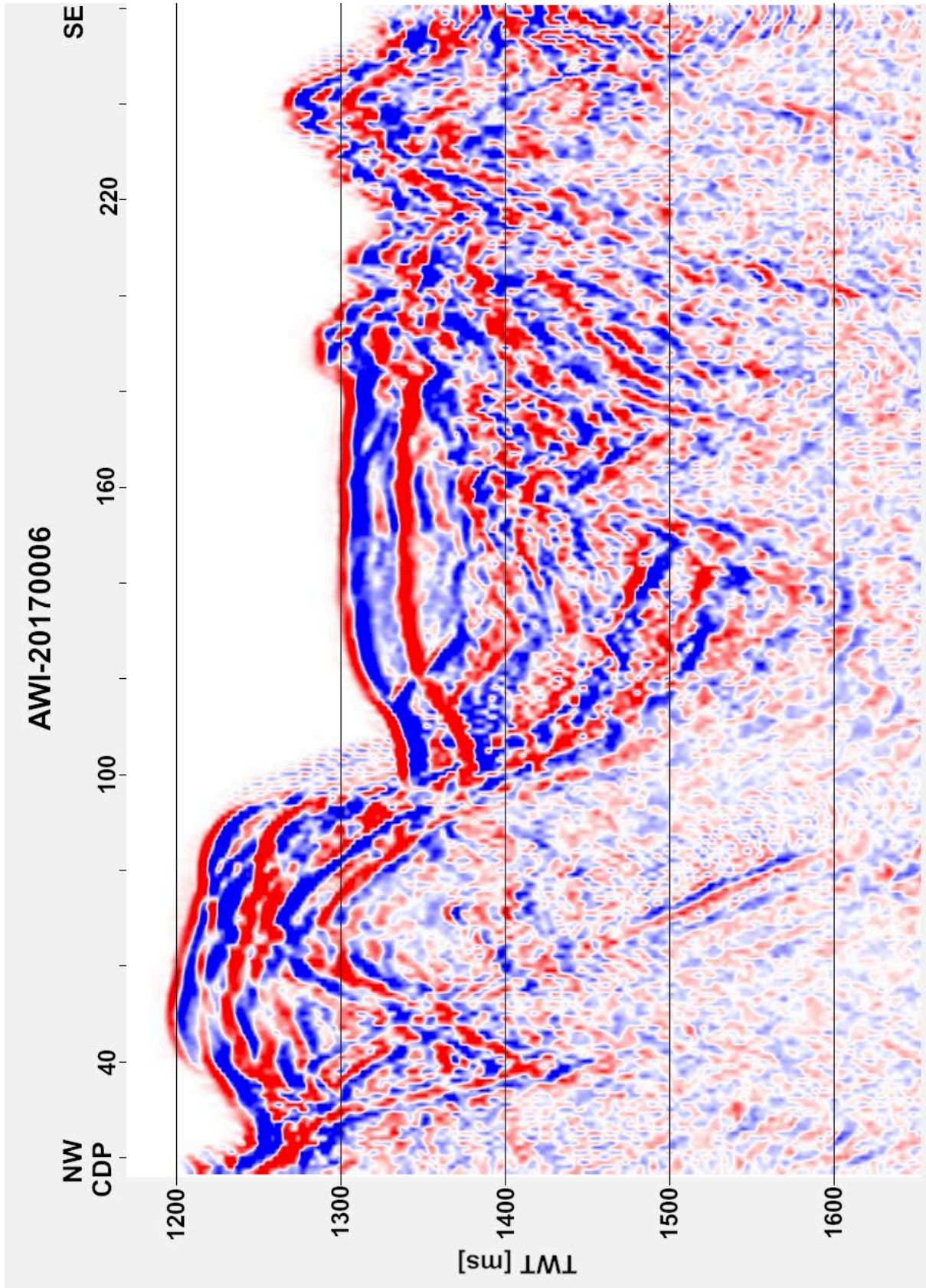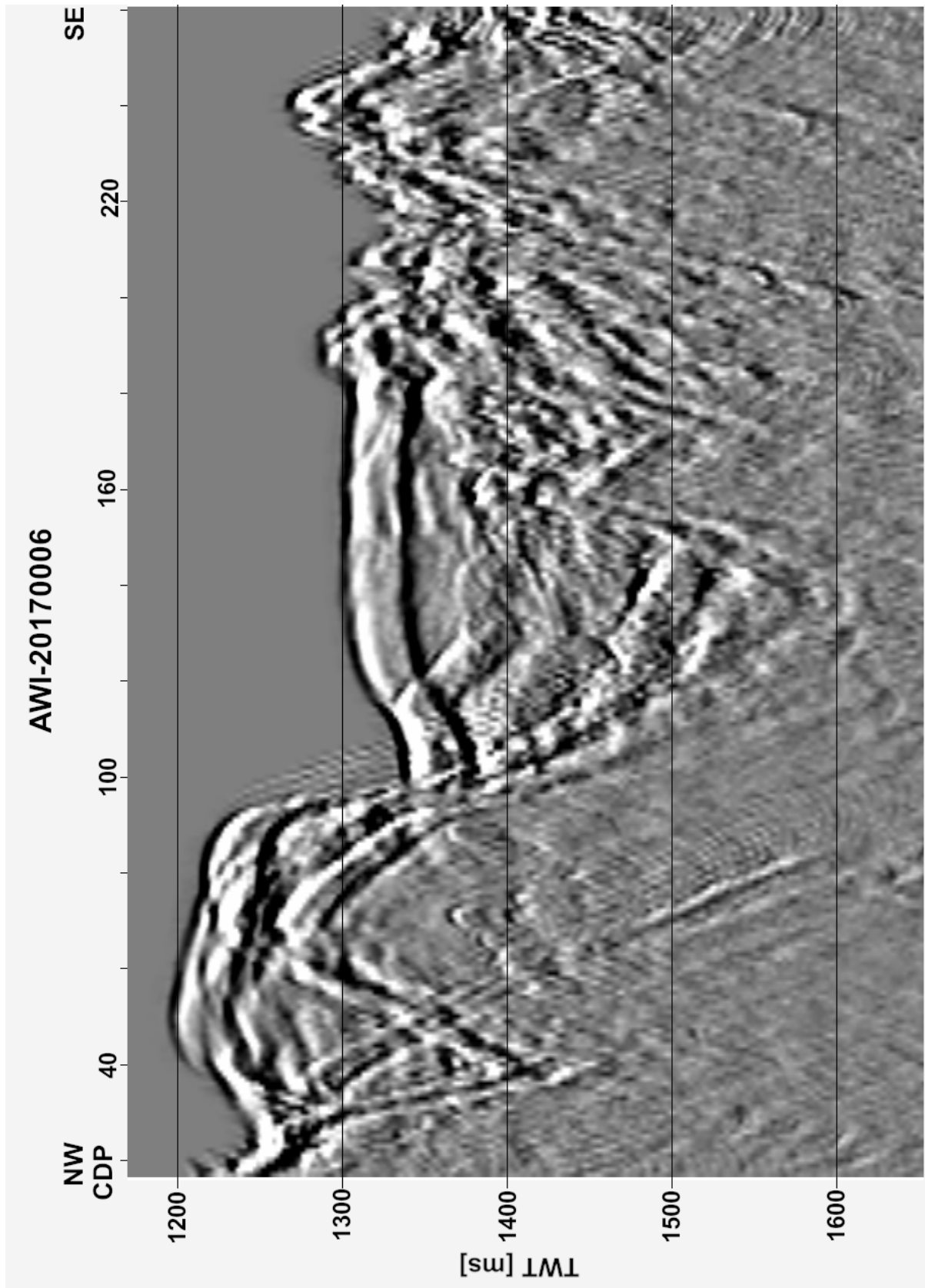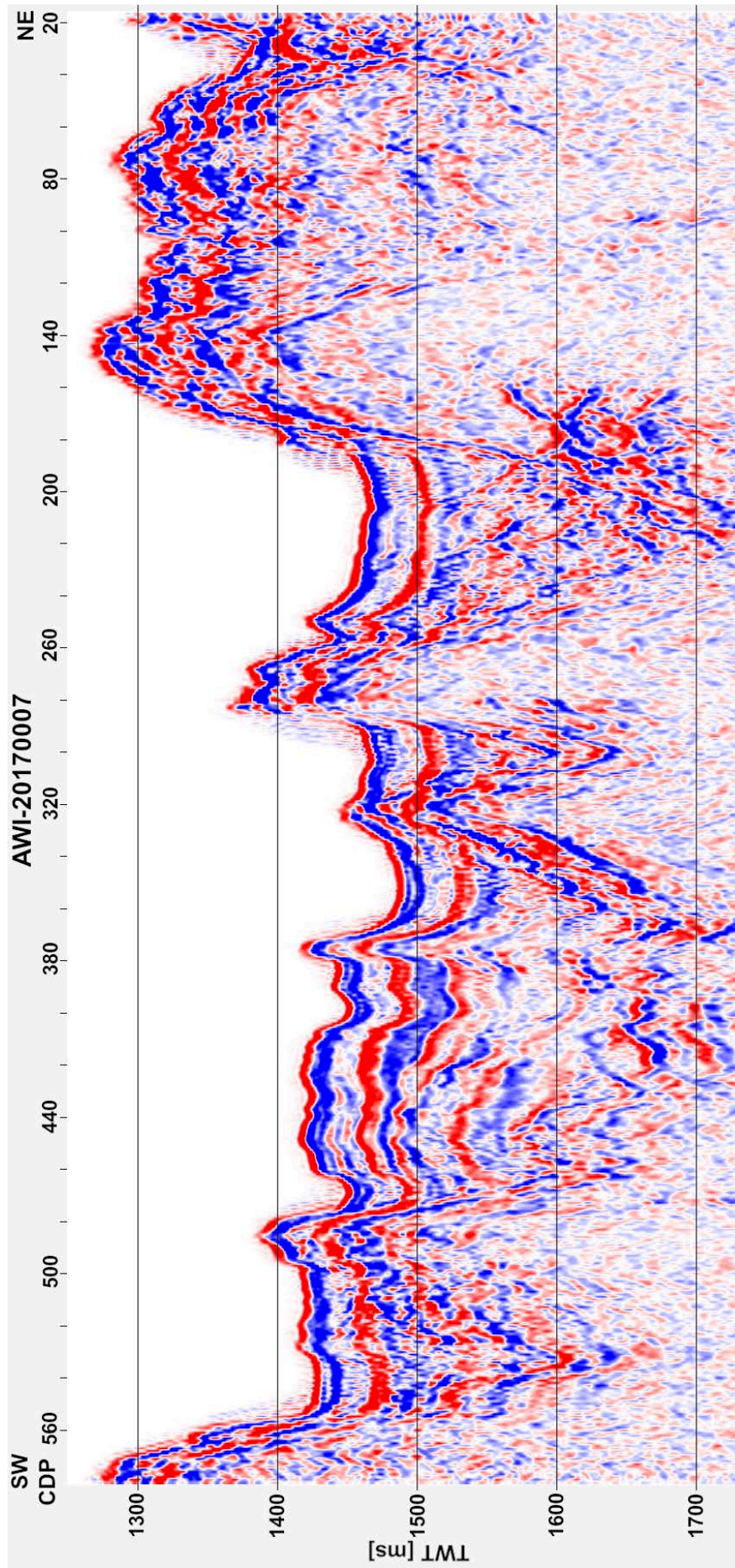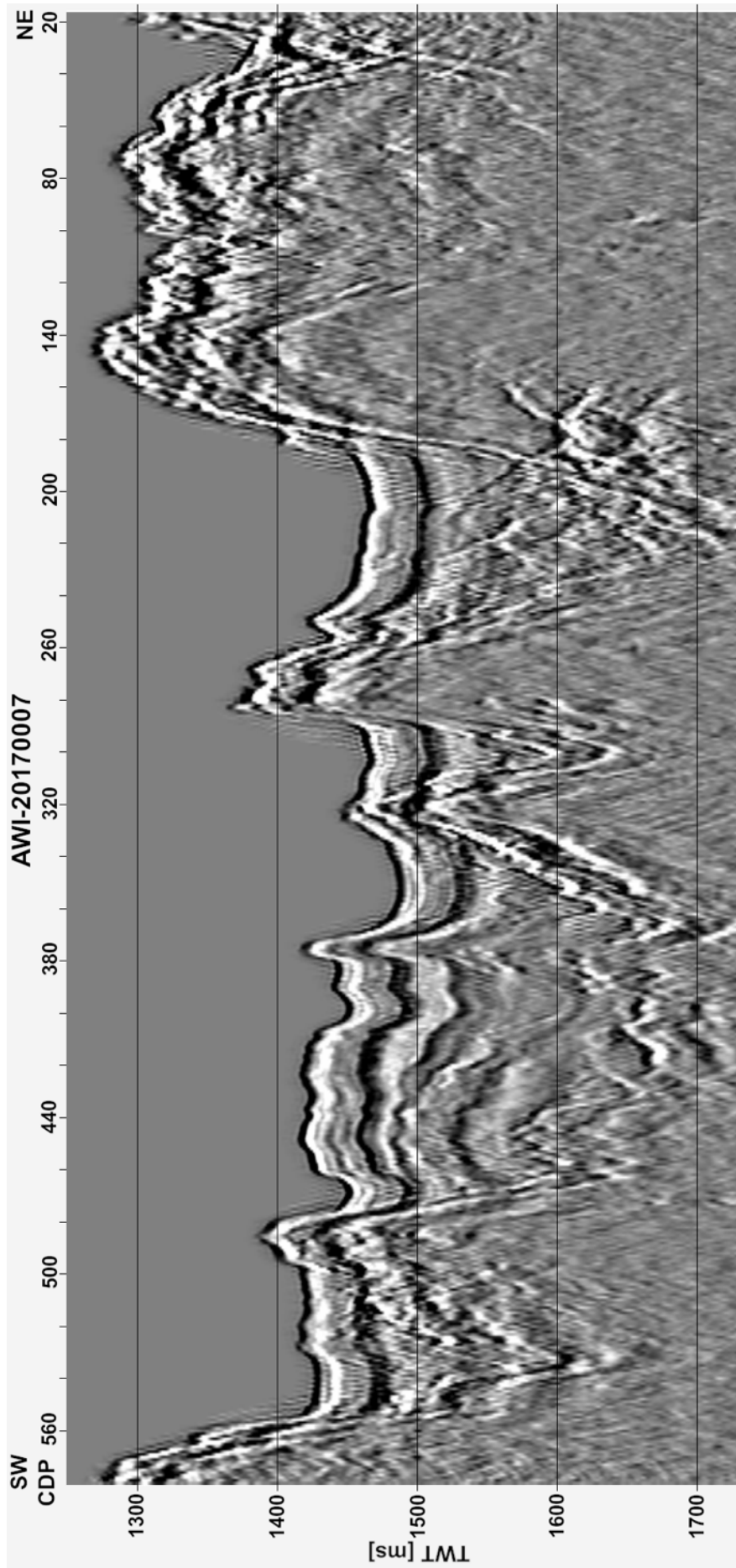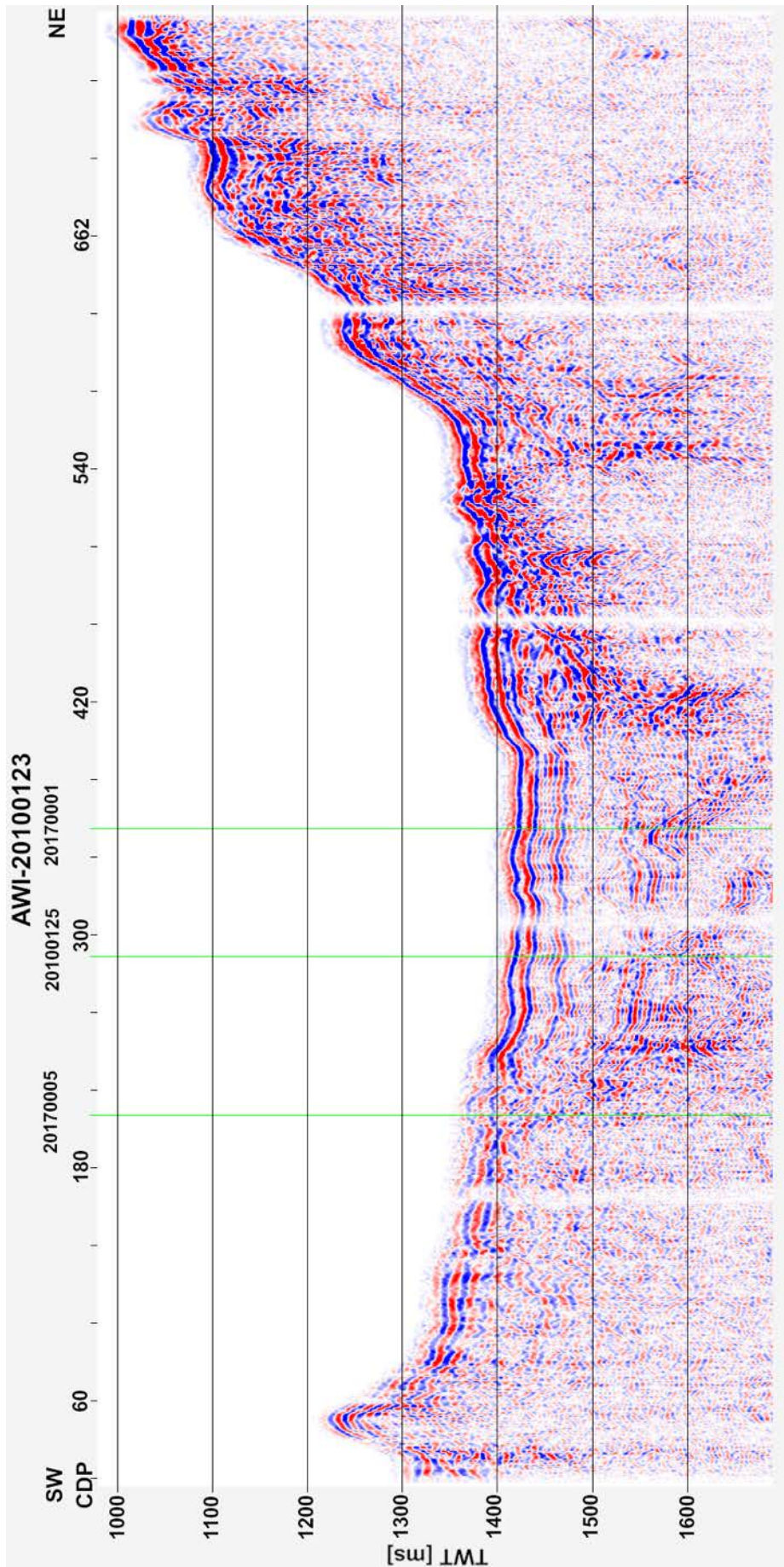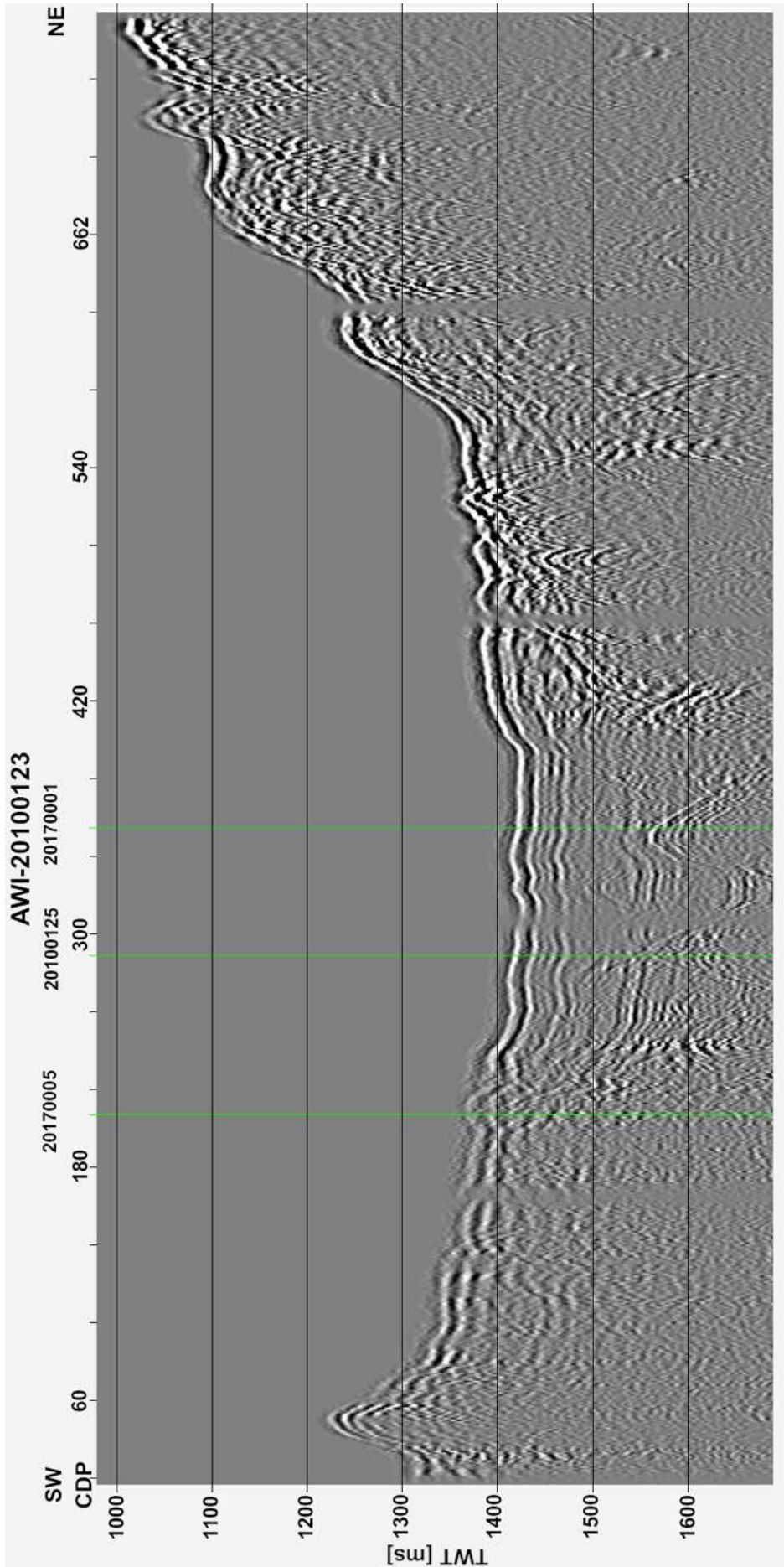
A. 6: Processed seismic profile AWI-20170003.

A. 7: Processed seismic profile AWI-20170004.

A. 8: Processed seismic profile AWI-20170004.

A. 9: Processed seismic profile AWI-20170005.

A. 10: Processed seismic profile AWI-20170005.
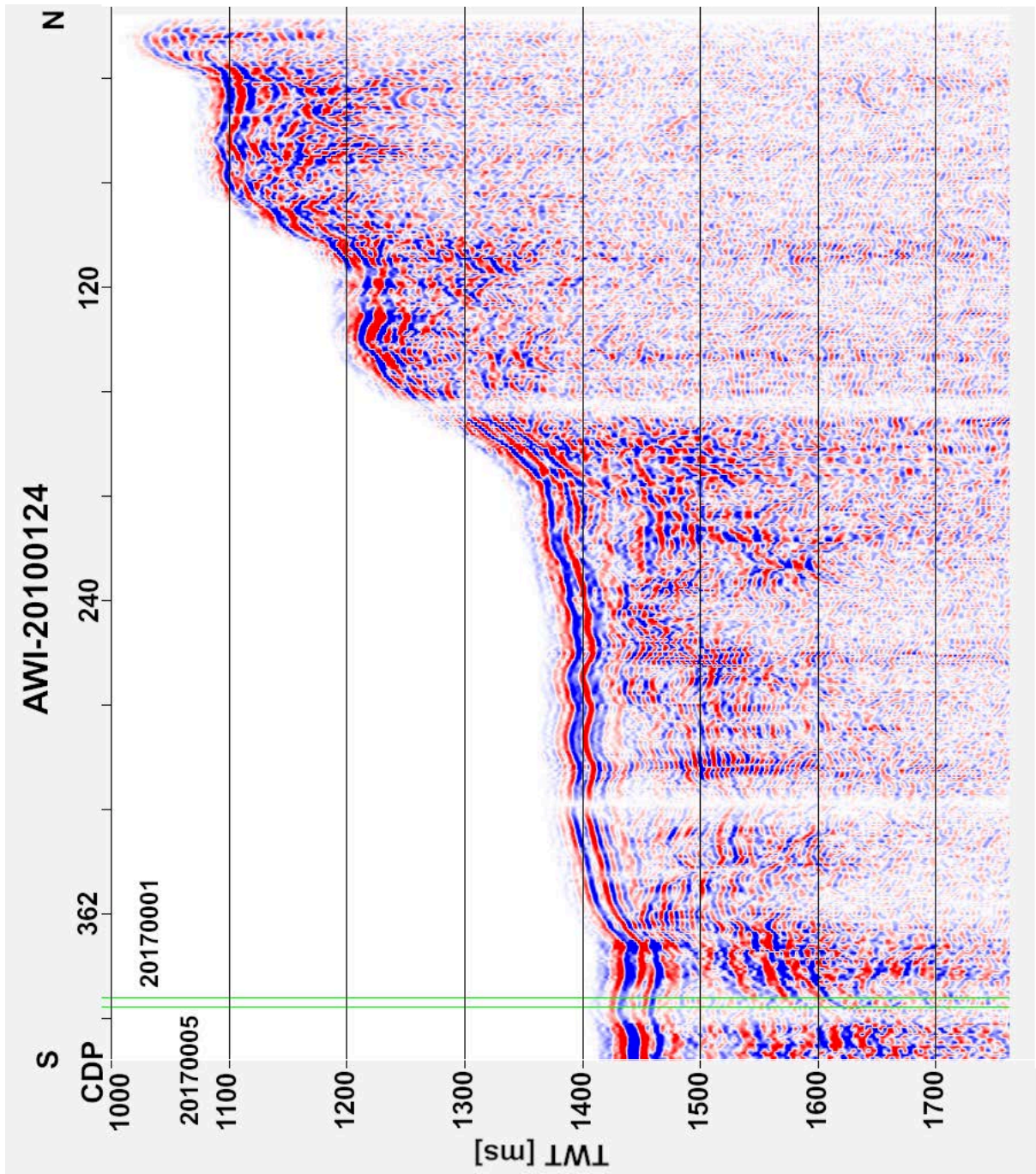
A. 11: Processed seismic profile AWI-20170006.

A. 12: Processed seismic profile AWI-20170006.

A. 13: Processed seismic profile AWI-20170007.

A. 14: Processed seismic profile AWI-20170007.

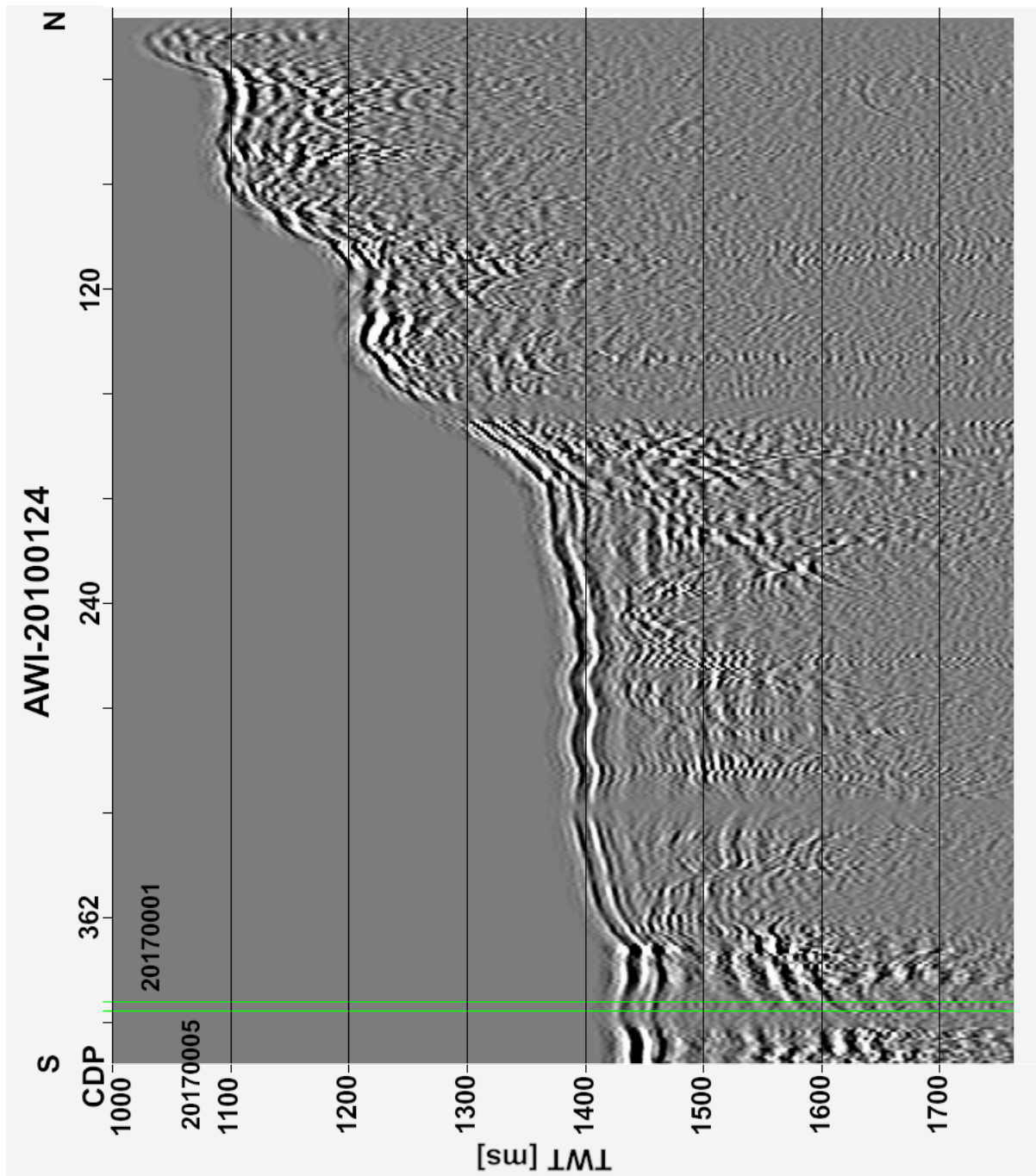## 10.2. Enlarged results of already processed profiles

A. 15: Already processed seismic profile AWI-20100123.

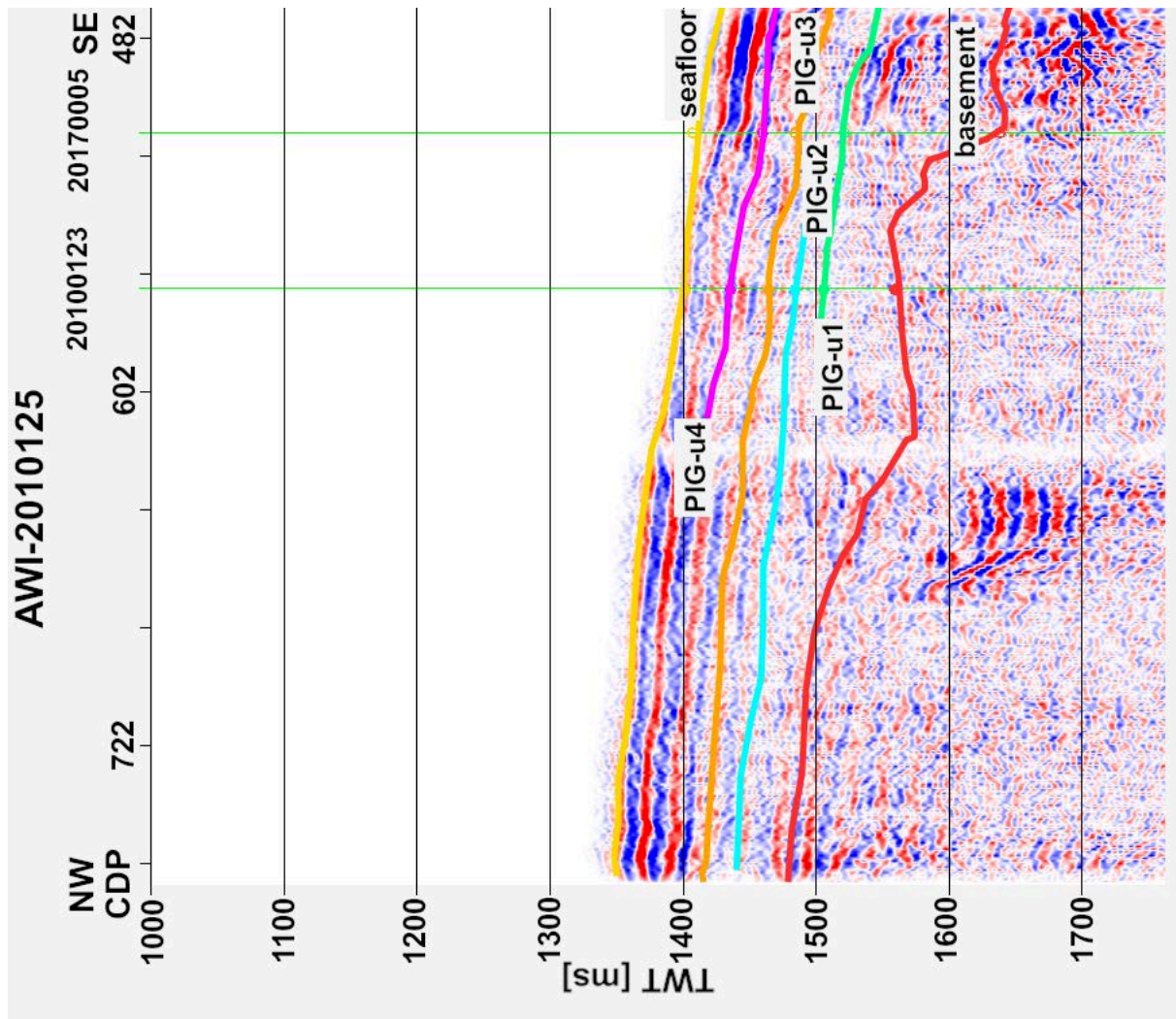*A. 16: Already processed seismic profile AWI-20100123.*

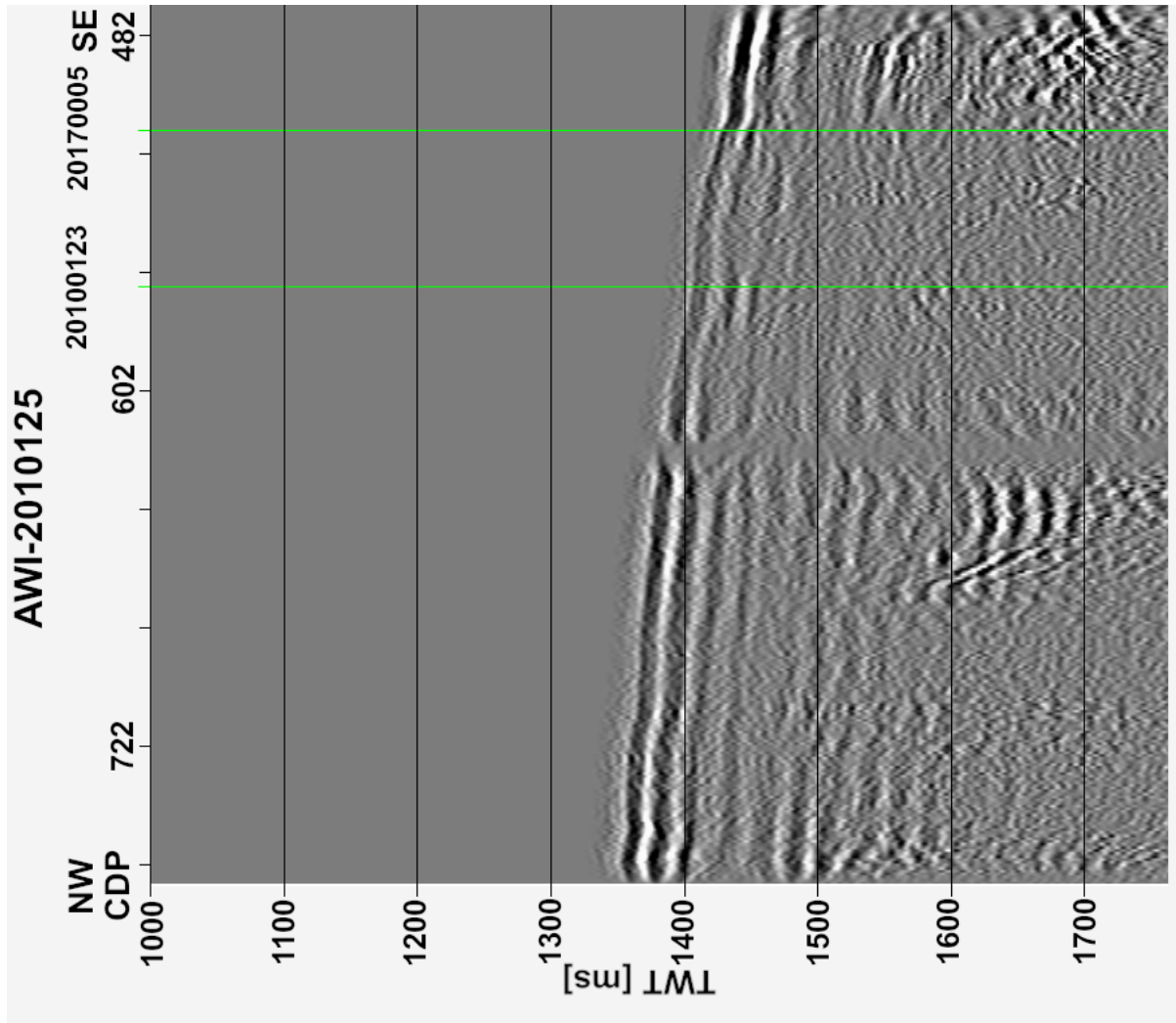*A. 17: Already processed seismic profile AWI-20100124.*

A. 18: Already processed seismic profile AWI-20100124.

A. 19: Already processed seismic profile AWI-20100125.

A. 20: Already processed seismic profile AWI-20100125.